SEMICONDUCTOR TRAVELING WAVE INTERACTION

By

Joseph Stanley Nadan

A dissertation submitted to the Graduate Faculty in Engineering in partial fulfillment of the requirements for the degree of Doctor of Philosophy, The City University of New York.

1969

This manuscript has been read and accepted for the Graduate Faculty in Engineering in satisfaction of the dissertation requirement for the degree of Doctor of Philosophy.

5-22-69
date

Chairman of Examining Committee

22 May 1969
date

Executive Officer

Prof. Paul Karmel

Prof. Carl Shulman

Prof. Morris Ettenberg

Chairman, Supervisory Committee

The City University of New York

ACKNOWLEDGEMENTS

I wish to express my gratitude to my mentor Professor Morris Ettenberg for his guidance, both technical and personal, throughout the course of my graduate studies.

The many detailed technical discussions and suggestions of Professors Paul Karmel, Carl Shulman, and Bayram Vural were most helpful and are gratefully acknowledged. The comments of Professor George Eichmann and the skill and assistance of Mr. H. D. Pressman in the preparation of experiments were most appreciated.

The author is indebted to the National Science Foundation for the Science Faculty Fellowship that was awarded for 1968. The encouragement of Dean Egon Brenner and the financial support received from the City College of the City University of New York and the New York State Science and Technology Foundation (Grant SF(7)3) are gratefully acknowledged.

Many thanks are also due my wife for her non-technical assistance in preparing the manuscript.

The services provided by the secretarial and laboratory staffs of the City College Department of Electrical Engineering are most appreciated.

TABLE OF CONTENTS

TABLE OF CONTENTS

TABLE OF CONTENTS

TABLE OF CONTENTS

LIST OF FIGURES

ABSTRACT

The interaction between slow electromagnetic waves and drifting carriers in a semiconductor is studied considering two species of charge carrier, collision, recombination, cold circuit, and diffusion loss mechanisms. It is shown that for high resistivity materials the effect of the minority carrier may be neglected resulting in a dominant carrier dispersion equation. A perturbational solution to this equation is studied by root locus technique to reveal the effects of the various parameters.

The dispersion equation of a slow wave circuit suitable for use in studying the above interaction is developed taking into account the effects of a multi-layered medium. Experimental results verifying the above theory are presented.

Interaction for highly asynchronous velocities are studied by extending the range of validity of the perturbational assumptions. The modal excitation problem is solved revealing that the collision dominated assumption may not be utilized.

Numerical results for this interaction, when using the above slow wave circuit, are presented showing that the construction of a circuit with a cut-off frequency of approximately one third the collision frequency is required to obtain a practical device.

A new numerical method is presented that is useful in solving n^{th} degree algebraic equations of the type found in wave interaction problems.

SPECIAL SYMBOLS

A, B, S	subscripts for carrier species type
C	Pierce's coupling coefficient
h	synchronization parameter
m	line number
n	harmonic number
S	growth rate variable
u	velocity
V	mean velocity
$Y(\theta_0)$	Fletcher's admittance function
Z_{ic}	interaction impedance
α_c	cold circuit attenuation
β_c	collision wave number
β_e	electronic wave number
β_n	phase shift per unit length
β_p	plasma wave number
β_Q	reduced plasma wave number
β_R	recombination wave number
θ_n	interline phase shift
λ_D	Debye wavelength
τ_e	energy relaxation time
τ_p	momentum relaxation time
τ_R	recombination lifetime
ν	collision frequency
ω_c	reduced collision frequency
ω_p	plasma frequency
ω_Q	reduced plasma frequency
ω_R	reduced recombination frequency

CHAPTER 1 - INTRODUCTION AND BACKGROUND

The interaction of drifting charge carriers in a semiconductor and slow electromagnetic waves on an external circuit was first hypothesized by J.R. Pierce [1] in 1955 in the form of a patent for the solid state analog of the vacuum traveling wave tube. In this device a semiconductor filament would replace the electron beam of the traveling wave tube as shown in Figure 1.1, thus not requiring an electron gun and its associated focusing devices. The drifting charge carriers in the semiconductor, analogous to the electrons in the vacuum device, would interact with the slow electromagnetic wave resulting in a convective instability. No analytical or experimental work was attempted at the time.

The first analytical work performed concerning this interaction appeared as an appendix to a report by Sandbank, et. al., on the velocity modulation of charge carriers in semiconductors [2]. In their analysis Solymar and Ash presented the beginnings of a one dimensional model of the semiconductor traveling wave amplifier. They assumed a single species of charge carrier with infinite recombination lifetime obtaining a characteristic equation for the interaction that is reduceable to the well known vacuum traveling wave tube case. The range of validity of this single carrier assumption was not considered for a system where two carrier species, electrons and holes, seem more appropriate.

In solving this equation by a perturbational technique Solymar and Ash made two, as it will be shown, incorrect assumptions; first, it was

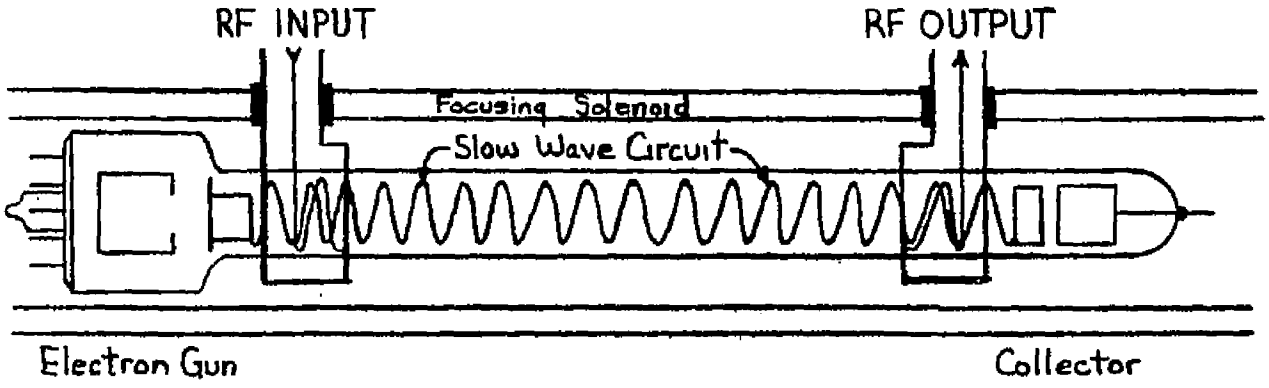

Figure 1.1a - Vacuum Traveling Wave Tube

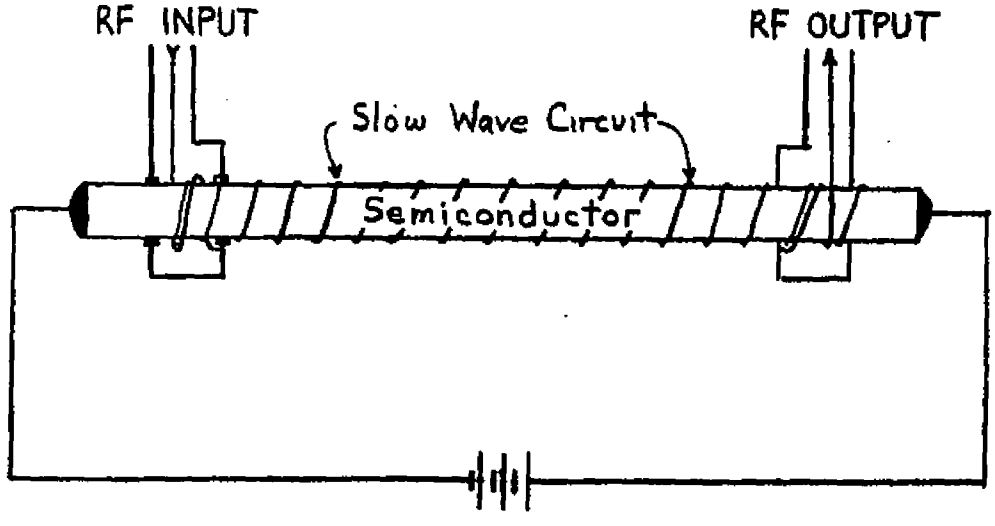

Figure 1.1b - Solid State Analog of Traveling Wave Tube

assumed that the four roots to the characteristic equation were widely separated and second, the cold circuit attenuation loss was assumed to be purely additive and not included in the perturbational solution, $\int$, i.e. Re (γ) = Re ($\int$) - Re (γ_o). These assumptions resulted in an expression for only the growing mode, one that is not reduceable to the well known vacuum traveling wave tube case.

In an attempt to evaluate the gain of a particular device Solymar and Ash utilized the interaction impedance calculated by Butcher [3] for infinitely thin ladder lines in free space. Since the tape line considered, the meander line, is dielectrically loaded and has finite boundaries this approximation is most questionable. The dispersion characteristics and interaction impedance of such a structure constructed on layered dielectric media are unknown.

The problem of mode excitation was not treated by Solymar and Ash.

Two numerical designs for n-type silicon devices were presented for liquid helium and room temperatures. The lack of data for the circuit precludes the confirmation of the calculated gain and its comparison with the fuller model to be developed.

Sumi [4] in 1966 published an analysis of traveling wave amplification by drifting carriers in semiconductors in which he predicted 100 db/mm gain for InSb device operated at 4GHz at liquid nitrogen temperature. The analysis consisted of evaluating the transverse admittance

at the surface of a collision dominated semiconductor and equating it to the transverse admittance at the surface of a developed helix, restricting the analysis to this particular structure and thus not having the same wide applicability as the Pierce type one dimensional model. There is strong experimental evidence [5,6] to indicate that the assumption of no surface charge or current at the semiconductor surface, used in equating the two admittances, is incorrect, thus invalidating the dispersion equation so found as illustrated in Figure 1.2. Zotter [7], using Sumi's analysis, has numerically evaluated the available gain for different semiconductor materials, as shown in Figure 1.3, predicting an even higher gain per millimeter.

The work of Sumi and Zotter is not reduceable to the well known vacuum traveling wave tube case because of the collision dominated assumption made. The mode excitation problem was not treated.

Vural and Steele [8] have extended Sumi's analysis to consider the interaction with a generalized admittance wall including the effects of surface charge and currents. While allowing one to determine the mode behavior for various assumed admittances it does however require the evaluation of the transverse admittance for the particular slow wave circuit under consideration. Unfortunately, as will be shown, the calculation of the transverse admittance of the meander line slow wave circuit requires the knowledge of higher order modes propagating along the structure; i.e. when calculated using only the dominant mode the admittance is zero.

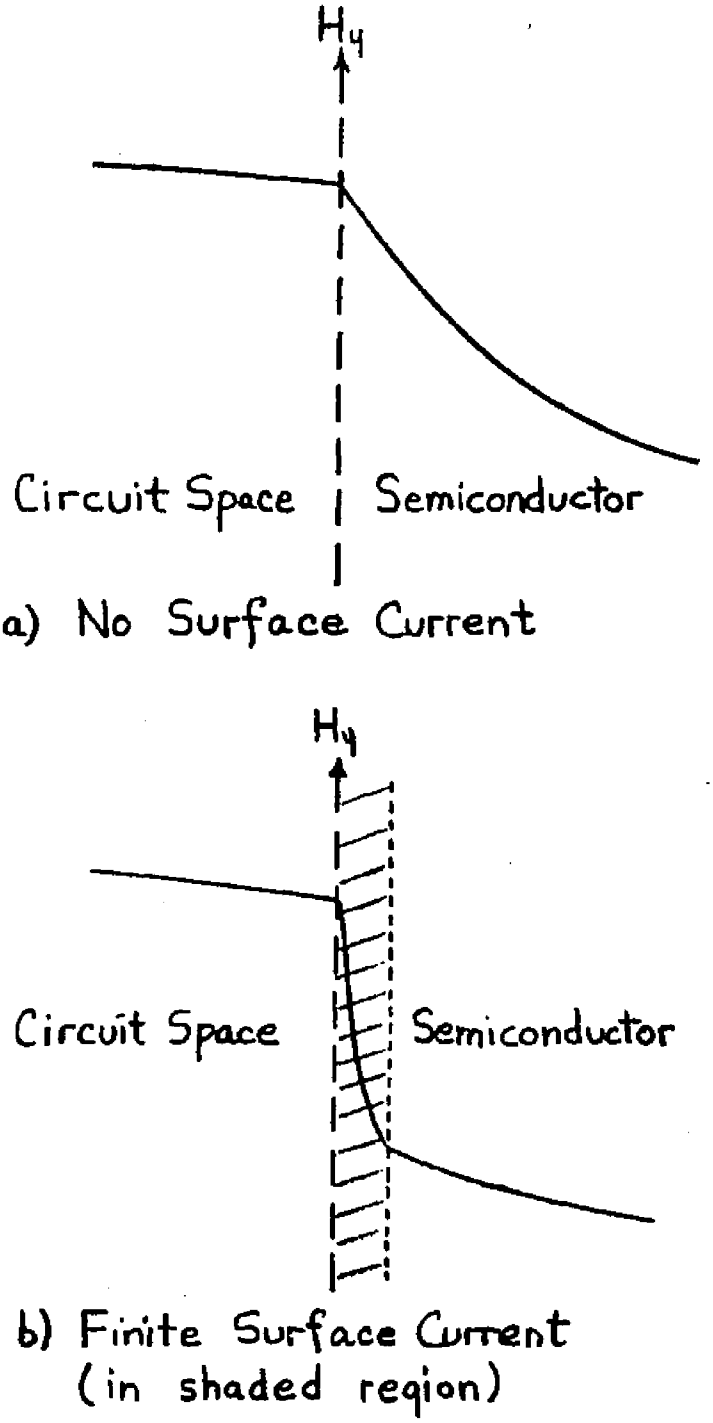

Figure 1.2 Effect of Surface Current on the Magnetic Field In a Semiconductor

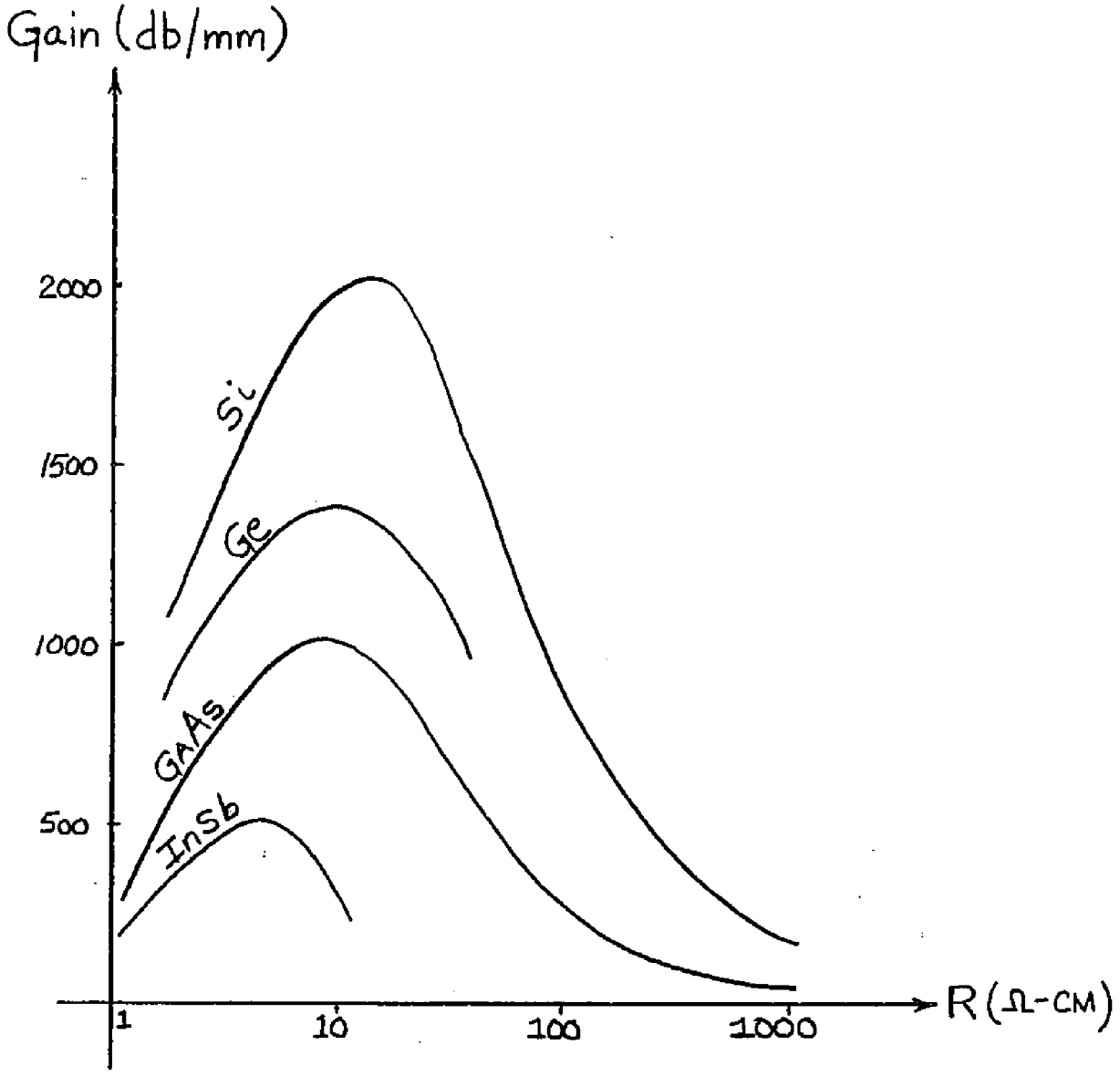

Figure 1.3 Maximum Gain vs. Resistivity for Semiconductor Materials
(based on Sumi's analysis - calculated by Zotter)

Study of this case in the inertia dominated limit reveals five constant amplitude modes which in the presence of non-zero admittance is modified to include a convective instability. The mode excitation problem was not treated.

Hammer [9,10], following the Solymar and Ash treatment but using a Taylor series expansion for the effective mass, has shown that the presence of negative differental mobility in the collision dominated limit inhibits the interaction when the mean electron exceeds the cold circuit phase velocity; however, when the mean electron velocity is less than the cold circuit phase velocity gain enhancement is predicted.

The study of the interaction of drifting carriers in a semiconductor and slow electromagnetic waves on an external circuit has been initiated by several authors revealing the need for further work. This work should be directed towards the development of a model that is applicable to a generalized slow wave circuit while still facilitating the evaluation of the individual case: in particular both the helix and dielectrically loaded meander line, and should include all the effects inherent to the semiconductor plasma. The model should be reduceable to the vacuum traveling wave tube case such that the effects of the semiconductor plasma may be ascertained. The mode excitations have to be determined to allow the calculation of device gain such that comparison with experiment may be made.

CHAPTER 2 - DISPERSION EQUATION FOR THE INTERACTION OF SLOW ELECTROMAGNETIC WAVES WITH DRIFTING CARRIERS IN A SEMICONDUCTOR.

The subject matter of this chapter is the development of a "one-dimensional" normalized dispersion equation characterizing the interaction of a slow electromagnetic wave with drifting carriers in a semiconductor. Although only longitudinal waves are considered, the coefficients of the dispersion equation are calculated by taking into account the transverse field variations. For completeness, the derivation is started at a fundamental point: namely the Boltzmann transport equation as derived by many authors [11,12,13].

2.1 The Boltzmann Equation

The distribution function of the s^{th} carrier species, $f_s(\vec{r},\vec{u},t)$, is defined as the density of s^{th} type carriers at the point $(\vec{r},\vec{u})$ in phase space. The most probable number of s^{th} type carriers in an infinitesmal volume $d^3r\,d^3u$ about $(\vec{r},\vec{u})$ is $f_s(\vec{r},\vec{u},t)\,d^3r\,d^3u$. The velocity space average of a quantity $g(\vec{r},\vec{u},t)$ is given by

$$\bar{g}(\vec{r},t) = \frac{\int g(\vec{r},\vec{u},t)\, f_s(\vec{r},\vec{u},t)\, d^3u}{\int f_s(\vec{r},\vec{u},t)\, d^3u} \qquad (2\text{-}1)$$

the denominator of (2-1) is recognized as the s^{th} type carrier species density in position space, to be referred to as "the carrier density",

n_s, given by

$$n_s(\vec{r},t) = \int f_s(\vec{r},\vec{u},t)\, d^3u \,, \tag{2-2}$$

such that

$$\bar{g}(\vec{r},t) = \frac{\int g(\vec{r},\vec{u},t) f_s(\vec{r},\vec{u},t)\, d^3u}{n_s(\vec{r},t)} \tag{2-3}$$

The Boltzmann equation may be derived by considering the various methods of altering $f_s(\vec{r},\vec{u},t)$. Carriers may move into and out of the region $(\vec{r},\vec{u})$ due to diffusion. The momentum (thus velocity) of a carrier may be altered by an externally applied force according to the law $\dot{\vec{k}} = \vec{F}/\hbar$.[14] A carrier may be "scattered" from one point in phase space to another. Unlike the gaseous plasma the collision terms are non-negligible because of the higher carrier densities in a solid-state plasma.

The many scattering mechanisms present in a solid include scattering by optical and acoustic laitice vibrations, scattering by lattice imperfections, scattering by ionized impurities, and lastly scattering by other carriers. The predominant scattering mechanism depends on the plasma selected and the carrier temperature; e.g. in non-polar semiconductors (germanium and silicon) optical phonon scattering determines the energy loss while acoustic phonon scattering controls the

momentum dissipation at moderate and high temperature, whereas scattering by lattice imperfections and ionized impurities predominates at low temperature [15]. Only the weakest of these mechanisms are present in a gaseous plasma.

Finally, carriers may be generated or recombine with another carrier species; e.g. conduction band electrons may recombine with either holes in the valence band, termed direct recombination because of the band to band transition, or with "traps", termed indirect recombination because recombination occurs via intermediate localized energy levels in the forbidden gap.

The Boltzmann equation is [16]

$$\frac{\partial f_s}{\partial t} + \vec{u}\cdot\nabla_r f_s + \frac{\vec{F}}{m^*}\cdot\nabla_u f_s = \left.\frac{\partial f_s}{\partial t}\right|_{coll.} + \left.\frac{\partial f_s}{\partial t}\right|_{g-r} \qquad (2\text{-}4)$$

The two terms on the right hand side representing respectively the rate of change of the distribution function due to collisions (scattering) and generation-recombination of carriers.

2.2 Macroscopic Equations Derived From the Boltzmann Equation.

The Boltzmann equation is a microscopic equation; i.e. it describes the individual carrier behavior. It is useful to derive general macroscopic laws by taking moments of the Boltzmann equation. This approach yields the continuity and momentum transfer equations, which are more useful because the dependent variables are macroscopic and

observable. This method, however, also results in an open set of equations that must be closed by making a simplifying hypothesis about one of the hydrodynamic moments.

The continuity equation (conservation of particle number) is derived by taking the zeroth moment of the Boltzmann equation; i.e. multiplying by u^o and integrating over velocity space [17], yielding

$$\frac{\partial n_s}{\partial t} + \nabla_r \cdot (n_s \vec{V}_s) = \int \frac{\partial f_s}{\partial t}\Big)_{coll.} d^3u + \int \frac{\partial f_s}{\partial t}\Big)_{g-r} d^3u . \qquad (2\text{-}5)$$

The momentum transfer equation (conservation of particle momentum) is derived by taking the first moment of the Boltzmann equation; i.e. multiplying by $\vec{u}^1$ and integrating over velocity space [18], yielding

$$\frac{\partial(n_s \vec{V}_s)}{\partial t} + \frac{\nabla_r \cdot \mathbb{P}}{m_s^*} + \nabla_r \cdot (n_s \vec{V}_s \vec{V}_s) - \frac{n_s \vec{F}}{m_s^*} = \int \vec{u} \frac{\partial f_s}{\partial t}\Big)_{coll.} d^3u + \int \vec{u} \frac{\partial f_s}{\partial t}\Big)_{g-r} d^3u , \qquad (2\text{-}6)$$

where $\mathbb{P} = m_s^* n_s \overline{(\vec{u}_s - \vec{V}_s)(\vec{u}_s - \vec{V}_s)}$ is a pressure tensor.

To proceed further one must evaluate the integrals in the continuity and momentum transfer equations. One would express the rate of change of the distribution function due to scattering in terms of the density of states and transition probability functions [19]. This, however, requires inferring these functions from either theory or experi-

ment. The phenomenological approach, that of approximating the scattering terms, yields simpler usable results.

First, one assumes that the equilibrium (zero convection current) distribution function is Maxwellian and isotropic in velocity; i.e.,

$$f_s(\vec{v}_s, \vec{u}, T_s)\Big|_{\vec{v}_s=0} = n_s\left(\frac{m_s^*}{2kT_s}\right)^{3/2} \exp\left(\frac{-m_s^* u^2}{2kT_s}\right) . \qquad (2\text{-}7)$$

Furthermore, one assumes that the effect of any distrubance is to alter the carrier temperature and mean velocity while not appreciably changing the form of the distribution function; i.e. the non-equilibrium distribution function is a displaced Maxwellian of higher temperature as shown in Figure 2.1. This technique allows extrapolation to "hot electrons" although it is known that at very high drift velocities departure from Maxwellian form may occur [20]. Upon removal of the disturbance the non-equilibrium distribution function, $f_s(\vec{v}_s, \vec{u}, T_s)$, relaxes to the equilibrium distribution function, $f_s(o, \vec{u}, T_l)$. The equilibrium condition is attained when both T_s decreases to T_l and the mean carrier velocity is zero. The rate of change of the distribution function due to collisions may be expanded as

$$\left(\frac{\partial f_s}{\partial t}\right)_{coll.} = \left(\frac{\partial f_s}{\partial v_s}\right)\left(\frac{\partial v_s}{\partial t}\right)_{coll.} + \left(\frac{\partial f_s}{\partial T_s}\right)\left(\frac{\partial T_s}{\partial t}\right)_{coll.} . \qquad (2\text{-}8)$$

Phenomenologically assuming that relaxation times for energy (temperature) and momentum (velocity) are valid; i.e.,

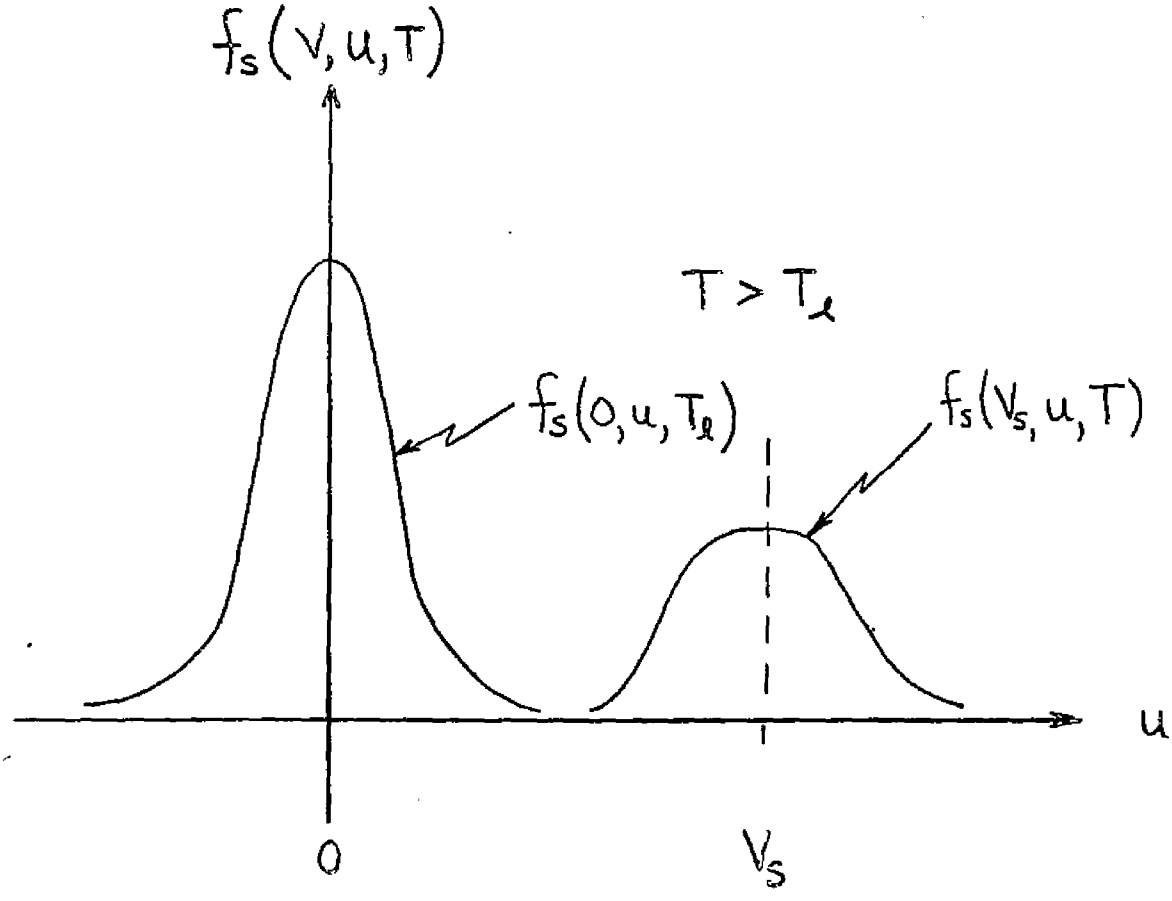

FIGURE 2.1 DISTRIBUTION FUNCTIONS

$f_s(0,u,T_e)$ – equilibrium Maxwellian

$f_s(V_s,u,T)$ – non-equilibrium drifted Maxwellian

$$\left.\frac{\partial T_s}{\partial t}\right|_{coll.} = -\frac{(T_s - T_\ell)}{\tau_e} \,, \tag{2-9}$$

and

$$\left.\frac{\partial V_s}{\partial t}\right|_{coll.} = -\frac{V_s}{\tau_p} \,, \tag{2-10}$$

results in

$$-\left.\frac{\partial f_s}{\partial t}\right|_{coll.} = \frac{f_s(V_s,u,T_\ell) - f_s(0,u,T_\ell)}{\tau_p} + \frac{f_s(0,u,T_s) - f_s(0,u,T_\ell)}{\tau_e} \,. \tag{2-11}$$

The effects of phonon emission caused by supersonic carriers [21] may be studied by expanding the relaxation times as functions of velocity and temperature; however, in this study τ_p and τ_e are assumed to be constant. Substitution of (2-11) in (2-5) and (2-6) results in collision integrals of the form

$$I_{n,\vec{V}_s} \triangleq \int \vec{u}^{\,n} f_s(\vec{V}_s,u,T)\, d^3u \,. \tag{2-12}$$

For n odd and $\vec{V}_s$ equal to zero, $I_{n,o} \equiv 0$, since u^n is odd and $f_s(o,u,T)$ is even. For n equal to zero, $I_{o,\vec{V}_s} \equiv \Omega_s$ independent of $\vec{V}_s$. Therefore,

$$\int \left.\frac{\partial f_s}{\partial t}\right)_{coll.} d^3u = 0 \,. \tag{2-13}$$

This is anticipated since intuitively it is expected that collisions cannot create or destroy particles. It is noted that the above does not depend on the Maxwellian form of $f_s(\vec{v}_s, u, T)$ but rather upon its eveness property. The integral

$$\int \vec{u} \left.\frac{\partial f_s}{\partial t}\right)_{coll.} d^3u \,, \tag{2-14a}$$

reduces to

$$I_{1,\vec{v}_s} = \frac{-\int \vec{u}\, f_s(\vec{V}_s, u, T_\ell)\, d^3u}{\tau_p} \tag{2-14b}$$

$I_{1,\vec{v}_s}$ is independent of τ_e ; i.e. the conservation of momentum is not effected by the energy relaxation time. Evaluating (2-14b) yields,

$$I_{1,\vec{v}_s} = -\frac{n_s \vec{V}_s}{\tau_p} \,. \tag{2-14c}$$

The generation-recombination terms are considered next. A derivation similar to that for the collision terms does not adequately represent many observed phenomena; e.g. minority carrier recombination as in the

Haynes-Shockley experiment. These effects are frequently represented by assuming a constant carrier generation rate, G_s, and a recombination rate that is proportional to the excess carrier concentration n_s, resulting in the continuity equation

$$\frac{\partial n_s}{\partial t} + \nabla_r \cdot (n_s \vec{V}_s) = G_s - \frac{\Delta n_s}{\tau_s} \quad . \tag{2-15}$$

In non-polar semiconductors τ_s (carrier recombination lifetime) is in the range 10^{-5} to 10^{-2} seconds and indirect recombination predominates. For polar semiconductors, in which direct recombination predominates, τ_s is in the range 10^{-8} to 10^{-6} seconds and may not be negigible. It is noted that the recombination lifetime may vary from sample to sample prepared from the same material because of differences in the treatment of the surfaces.

Substitution of (2-14c) in (2-6) yields

$$\frac{\partial (n_s \vec{V}_s)}{\partial t} + \frac{\nabla_r \cdot \mathbb{P}}{m_s^*} + \nabla_r \cdot (n_s \vec{V}_s \vec{V}_s) - \frac{n_s \vec{F}}{m_s^*} = -\frac{n_s \vec{V}_s}{\tau_p} \quad . \tag{2-16}$$

Assuming that the pressure tensor is isotropic and defining temperature by the equation of state $P \triangleq n k T_s$ to terminate the moment equations results in

$$\frac{d\vec{V}_s}{dt} + \frac{\vec{V}_s}{\tau_p} = \frac{\vec{F}}{m_s^*} - v_{th}^2 \frac{\nabla_r n_s}{n_s} \quad , \tag{2-17}$$

where the thermal velocity of the s^{th} carrier species is defined as $v_{th}^2 = 3kT_s / m_s^*$.

2.3 Dispersion Equation

The dispersion equation for the system; i.e. the relationship between wave vector and excitation frequency for the semiconductor and circuit is found by applying the principle of self consistency to the one dimensional model. First, the RF convection current density in the semiconductor is calculated from an assumed electric field in the circuit. The electronic admittance is defined as the ratio of the RF convection current density to the circuit RF electric field when calculated in such a manner. Next, the circuit RF electric field is calculated from an assumed RF convection current density in the semiconductor. The circuit admittance is defined as the ratio of the RF convection current density to the circuit RF electric field when calculated in this manner. The circuit admittance is then equated to the electronic admittance.

To derive the above admittances wave dependence for the variables of the form $\exp(j\omega t - \gamma z)$ is assumed. Additionally, small signal theory is used to write

$$\begin{aligned} \vec{J} &= \vec{J}_0 + \vec{J}_1 \exp(j\omega t - \gamma z), \\ \vec{E}_c &= \vec{E}_1 \exp(j\omega t - \gamma z), \\ \vec{V} &= \vec{V}_0 + \vec{V}_1 \exp(j\omega t - \gamma z), \end{aligned} \tag{2-18}$$

and $$n = n_0 + n_1 \exp(j\omega t - \gamma z),$$

where it has been assumed that higher order terms are negligibly small and E_c is the circuit electric field. Two carrier species, e.g. electrons and holes, are considered being represented by the subscripts A and B. The convection current density is therefore

$$\vec{J} = \sum_s q_s n_s \vec{V}_s = q_A n_A \vec{V}_A + q_B n_B \vec{V}_B . \qquad (2\text{-}19)$$

Substitution of (2-18) into the continuity equations for carriers A and B results in

$$j\omega n_{1A} - \gamma (n_{0A} V_{1A} + n_{1A} V_{0A}) = -\frac{n_{1A}}{\tau_{RA}} , \qquad (2\text{-}20)$$

and

$$j\omega n_{1B} - \gamma (n_{0B} V_{1B} + n_{1B} V_{0B}) = -\frac{n_{1B}}{\tau_{RB}} . \qquad (2\text{-}21)$$

Substitution of (2-18) into the momentum transfer equations for carriers A and B results in

$$(j\omega - \gamma V_{0A} + \nu_A) V_{1A} = \eta_A^* E_{T1} + v_{th_A}^2 \frac{\gamma n_{1A}}{n_{0A}} , \qquad (2\text{-}22)$$

and

$$(j\omega - \gamma V_{0B} + \nu_B) V_{1B} = \eta_B^* E_{T1} + v_{th_B}^2 \frac{\gamma n_{1B}}{n_{0B}} \quad . \tag{2-23}$$

The total electric field in the semiconductor may be written as the summation of the circuit electric field and the localized space charge electric field; i.e.,

$$\vec{E}_T = \vec{E}_C + \vec{E}_{SP} \quad . \tag{2-24}$$

The Lorentz force is neglected in (2-23) since $|V \times B|_z \ll |E_c|$. Substitution of (2-18) in Poisson's equation $\nabla_r \cdot \vec{D} = \rho_f$ completes the set of equations necessary to derive the electronic admittance. Defining the effective permittivity of the semiconductor plasma, ϵ, by $\vec{D} = \epsilon \vec{E}$, (Derived for a two component plasma in Appendix 1) results in $\nabla_r \cdot \vec{E}_T = \rho_f / \epsilon$. Since the circuit electric field exists without space charge, $\nabla_r \cdot \vec{E}_C = 0$, results in

$$\nabla_r \cdot \vec{E}_T = \nabla_r \cdot (E_C + E_{SP}) = \nabla_r \cdot E_{SP} \approx \nabla_z \cdot E_{SP} = \frac{\rho_f}{\epsilon} , \tag{2-25}$$

or

$$-\gamma E_{SP} = \frac{q_A n_{1A} + q_B n_{1B}}{\epsilon} \quad . \tag{2-25a}$$

The RF densities are found as functions of the RF velocities from (2-20, 21).

$$n_{1S} = \frac{\gamma n_{0S} V_{1S}}{\omega_{RS}} \tag{2-26}$$

where the "reduced" recombination frequency, ω_{RS}, is defined by

$$\omega_{RS} \triangleq (j\omega - \gamma V_{0S} + \tau_{RS}^{-1}). \tag{2-27}$$

Substituting (2-24, 25a) into the momentum transfer equations (2-22, 23) results in

$$\omega_{CA} V_{1A} = \eta_A^* E_1 - \eta_A^* \left[\frac{q_A n_{1A} + q_B n_{1B}}{\gamma \epsilon}\right] + v_{th_A}^2 \frac{\gamma n_{1A}}{n_{0A}}, \tag{2-28}$$

and

$$\omega_{CB} V_{1B} = \eta_B^* E_1 - \eta_B^* \left[\frac{q_A n_{1A} + q_B n_{1B}}{\gamma \epsilon}\right] + v_{th_B}^2 \frac{\gamma n_{1B}}{n_{0B}}, \tag{2-29}$$

where the "reduced" collision frequency, ω_{CS}, is defined by

$$\omega_{CS} \triangleq (j\omega - \gamma V_{0S} + \nu_S). \tag{2-30}$$

Substituting (2-26) into (2-28, 29) and defining the plasma frequency of the s^{th} type carrier, ω_{ps}, as

$$\omega_{ps}^2 \triangleq \frac{\eta_s^* q_s n_{os}}{\epsilon} , \tag{2-31}$$

results in the set of coupled equations,

$$\begin{pmatrix} (\omega_{CA}\omega_{RA} + \omega_{PA}^2 - v_{th_A}^2\gamma^2) & R\omega_{PB}^2 \\ R^{-1}\omega_{PA}^2 & (\omega_{CB}\omega_{RB} + \omega_{PB}^2 - v_{th_B}^2\gamma^2) \end{pmatrix} \begin{pmatrix} V_{IA} \\ V_{IB} \end{pmatrix} = \begin{pmatrix} \eta_A^*\omega_{RA}E_I \\ \eta_B^*\omega_{RB}E_I \end{pmatrix}, \tag{2-32}$$

where

$$R \triangleq \frac{\eta_A^*\omega_{RA}}{\eta_B^*\omega_{RB}} . \tag{2-33}$$

Defining

$$\omega_s^2 = \omega_{cs}\omega_{Rs} + \omega_{ps}^2 - v_{th_s}^2\gamma^2 , \tag{2-34}$$

and solving (2-32) results in the RF velocities

$$V_{IA} = \frac{\eta_A^*\omega_{RA}(\omega_{cB}\omega_{RB} - v_{th_B}^2\gamma^2)E_I}{\omega_A^2\omega_B^2 - \omega_{PA}^2\omega_{PB}^2} , \tag{2-35}$$

and

$$V_{1B} = \frac{\eta_B^* \omega_{RB}(\omega_{CA}\omega_{RA} - \upsilon_{thA}^2\gamma^2)\, E_1}{\omega_A^2\omega_B^2 - \omega_{PA}^2\omega_{PB}^2} \,. \tag{2-36}$$

The RF convection current density is found from (2-19) as

$$J_1 = q_A(n_{OA}V_{1A} + n_{1A}V_{OA}) + q_B(n_{OB}V_{1B} + n_{1B}V_{OB}). \tag{2-37}$$

ubstituting (2-26, 35, 36) into (2-37) results in the electronic admittance of a two component plasma,

$$\left.\frac{J_1 A}{E_1}\right)_{elec.} = \frac{\epsilon A\left[\frac{\omega_{PA}^2}{\tau_{RA}}\left(\omega_{CB}\omega_{RB} - \upsilon_{th_B}^2\gamma^2\right)\left(1 + j\omega\tau_{RA}\right) + \frac{\omega_{PB}^2}{\tau_{RB}}\left(\omega_{CA}\omega_{RA} - \upsilon_{th_A}^2\gamma^2\right)\left(1 + j\omega\tau_{RB}\right)\right]}{\omega_A^2\omega_B^2 - \omega_{PA}^2\omega_{PB}^2} \,. \tag{2-38}$$

The electronic admittance includes the effects of carrier lattice collisions, diffusion recombination and space charge through the parameters, ω_{CS}, $\upsilon_{th_S}^2$, ω_{RS}, and ω_{PS}^2 respectively. Diffusion and space charge are two entirely different loss mechanisms; diffusion loss resulting from the carrier density gradient while space charge loss is caused by the mutual forces between drifting charged carriers.

In deriving the electronic admittance, $\frac{J_1 A}{E_1}$, the effects of a

transverse electric field variation were neglected in Poisson's equation. These effects may be included by utilizing a reduced plasma frequency, $\omega_{QS}^2 < \omega_{PS}^2$. [22, 23] +

The circuit RF electric field excited by an impressed RF convection current density is next calculated [24] by expanding in terms of the normal modes resulting in -

$$E_T = -J_1 A \left[\sum_n \frac{Z_n \gamma^2 \gamma_n}{\gamma^2 - \gamma_n^2} + \frac{j}{\omega \epsilon A} \right] , \qquad (2\text{-}39)$$

+ Poisson's equation $\nabla_T \cdot E_T = \rho_f / \epsilon$ may be rewritten without approximation as

$$\nabla_z \cdot E_{SP} = \frac{\rho_f}{\epsilon} \left[1 + \frac{\nabla_t \cdot E_{SP}}{\nabla_z \cdot E_{SP}} \right]^{-1} .$$

In the previous derivation it has been assumed that $\nabla_t \cdot E_{SP} = 0$. The concept of utilizing a reduced plasma frequency is to improve upon this approximation by calculating this term in the following manner. As will be shown, $\nabla_z \cdot E_{SP} = -\gamma E_{SP} \approx -j\beta_e E_{SP}$ such that the correction term is

$$\left[1 + j \frac{\nabla_t \cdot E_{SP}}{\beta_e E_{SP}} \right]^{-1}$$

and depends on the transverse boundary conditions. This correction term is related to the plasma frequency reduction factor ω_Q^2 / ω_P^2 . This term can in principle be evaluated from the geometrical configuration of the boundary.

where Z_n is the "interaction impedance" of the n^{th} space harmonic of E_T defined as

$$Z_n \triangleq \frac{|E_{zn}|^2}{2\beta_n^2 P} \quad . \qquad (2\text{-}40)$$

Consider the case when $\gamma \approx \pm \gamma_o$. For $n \neq 0$, the term $\gamma^2 - \gamma_n^2$ will be large when compared to $\gamma^2 - \gamma_o^2$. Additionally, the numerical value of the term $Z_n \gamma^2 \gamma_n / (\gamma^2 - \gamma_n^2)$ will not be appreciably altered by changing various parameters. Hence (2-39) may be rewritten as

$$E_T = -J_1 A \left[\frac{Z_n \gamma^2 \gamma_o}{\gamma^2 - \gamma_o^2} + \frac{j}{m_1 \beta_e A} \right] \qquad (2\text{-}41)$$

where m_1 is a constant, having dimensions of admittance, that represents the effects of all the passive modes $(n \neq 0)$ and the term $+j/\omega \epsilon A$. The first term is derived from a field that has approximately the same spatial variation as the circuit field; i.e. $\gamma \approx \pm \gamma_o$. From (2-24) it is seen that the second term may be interpreted as the space charge field. Hence,

$$\left. \frac{J_1 A}{E_1} \right|_{CKT} = \frac{\gamma_o^2 - \gamma^2}{\gamma^2 \gamma_o Z_o} \quad . \qquad (2\text{-}42)$$

The dispersion equation is found by applying the principle of selfconsistency to J_1A/E_1 ; i.e. equating (2-42) to (2-38), or by applying the principle of self-consistency to J_1A/E_T . The former of these requires the evaluation of the plasma frequency reduction factor while the latter requires the evaluation of the admittance m_1 . Since data is more readily available for plasma frequency reduction factors [25] the former approach is taken resulting in the dispersion equation

$$\frac{\epsilon A\left[\frac{\omega_{QA}^2}{\tau_{RA}}\left(\omega_{CB}\omega_{RB}-\mu_{H_B}^2\gamma^2\right)\left(1+j\omega\tau_{RA}\right)+\frac{\omega_{QB}^2}{\tau_{RB}}\left(\omega_{CA}\omega_{RA}-\mu_{H_A}^2\gamma^2\right)\left(1+j\omega\tau_{RB}\right)\right]}{\omega_A^2\omega_B^2-\omega_{QA}^2\omega_{QB}^2}=\frac{\gamma_o^2-\gamma^2}{\gamma^2\gamma_o Z_n}\,. \qquad (2\text{-}43)$$

2.4 Collision Dominated Dispersion Equation

The dispersion equation of the interaction (2-43) is a sixth degree algebraic equation in γ with complex coefficients. It is therefore useful to examine the equation for the semiconductor case to see how it may be simplified for numerical calculation. The interaction is said to be collision dominated when the condition $\nu_s >> (j\omega-\gamma V_{os})$ is satisfied for all carrier species, for which $\omega_{cs} \rightarrow \nu_s$. Assuming that the effects of diffusion are negligible (as will be shown), and considering the case when the recombination lifetime is arbitrarily large, $\omega\tau_{RS} >> 1$, such that $\omega_{RS} \rightarrow (j\omega-\gamma V_{os})$, the dispersion equation may be rewritten as

$$\frac{\frac{\beta_{QA}^2}{\beta_{CA}}\left(j\beta_{eB}-\gamma_0\right)+\frac{\beta_{QB}^2}{\beta_{CB}}\left(j\beta_{eA}-\gamma\right)}{\frac{\beta_{QA}^2}{\beta_{CA}}\left(j\beta_{eB}-\gamma\right)+\frac{\beta_{QB}^2}{\beta_{CB}}\left(j\beta_{eA}-\gamma\right)+\left(j\beta_{eA}-\gamma\right)\left(j\beta_{eB}-\gamma\right)}=\frac{\gamma_0^2-\gamma^2}{j\omega\epsilon\gamma^2\gamma_0 Z_n A}, \quad (2\text{-}44)$$

a quartic equation in γ with complex coefficients. Assuming the solutions for γ will have a magnitude approximately equal to the electronic wave number allows the derivation of a condition for which the interaction may be characterized by the dominant carrier; i.e. when

$$\frac{\beta_{QA}^2}{\beta_{CA}} \gg \frac{\beta_{QB}^2}{\beta_{CB}} \quad (2\text{-}45)$$

equation (2-44) may be approximated as

$$\frac{\beta_{QA}^2}{\beta_{CA}\left(j\beta_{eA}-\gamma\right)} = \frac{\gamma_0^2-\gamma^2}{j\omega\epsilon\gamma^2\gamma_0 Z_n A} . \quad (2\text{-}46)$$

The dominant carrier condition (2-45) may be rewritten for n and p - type materials respectively as

$$n_0 \gg n_i\left(\frac{m_e^* \mu_e}{m_H^* \mu_H}\right), \quad (2\text{-}47a)$$

$$p_0 \gg n_i\left(\frac{m_H^* \mu_H}{m_e^* \mu_e}\right), \quad (2\text{-}47b)$$

thus defining for each material a maximum resistivity for which this approximation is valid. (A tabulation for different materials is given in table 2.1) Equation (2-46) is not reduceable to the vacuum traveling wave tube case because of the collision dominated assumption made.

2.5 Dominant Carrier Dispersion Equation

The dominant carrier dispersion equation may be derived in an alternate manner that retains the collision, diffusion, and recombination dependence. Letting $\omega_{QB}^2 \to 0$, the dispersion equation (2-43) reduces to

$$\frac{\epsilon A \beta_{QA}^2}{\left[(j\beta_{eA}-\gamma+\beta_{RA})(j\beta_{eA}-\gamma+\beta_{cA})+\beta_{QA}^2(1-\lambda_{DA}^2\gamma^2)\right]} = \frac{\gamma_0^2-\gamma^2}{\gamma^2\gamma_0 Z_n\left(\frac{1+j\omega\tau_{RA}}{\tau_{RA}}\right)}, \quad (2\text{-}48)$$

and has been written to display the effects of carrier recombination. When $\omega\tau_{RA} >> 1$, the case of negligible carrier recombination as in Germanium and Silicon, equation (2-48) reduces to the case studied by Solymar and Ash [26] . The major effect of nonnegligible carrier recombination is to modify the interaction impedance to

$$Z_{n\tau} = Z_n\left[1 - j(\omega\tau_{RA})^{-1}\right], \quad (2\text{-}49)$$

thus affecting the growth rate.

Semiconductor Material	$\frac{m_n^*}{m_e}$	$\frac{m_H^*}{m_e}$	μ_n $cm^2/V\text{-}sec$	μ_H $cm^2/V\text{-}sec$	$\frac{m_n^* \mu_n}{m_H^* \mu_H}$	$n_i\ (cm)^{-3}$	Maximum Resistivity	Theoretical Intrinsic Resistivity
Ge	0.55	0.3	3800	1800	3.875	2.4×10^{13}	2Ω-CM	46 Ω-CM
Si	1.09	0.5	1300	500	5.67	1.4×10^{10}	600Ω-CM	240 KΩ-CM
GaAs	0.072	0.65	8500	400	2.355	9×10^{6}	3.5 MΩ-CM	78 MΩ-CM
InSb	0.013	0.18	70 000	1 000	5.05	1.5×10^{16}	0.001 Ω-CM	0.006Ω-CM

Table 2.1 MAXIMUM RESISTIVITY for which the DOMINANT CARRIER DISPERSION EQUATION IS VALID AT 300°K

Since $\left(\frac{m_n^* \mu_n}{m_H^* \mu_H}\right) > 1$, the maximum resistivity for P-type materials is approximately equal to the theoretical intrinsic resistivity.

2.5a Perturbational Solution of the Dominant Carrier Dispersion Equation

The cold circuit transmission line supports two waves, circuit waves, that propagate in opposite directions along the line. When carriers are drifted through the semiconductor the "system" supports six waves; the four additional waves being called carrier waves, electrokinetic waves, and/or space charge waves. The perturbational solution of the dominant carrier dispersion equation will, because of its reduced degree, result in two circuit and two carrier waves.

Perturbations of the cold circuit waves are attempted for two reasons; first, it is expected that if the interaction is weak, then $\gamma \approx \pm \gamma_0$, and second, to obtain a strong interaction, corresponding to an appreciable Z_n, the circuit admittance should be minimized. This condition is satisfied when $\gamma^2 - \gamma_0^2 \approx 0$. Let

$$\gamma = j\beta_{eA} - \delta \,, \tag{2-50}$$

and

$$\gamma_0 = \alpha_0 + j\beta_0 = \alpha_0 + j(\beta_{eA} + h_A) \,. \tag{2-51}$$

The circuit admittance is approximated as

$$\left.\frac{J_1 A}{E_1}\right)_{CKT} = \frac{-2(\delta + \alpha_0 + j h_A)}{\beta_{eA}^2 Z_{nT}} \,, \tag{2-52}$$

contingent upon the conditions $|\beta_{eA}| >> |\alpha_o|$, $|\beta_{eA}| >> |\delta|$, and most importantly $|\beta_{eA}| >> |h_A|$, thus restricting the range of perturbational validity to near synchronism.

The perturbed dominant carrier dispersion is therefore the cubic

$$S^3 + (\beta'_{CA}+\beta'_{RA}+\alpha'_o+jh'_A)S^2 + \Big[(\beta'_{CA}+\beta'_{RA})(\alpha'_o+jh'_A)+\beta'_{CA}\beta'_{RA}+ \beta'^2_{QA}(1+\lambda^2_{DA}\beta^2_{eA})\Big]S + \Big([\beta'_{CA}\beta'_{RA}+\beta'^2_{QA}(1+\lambda^2_{DA}\beta^2_{eA})] \cdot [\alpha'_o+jh'_A]+j\Big) = 0 \quad , \tag{2-53}$$

where C is Pierce's coupling coefficient defined as

$$C \triangleq \left(\frac{Z_{rr}J_{oA}A\eta^*_A}{2V^2_{oA}}\right)^{1/3} , \tag{2-54}$$

and the prime, henceforth to be suppressed, denotes division by $\beta_{eA}C$. The perturbational solution to the dominant carrier dispersion equation is reduceable to the vacuum traveling wave tube case studied by Pierce [27] with provision for studying the effects present in semiconductor plasma.

The effect of diffusion is seen to be negligible since for most semiconductors,

$$|\lambda^2_D\beta^2_e| = \left|\left(\frac{\omega}{\omega_p}\right)^2\left(\frac{v_{th}}{v_o}\right)^2\right| << 1 \quad . \tag{2-55}$$

For $V_o = v_{th}$, ω would have to be approximately ω_p, 10^{12} sec^{-1}, for diffusion effects to occur.

2.6 The Effects of Collision and Cold Circuit Attenuation on the Perturbed Solution of the Dominant Carrier Dispersion Equation at Synchronism

The synchronous case is studied because it is the simplest mathematically and is the best perturbational approximation. Additionally, let the carrier recombination lifetime be arbitrarily large and the reduced plasma wave number negligibly small but non-zero. Equation (2-53) reduces to

$$S^3 + S^2(\beta_{CA} + \alpha_o) + S(\alpha_o \beta_{CA}) + j = 0 \qquad (2\text{-}56)$$

The collision and cold circuit attenuation loss mechanisms are not purely additive as suggested by Solymar and Ash[28].

There exists a solution to (2-56) with positive real part for all values of the real coefficients β_{CA} and α_o. This corresponds to the presence of a convective instability (gaining wave) even though appreciable collision damping may be present.

The above statement may be proved as follows. Inspection of the coefficients reveals that a pure real or pure imaginary solution is not possible except for infinite loss, a case never occurring in practice. Consider the lossless case, $\alpha_o = \beta_{CA} = 0$. Equation (2-56) reduces to $S^3 + j = 0$ whose solution is known to have a root with positive real part; i.e. $S_o = (+\sqrt{3} - j)/2$ in the fourth quadrant of the S-plane. Since the roots of a polynomial equation are continuous functions of the coefficients (Hurwitz's theorem), and may not cross the axes, the positive real part root is constrained to the fourth quadrant. Q.E.D.

The effects of the variation of either loss parameter may be studied by root locus technique. Letting $\alpha_o = 0$, and rewriting (2-56) in root locus form results in

$$1 + \frac{\beta_{CA} S^2}{S^3 + j} = 0 \qquad (2\text{-}57)$$

The points of origin of the loci are the solution to the lossless case $S^3 + j = 0$. The points of convergence of the loci are the double zero at the origin and one zero at infinity. The complete root locus is shown in Figure 2.2. Increasing the collision frequency (decreasing the momentum relaxation time) decreases the growth rate of the root in the fourth quadrant. Even for large β_{CA} there is net growth. It is noted that the magnitude of β_{CA} is not one of perturbational assumptions.

When $\alpha_o \neq 0$, (2-56) may be rewritten in root locus form

$$1 + \frac{\alpha_o S (S + \beta_{CA})}{S^3 + S^2 \beta_{CA} + j} = 0 \qquad (2\text{-}58)$$

The points of origin of the loci are the zeros of $S^3 + S^2 \beta_{CA} + j$ which is the previous root locus studied. The points of convergence are one zero at $S = -\beta_{CA}$, one zero at the origin and one zero at infinity. The complete root locus is shown in Figure 2.3. The effect of cold circuit attenuation is to reduce further the net growth rate.

2.7 The Effects of Space Charge and Diffusion on the Perturbed Solution of the Dominant Carrier Dispersion Equation at Synchronism.

When the only mechanisms present are space charge and diffusion, equation (2-56) reduces to

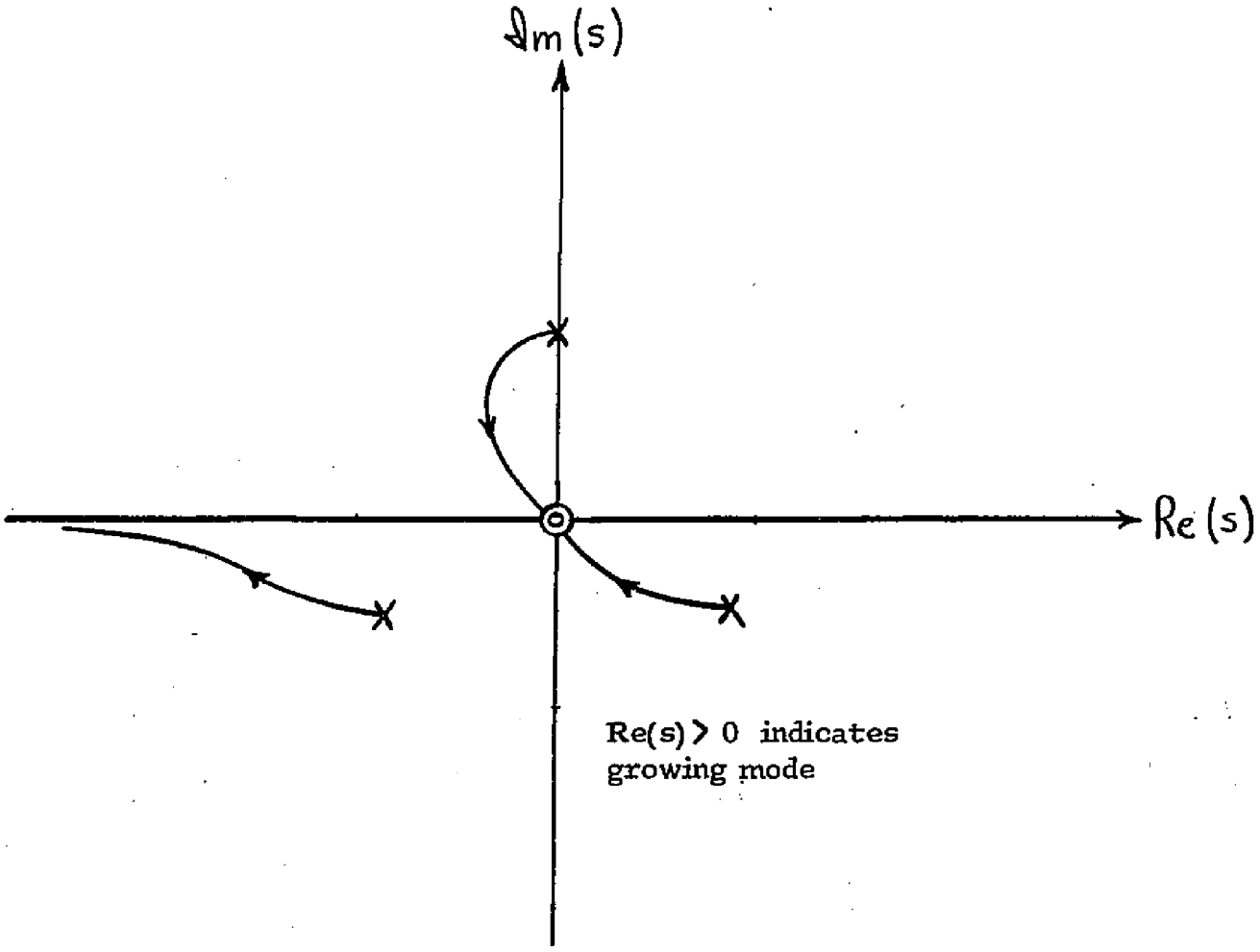

Figure 2.2 Root locus of synchronous dominant carrier dispersion equation for $\alpha_o = 0$.

Points of origin are indicated by X. Points of convergence are indicated by 0. Arrows indicate increasing gain constant β_{CA}. This locus is calculated for the case when only collision loss is present.

$$1 + \frac{\beta_{CA} S^2}{S^3 + j} = 0 .$$

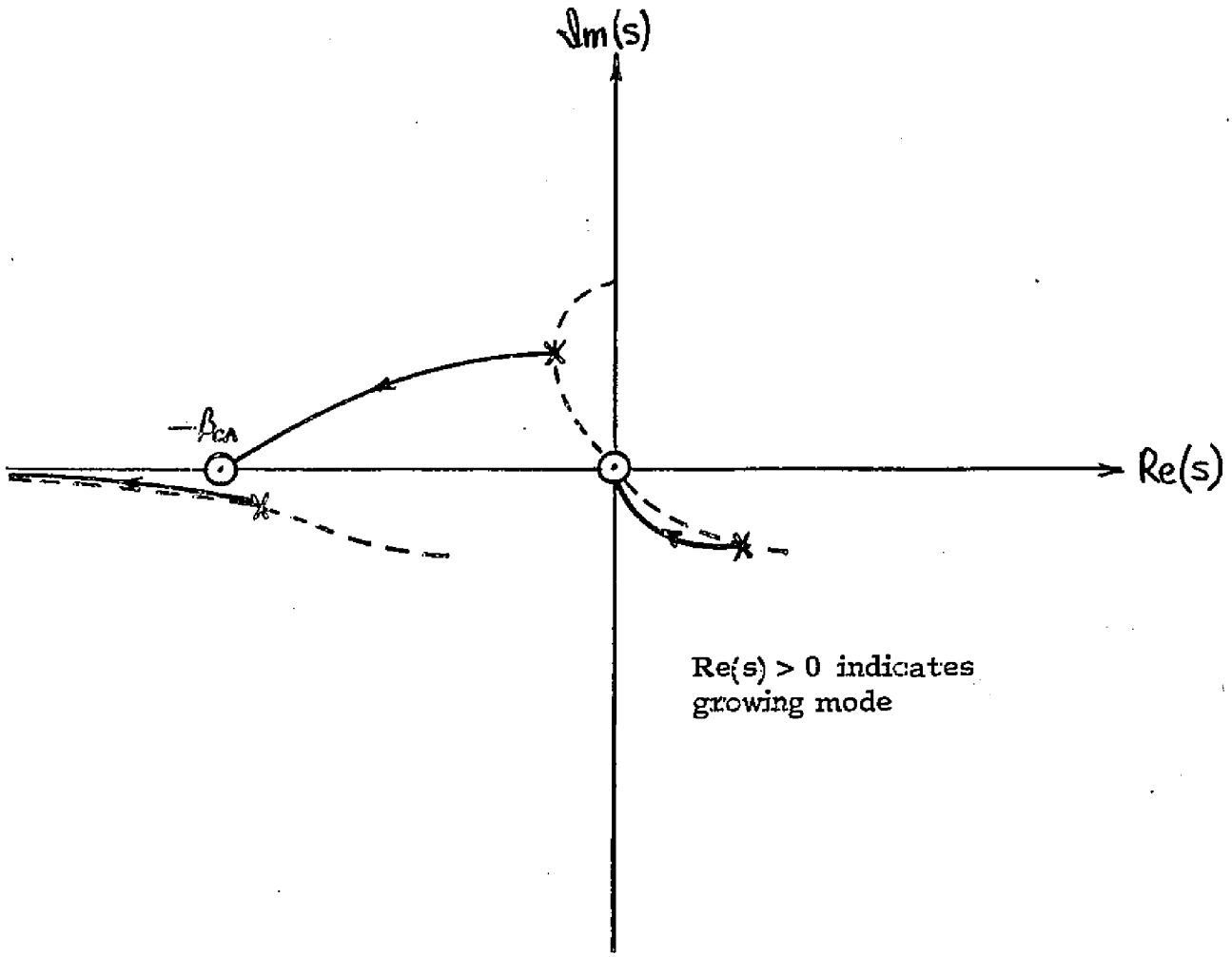

Figure 2.3 Root locus of synchronous dominant carrier dispersion equation

Points of origin are indicated by X, as determined by the collision wave number, β_{CA}. Points of convergence are indicated by 0. The dashed curve is the root locus for the case $\alpha_o = 0$. Arrows indicate increasing gain constant α_o. This locus is calculated for the case when collision loss and cold circuit attenuation are present.

$$1 + \frac{\alpha_o S(S + \beta_{CA})}{S^3 + \beta_{CA} S^2 + j} = 0$$

$$1 + \frac{\beta_{QA}^2(1+\lambda_{DA}^2\beta_{eA}^2)S}{S^3+j} = 0. \qquad (2\text{-}59)$$

The complete root locus is shown in Figure 2.4. It is noted that there is always one pure imaginary solution corresponding to an unattenuated mode. The growth rate of the root in the fourth quadrant decreases with increasing plasma wave number and Debye wavelength although as previously explained the latter effect is minor.

When all loss mechanisms are present, the dispersion equation (2-56) reduces to

$$S^3+S^2(\beta_{CA}+\alpha_0)+S\left[\beta_{CA}\alpha_0+\beta_{QA}^2(1+\lambda_{DA}^2\beta_{eA}^2)\right]+\alpha_0\beta_{QA}^2(1+\lambda_{DA}^2\beta_{eA}^2)+j=0, \qquad (2\text{-}60)$$

the effects of recombination being considered negligible. Rewriting (2-60) in root locus form

$$1 + \frac{\beta_{QA}^2(1+\lambda_{DA}^2\beta_{eA}^2)(S+\alpha_0)}{S^3+S^2(\beta_{CA}+\alpha_0)+S(\beta_{CA}\alpha_0)+j} = 0, \qquad (2\text{-}60a)$$

where the denominator, determing the points of origin of the loci, corresponds to equation (2-58) that has already been studied. The points of convergence are one zero at $S = -\alpha_0$, one zero at the origin and one zero at infinity.

The complete root locus is shown in Figure 2.5. As the plasma wave number increases a value is reached such that all three roots have negative real part. There exists, therefore, a maximum value for β_{qA}^2, β_{qAM}^2, such

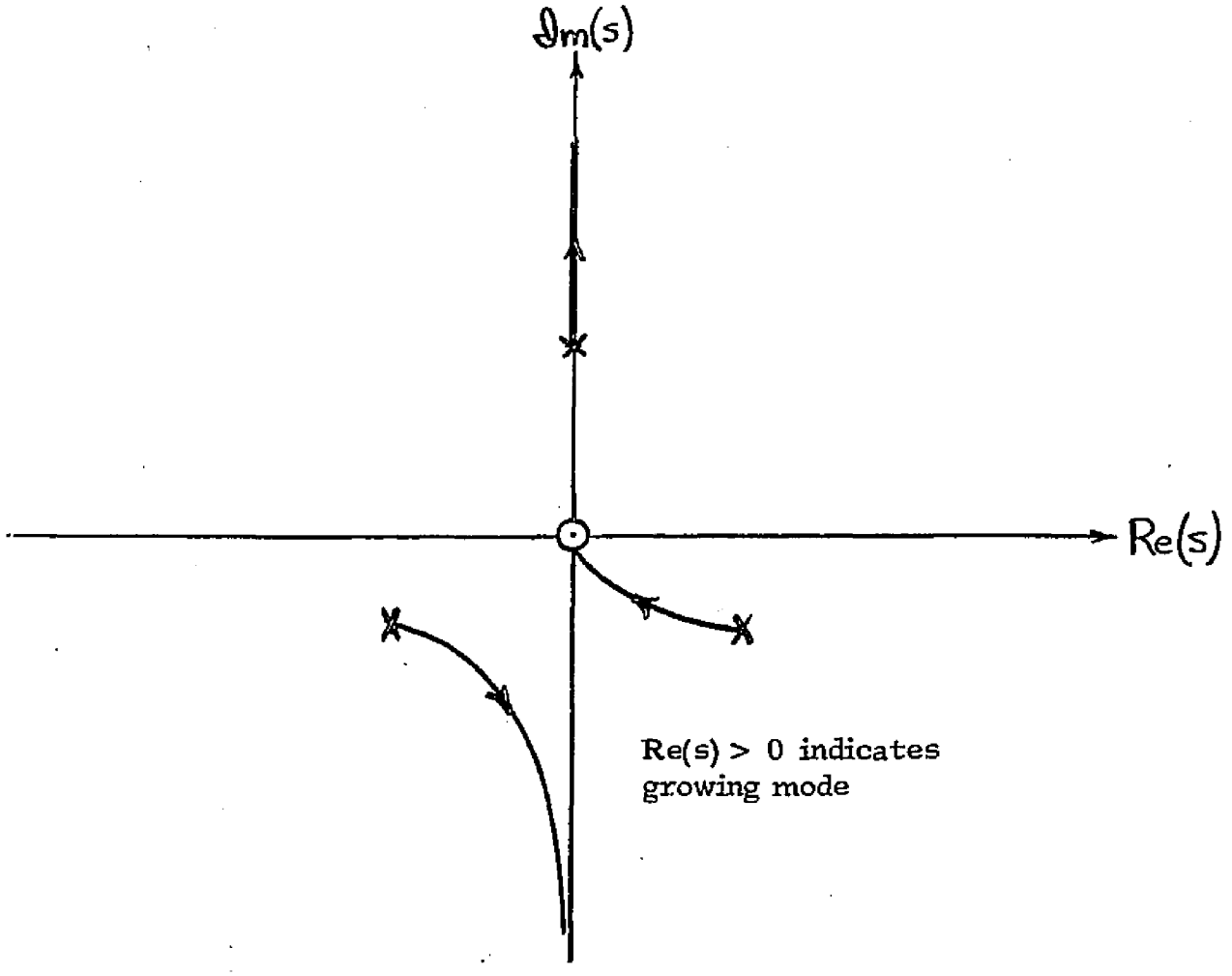

Figure 2.4 Root locus of synchronous dominant carrier dispersion equation, $\beta_q \neq 0$

Arrows indicate increasing reduced plasma wave number β_{qA}. Loss mechanisms considered are diffusion and space charge.

$$1 + \frac{\beta_{qA}^2 (1 + \lambda_{DA}^2 \beta_{eA}^2) S}{S^3 + j} = 0$$

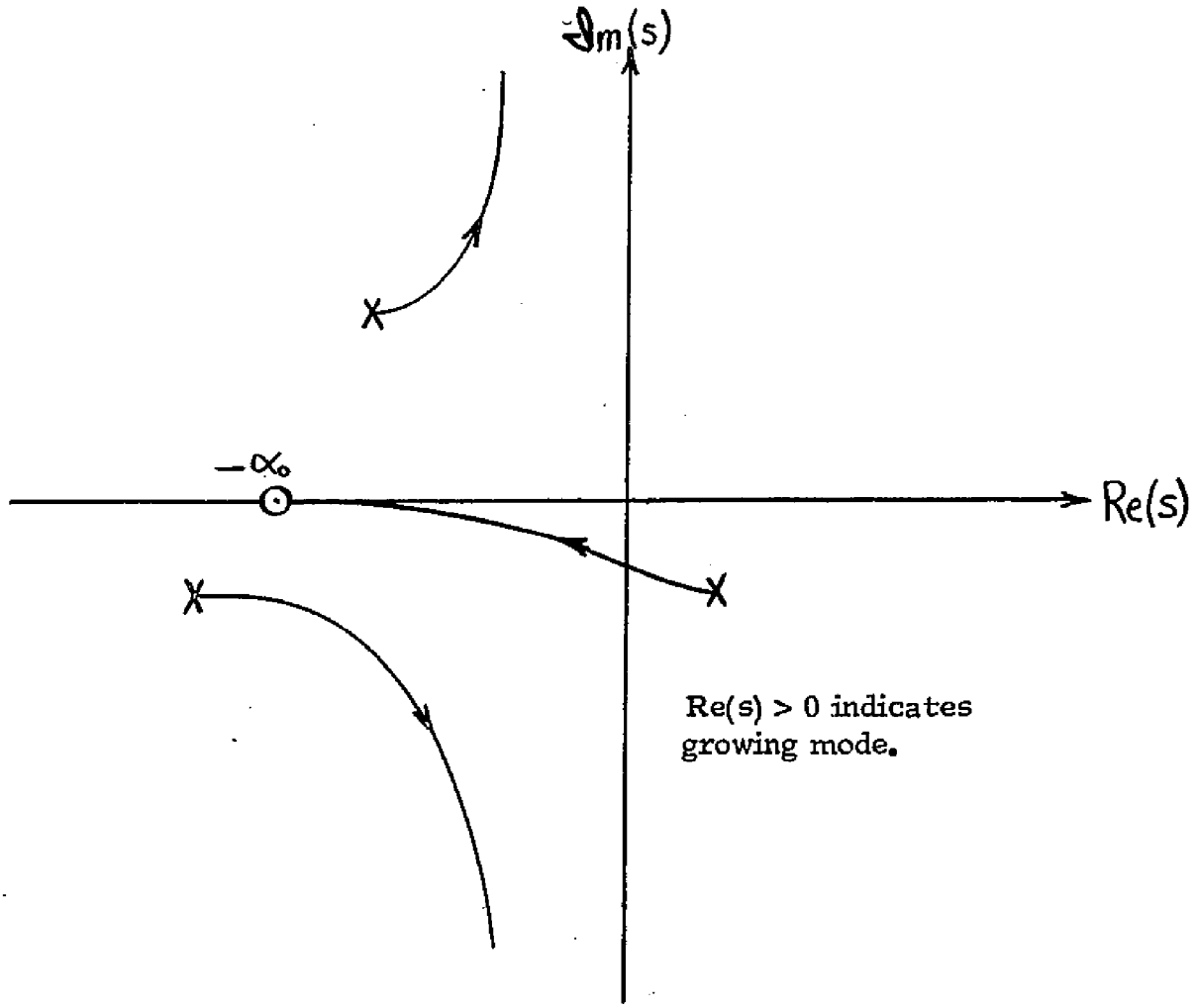

Figure 2.5 Root locus of synchronous dominant carrier dispersion equation
(all loss mechanisms)

Arrows indicate increasing reduced plasma wave number β_{qA}. Locus indicates that there exists a maximum value of β_{qA} such that a growing wave exists. Loss mechanisms considered are collision, cold circuit attenuation, diffusion, and space charge.

$$1 + \frac{\beta_{qA}^2 (1 + \lambda_{DA}^2 \beta_{eA}^2)(S + \alpha_o)}{S^3 + S^2(\beta_{CA} + \alpha_o) + S(\beta_{CA}\alpha_o) + j} = 0 \quad .$$

that a convective instability exists for finite β_{CA} and α_o. Substitution of $S = jS_o$ in (2-60) results in the simultaneous equations

$$S_o^3 - S_o\left[\beta_{QAM}^2(1+\lambda_{DA}^2\beta_{eA}^2) + \beta_{CA}\alpha_o\right] - 1 = 0, \qquad (2\text{-}61)$$

and

$$S_o^2(\beta_{CA}+\alpha_o) - \alpha_o\beta_{QAM}^2(1+\lambda_{DA}^2\beta_{eA}^2) = 0, \qquad (2\text{-}62)$$

for imaginary and real parts respectively. The imaginary axis crossing occurs at

$$S = -j\left[\frac{\alpha_o\beta_{QAM}^2(1+\lambda_{DA}^2\beta_{eA}^2)}{(\beta_{CA}+\alpha_o)}\right]^{1/2} \qquad (2\text{-}63)$$

Substitution of (2-63) in (2-61) results in a cubic equation for β_{QAM} as a function of ($\beta_{CA}, \alpha_o, \lambda_{DA}, \beta_{eA}$). Although a method for solving the cubic exists[29] a formula for the solution as a function of the coefficients does not. Another technique will be used to solve for the maximum allowable carrier density for net growth to exist.

2.8 The Effects of Carrier Recombination on the Perturbed Solution of the Dominant Carrier Dispersion Equation at Synchronism.

When the only mechanism present is carrier recombination, equation (2-56) reduces to

$$1 + \frac{\beta_{RA}S^2}{S^3 + j} = 0, \qquad (2\text{-}64)$$

although Pierce's coupling coefficient, C, as defined by equation (2-54), is no

longer pure real. It is noted that equation (2-64) has the same form as equation (2-57), the case when only collision loss is present. It differs from that case in that the "gain constant" $\beta_{RA}/\beta_e C$ is no longer pure real. The root locus, however, has the same points of origin and convergence. The effect of decreasing the recombination lifetime, i.e. increasing the recombination wave number β_{RA}, is to decrease the growth rate as shown in Figure 2.2.

2.9 Reflected Circuit Wave Perturbational Solution of the Dominant Carrier Dispersion Equation

The system's quartic dispusion equation was found in Section 2.4. Three forward traveling wave solutions were found as perturbations of the forward traveling circuit wave. The fourth solution is found as a perturbation of the circuit wave traveling in the direction opposite to the drifting carriers. This wave is called the reflected circuit wave and is excited by improper termination of the slow wave circuit at the output. Therefore, let

$$\gamma = -j\beta_e - \delta . \tag{2-65}$$

The circuit admittance is approximated as

$$\left.\frac{J_1 A}{E_1}\right|_{CKT} = \frac{-2(\delta - \alpha_o - j h_A)}{\beta_{eA}^2 Z_{rt}} , \tag{2-66}$$

also contingent upon the conditions $|\beta_{eA}| >> |\alpha_o|$, $|\beta_{eA}| >> |\delta|$, and $|\beta_{eA}| >> |h_A|$. The perturbed dispersion equation becomes

$$S = \alpha_o + j h_A + \left[\frac{2}{C}\left(\frac{2}{C} - j\beta_{CA}\right) - j\beta_{QA}^2\left(1 + \lambda_{DA}^2\beta_{eA}^2\right)\right]^{-1} , \tag{2-67}$$

the effects of recombination being considered negligible. The $Re(s) > 0$ is expected since the wave attenuates as it travels in the negative z direction.

2.10 Conclusions

For most semiconductors, with the exception of high resistivity germanium, the effect of the minority carrier may be neglected resulting in the dominant carrier dispersion equation. The solutions to this equation are two circuit and two carrier waves, a situation directly analogous to the vacuum traveling wave tube. A theorem was proved revealing the existence of a convective instability (gaining carrier wave) in the presence of collision damping and cold circuit attenuation for high resistivity semiconductor although the growth rate becomes vanishingly small. Root locus techniques were found to be useful to reveal the existence of a maximum carrier density for which a convective instability exists at synchronism. The effects peculiar to the semiconductor decrease the growth rate and require device operation at very low drift velocity, i.e. velocities three orders of magnitude less than the intrinsic velocity of semiconductor thus necessitating the development of a slow wave circuit with a slowing factor of approximately one thousand.

CHAPTER 3 - THE STUB - LOADED MEANDER LINE SLOW WAVE CIRCUIT

The purpose of this chapter is to characterize a slow wave circuit suitable for use in studying the interaction by evaluating two of the circuit's parameters; namely, γ_o, the cold circuit propagation constant, and Z_n, the interaction impedance of the n^{th} space harmonic as defined by equation (2-40).

Planar slow wave circuits are particularly well suited for devices utilizing the studied interaction. Very large slowing factors are required because the maximum attainable non-saturated carrier drift velocity is several orders of magnitude less than the intrinsic phase velocity of semiconductors. Fabrication by evaporation deposition and/or photolithographic etching facilitates the construction of circuits with the necessary dimensions. Additionally, by selecting a high thermal conductivity substrate, the circuit is able to dissipate large amounts of power before physically deforming.

3.1 Description of the Slow Wave Circuit

The structure investigated is the stub-loaded meander line as shown in Figure 3.1. The circuit's aspect ratio is defined as the ratio of the interline shorting link to center line distance, a, to the half width, b, i.e.

$$\text{aspect ratio} \triangleq \frac{a}{b}. \qquad (3\text{-}1)$$

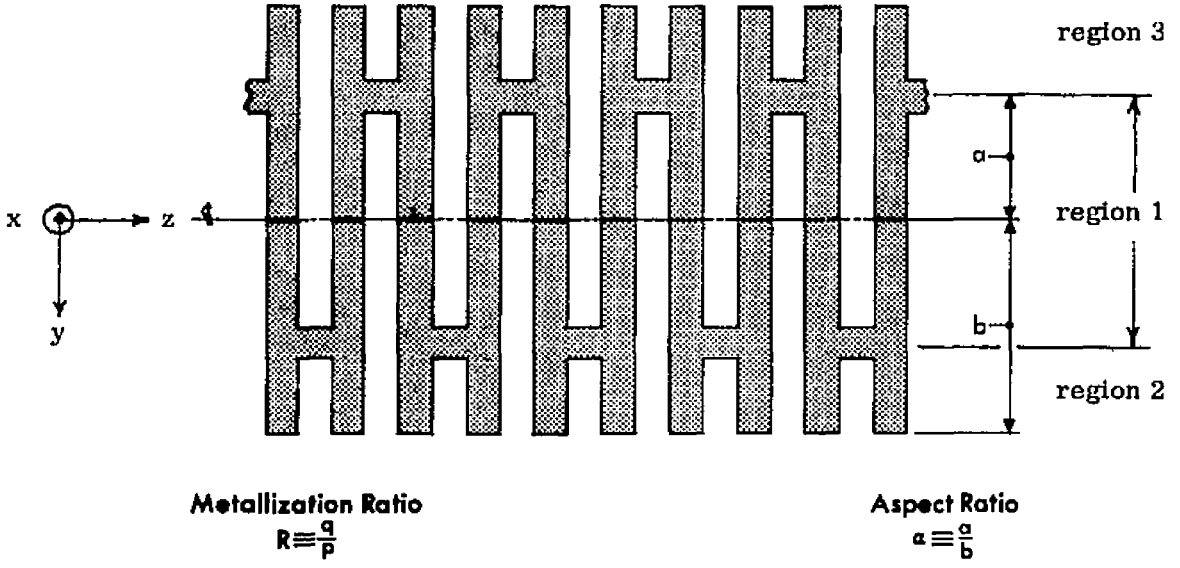

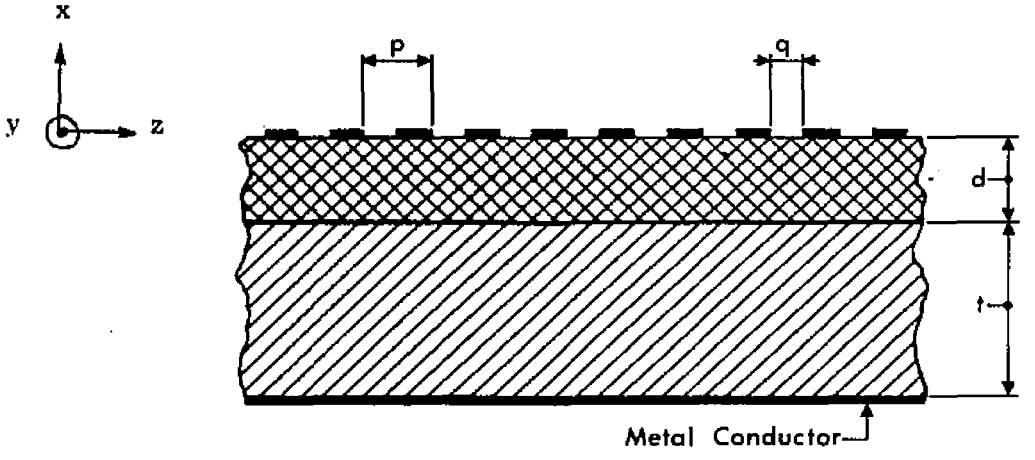

Figure 3.1 Stub Loaded Meander Line.

The metallization ratio is defined as the ratio of the interline distance, q, to the half period, p, i.e.

$$\text{metallization ratio} \triangleq \frac{q}{p} . \qquad (3\text{-}2)$$

The thickness of the conducting tape is taken as nominally zero. The passivation layer, or in the case of some devices the printed circuit board, is of thickness d. A dielectric plate of thickness t is used to obtain additional slowing.

The circuit may be thought of as a transmission line in the transverse direction and a periodic structure in the longitudinal direction. As such, the approximate slowing factor is 2a/p.

3.2 Fletcher's Method of Analysis

While an exact electromagnetic analysis of the circuit is desirable it is not achievable because an infinite number of modes are required to satisfy the boundary conditions exactly. The circuit is analyzed using an approximate method introduced by Fletcher [30] and later corrected and extended by Walling [31]. The boundary conditions are expressed in terms of transmission line voltages and currents that are calculated from the lowest order electromagnetic fields. To solve the field problem each field component is approximated by a sum of space harmonics that propagate as TEM waves in the plane of the line; i.e. it is assumed that the majority of the stored energy is in the TEM components of the total field.

If the entire slow wave circuit is filled with a single homogeneous material the boundary conditions are satisfied exactly by a TEM_y mode, (except at the interline shorting link which is far from the active area of the semiconductor) where the subscript y denotes a transverse direction. In the case at hand, in which there are several different media, a unique effective intrinsic phase velocity is derived by extending the work of Chen [32] and Haddad [33] on traveling wave maser structures. The approximate solutions found represent only the lowest order TEM mode that may be excited in the circuit; i.e. higher order mode amplitudes are considered negligible although required to precisely satisfy the boundary conditions.

The longitudinal power transfer is calculated by multiplying the stored energy per unit length by the energy velocity. It has been shown [34] that the energy velocity in a periodic circuit equals the group velocity. It is noted that this is the only method of calculating the longitudinal power transfer because the exact field components are not known. Since the nature of the approximation is to set $E_y = H_y = 0$, calculation of longitudinal power transfer by the average Poynting vector method would lead to the incorrect result.

3.3 Dispersion Equation of the Stub-Loaded Meander Line

The voltage in the i^{th} region of the m^{th} transmission line is written as

$$V_{im}(x_\ell, y, z, t) = \sum_{n=0}^{N} F_{imn}(x_\ell, y) \exp\left[j(\omega t - \beta_n z)\right] \tag{3-3}$$

where x_ℓ is the position of the tape, and β_n is the phase shift per unit length of the n^{th} space harmonic, given by

$$\beta_n = \beta_o + \frac{2n\pi}{P} = \beta_o + \frac{n\pi}{p} . \tag{3-4}$$

The phase shift between one line and its neighbor, θ_n, is given by

$$\theta_n = \beta_n p = \theta_o + n\pi , \tag{3-5}$$

where θ_o is real and $0 \leq \theta_o \leq \pi$.

For biperiodic circuits (circuits with two bars per period; i.e. $P = 2p$) only two space harmonics are distinguishable at the tapes as shown in Figure 3.2. Since the boundary conditions are expressed only for the tape position the summation in (3-3) may be terminated at n = 1. It should be emphasized that this restriction to only two voltage space harmonics in the derivation of the dispersion equation does not prevent one from subsequently deriving the amplitudes of the electromagnetic field space harmonics, using the dispersion equation so found, in conjunction with an approximate field theory.

Equation (3-3) may be rewritten to reveal the assumed TEM_y mode in the three regions of the structure

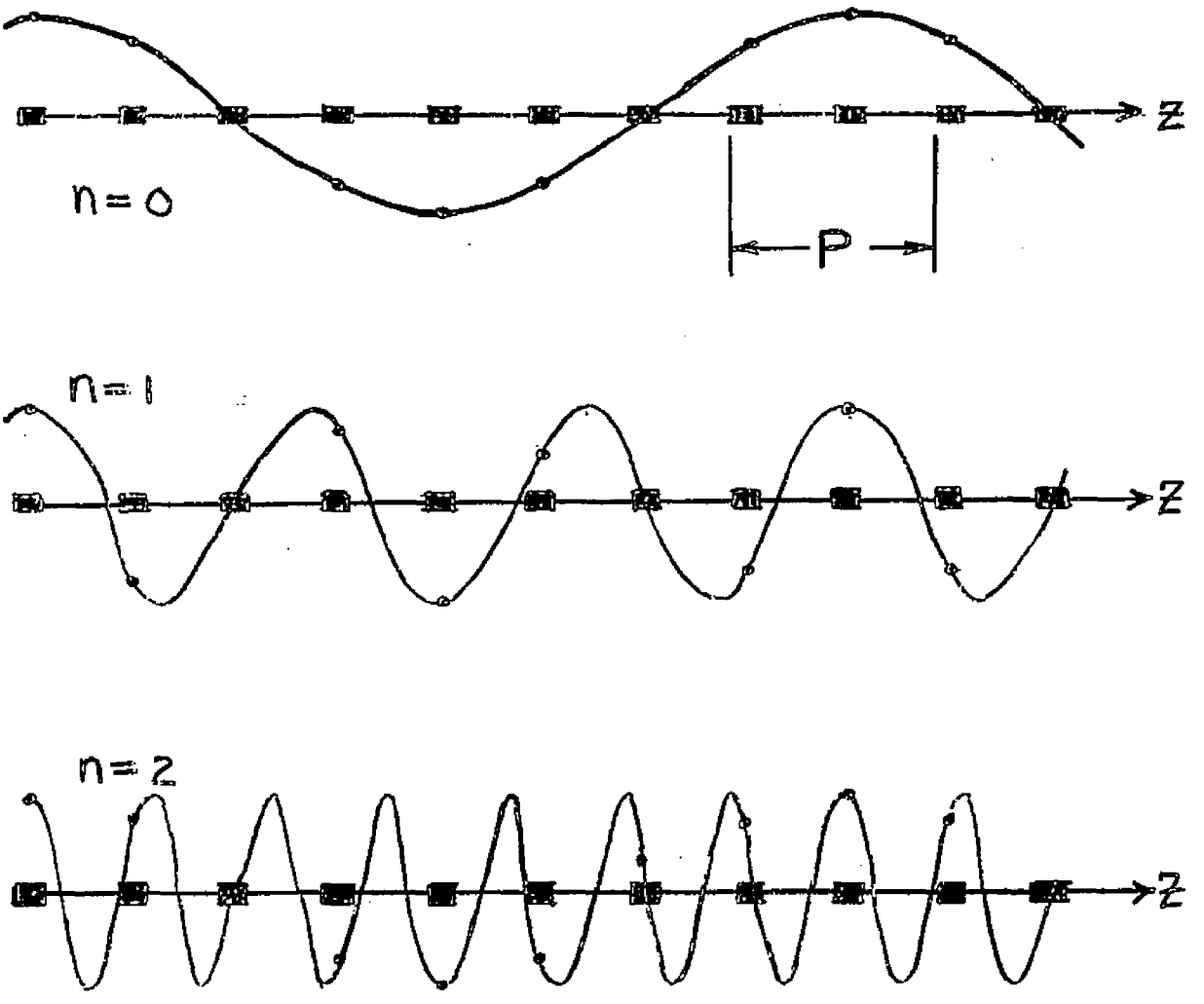

Figure 3.2 Space Harmonic Relationships in a Biperiodic Circuit

Consider $\cos \beta_n z = \cos(\beta_0 + \frac{2n\pi}{P}) z$. Evaluating at $z = \frac{mP}{M}$ where M is the number of bars per period and m is the index of a particular bar results in

$$\cos \beta_n z = \cos \left[\frac{\beta_0 m P}{M} + 2n\pi \left(\frac{m}{M} \right) \right] ,$$

which for M = 2 may take on only two independent values for a given bar for all n .

$$V_{\substack{1m\\2m\\3m}} = \left(A_{\substack{1\\5\\9}} \cos\varphi + A_{\substack{2\\6\\10}} \sin\varphi\right) e^{-jm\theta_o} + \left(A_{\substack{3\\7\\11}} \sin\varphi + A_{\substack{4\\8\\12}} \cos\varphi\right) e^{-jm(\theta_o+\pi)} , \qquad (3\text{-}6)$$

where $\varphi = 2\pi y/\lambda_{eff}$. The current in the m^{th} line is found from the transmission line equation,

$$I_{im} = j Y_i(\theta) \frac{\partial V_{im}}{\partial \varphi} , \qquad (3\text{-}7)$$

where $Y_i(\theta)$ is Fletcher's Admittance Function defined as

$$Y_i(\theta) \triangleq \frac{I_{im}}{V_{im}} , \qquad (3\text{-}8)$$

evaluated for a wave traveling in the +y direction. Hence,

$$I_{\substack{1m\\2m\\3m}} = j Y_{\substack{1\\2\\3}}(\theta_o)\left(A_{\substack{2\\6\\10}} \cos\varphi - A_{\substack{1\\5\\9}} \sin\varphi\right) e^{-jm\theta_o} + j Y_{\substack{1\\2\\3}}(\theta+\pi)\left(A_{\substack{3\\7\\11}} \cos\varphi - A_{\substack{4\\8\\12}} \sin\varphi\right) e^{-jm(\theta_o+\pi)} . \qquad (3\text{-}9)$$

The circuit boundary conditions are enumerated in table 3.1.

Imposing the condition that a non-trivial solution exists (derivation in Appendix 2) results in the determinantal equation,

$$\tan(ka)\tan(kb)\,X(\theta_o) - \tan^2\left(\frac{\theta_o}{2}\right) = 0 , \qquad (3\text{-}10)$$

where $k \triangleq 2\pi/\lambda_{eff}$ and $X(\theta_o) \triangleq Y(\theta_o)/Y(\theta_o+\pi)$. $X(\theta_o)$, the ratio of two real admittances, is positive real. When the aspect

Position	Voltage	Current
$y=+a$	$V_1(m+1)=V_2(m+1)$	$I_1(m+1)-I_2(m+1)$
	$V_1(m)=V_2(m)$	$+I_1(m+2)-I_2(m+2)$
	$V_1(m+1)=V_1(m+2)$	$=0$
$y=-a$	$V_1(m+1)=V_3(m+1)$	$I_1(m)-I_3(m)$
	$V_1(m)=V_3(m)$	$+I_1(m+1)-I_3(m+1)$
	$V_1(m)=V_1(m+1)$	$=0$
$y=+b$		$I_2(m)=0$
		$I_2(m+1)=0$
$y=-b$		$I_3(m)=0$
		$I_3(m+1)=0$

Table 3.1 Stub-Loaded Meander Line Boundary Conditions

ratio is one ($a = b$) there exists a solution θ_o for all k; i.e. the circuit is all pass. For this case, the meander line without stub loading, $\tan(ka)\tan(kb) = \tan^2(ka) \geq 0$; precisely the condition for a solution to exist.

When the meander line is stub-loaded ($a < b$) the circuit is bandpass. The cutoff regions are determined by $\tan(ka)\tan(kb) < 0$. The cutoff frequencies are therefore

$$f_{ca} = \frac{v_{eff}}{4a}, \qquad (3\text{-}11a)$$

and

$$f_{cb} = \frac{v_{eff}}{4b}, \qquad (3\text{-}11b)$$

where the subscripts a and b denote sign changes in the respective tangents.

The dispersion characteristics of a periodic circuit are not completely represented by the most elementary solution to the dispersion equation [35]. Since the circuit is symmetric about any plane, $z = (m+\frac{1}{2})p$, there must correspond to each solution θ_o, the possibility of a reflected wave $-\theta_o$. Additionally, the space harmonics of this reflected wave exist as $\theta_n = -\theta_o + n\pi$.

To calculate the complete dispersion characteristics the Fletcher Admittance Function, $\chi(\theta_o)$, must be evaluated. Before doing this, however, several conclusions are summarized. First, the meander line, with and without stub loading, can support both forward and backward

waves. Second, the line without stub loading has the largest bandwidth and highest slowing factor. It has been noted by several authors [36, 37] that one may increase the interaction impedance of a slow wave circuit by sacrificing slowing factor. This is indeed the case as will be shown in section 3.8c.

3.4 Fletcher's Admittance Function

Fletcher's Admittance Function is evaluated for two different experimental configurations. The first of these is the "cold test" experiment open-type slow wave circuit shown in Figure 3.3. The circuit is open such that it may be probed to reveal the field configuration. The second is the "hot test" experiment closed-type slow wave circuit shown in Figure 3.4. This circuit is covered and closed to achieve additional slowing through dielectric loading. In both of the above it is assumed that the circuit is uniform in the y direction, except at the shorting link; therefore the Fletcher's Admittance Functions of the three regions are equal, i.e. $Y_1(\theta_o) = Y_2(\theta_o) = Y_3(\theta_o) = Y(\theta_o)$.

Fletcher's Admittance Function if found by calculating the current flowing on the m^{th} tape, I_m, when a voltage exists of the form,

$$V_m = A_o e^{-j\varphi} e^{-jm\theta_o}. \qquad (3\text{-}12)$$

Assuming that the electric field is uniform between the tapes yields

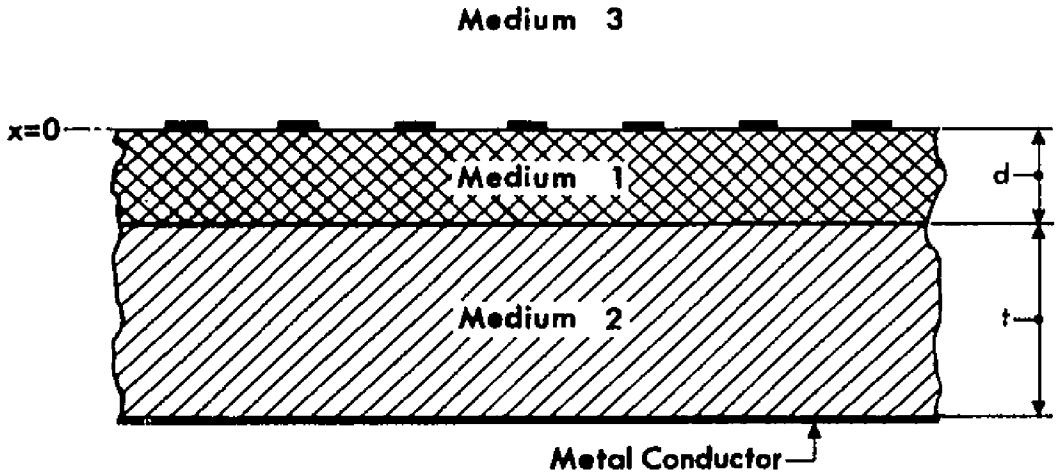

Figure 3.3 Open Type Slow Wave Circuit Cross Section.

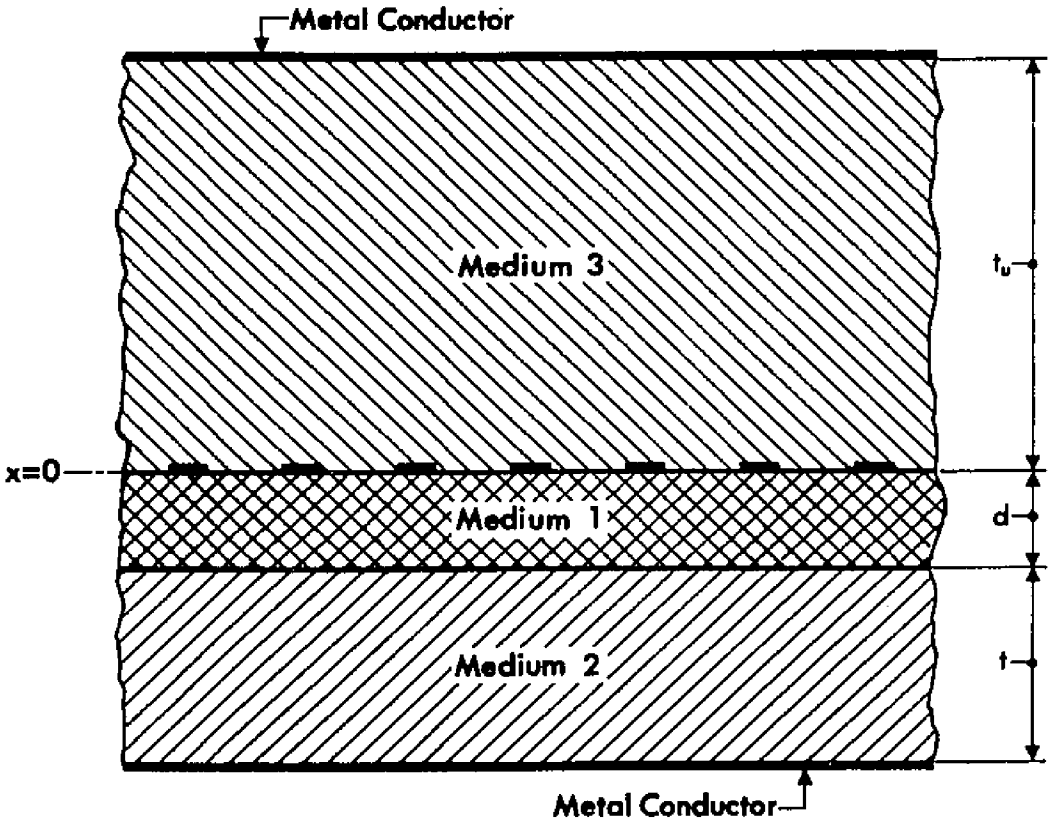

Figure 3.4 Closed Type Slow Wave Circuit Cross Section.

$$E_z\Big|_{x=0} = -\frac{(V_{m+1}-V_m)}{q} = E_o e^{-j(m+\frac{1}{2})\theta_o} e^{-j\varphi} \; , \qquad (3\text{-}13)$$

where $E_o = 2jA_o \sin(\frac{\theta_o}{2})/q$. It is necessary at this point to proceed with the development of $Y(\theta_o)$ for each case independently.

3.4a Fletcher's Admittance Function of an Open-Type Planar Slow Wave Circuit

The electric fields in the three different media are written as

$$E_{z1} = \sum_{n=-\infty}^{\infty} \left[F_{n1o} \frac{\sinh k_{x1}(d+x)}{\sinh k_{x1} d} + F_{n1e} \frac{\cosh k_{x1}(d+x)}{\cosh k_{x1} d} \right] e^{-j\varphi} e^{-j\beta_n z} \; , \qquad (3\text{-}14a)$$

$$E_{z2} = \sum_{n=-\infty}^{\infty} F_{n2} \frac{\sinh k_{x2}(d+t+x)}{\sinh k_{x2}(d+t)} e^{-j\varphi} e^{-j\beta_n z} \; , \qquad (3\text{-}14b)$$

$$E_{z3} = \sum_{n=-\infty}^{\infty} F_{n3} e^{-|k_{x3}| x} e^{-j\varphi} e^{-j\beta_n z} \; , \qquad (3\text{-}14c)$$

where the absolute value of k_{x3} is chosen in (3-14c) to insure that all space harmonics decay away from the circuit and

$$k_{\substack{x1 \\ x2 \\ x3}}^2 - \left[\left(\frac{2\pi}{\lambda_{eff}}\right)^2 + \beta_n^2 \right] + k_{\substack{o1 \\ o2 \\ o3}}^2 = 0 \; . \qquad (3\text{-}15)$$

The F_{n1o}, F_{n1e}, F_{n2}, and F_{n3} are the various mode coefficients. The numbered subscripts refer to the different media as illustrated in

Figure 3.3. Solutions have been selected to satisfy the boundary conditions for E_z at $x = -(d + t)$ and $x \to \infty$.

The mode coefficients are evaluated by imposing suitable boundary conditions at each interface. Equating $E_{z1}(x=0)$, $E_{z3}(x=0)$, and $E_z\big|_{x=0}$ yields

$$\sum_{n=-\infty}^{\infty} (F_{n1o} + F_{n1e}) e^{-j\varphi} e^{-j\beta_{nz}} = \sum_{n=-\infty}^{\infty} F_{n3}\, e^{-j\varphi} e^{-j\beta_{nz}} \qquad (3\text{-}16)$$

$$= \begin{cases} E_o\, e^{-j(m+\frac{1}{2})\theta_o} e^{-j\varphi}, & \text{for } (m+\tfrac{1}{2})p - \tfrac{q}{2} < z < (m+\tfrac{1}{2})p + \tfrac{q}{2}, \\ 0, & \text{otherwise.} \end{cases}$$

Multiplying by $e^{+j\beta_{nz}}$ and integrating over the orthogonality interval $z = mp$ to $z = (m + 1)p$ results in

$$(F_{n1o} + F_{n1e})p = F_{n3}p = \int_{(m+\frac{1}{2})p - \frac{q}{2}}^{(m+\frac{1}{2})p + \frac{q}{2}} E_o\, e^{-j(m+\frac{1}{2})\theta_o} e^{+j\beta_{nz}}\, dz. \qquad (3\text{-}17)$$

Evaluating the integral yields

$$F_{n3} = E_o R_{met}\, Sa\left(\frac{\theta_n R_{met}}{2}\right) e^{+j(m+\frac{1}{2})(\theta_n - \theta_o)}, \qquad (3\text{-}18)$$

where R_{met} is the metallization ratio q/p and $Sa(x) = \sin x/x$ the sampling function. Inspection of the exponential reveals that since

both m and n are integers

$$\exp\left[j\left(m+\tfrac{1}{2}\right)\left(\theta_n-\theta_o\right)\right]=\exp\left[j\left(m+\tfrac{1}{2}\right)2n\pi\right]=\left(-1\right)^n, \qquad (3\text{-}19)$$

where use has been made of the relationship $\theta_n = \theta_o + 2n\pi$.

It is noted that the relationship is different than equation (3-5) because in evaluating the Fletcher's Admittance Function of a typical cross section the period P equals the interline spacing p. Therefore $\beta_n = \beta_o + \frac{2n\pi}{P} = \beta_o + \frac{2n\pi}{p}$. Substitution of (3-19) in (3-18) yields.

$$F_{n3} = \left(-1\right)^n E_o R_{MET} Sa\left(\frac{\theta_n R_{MET}}{2}\right) . \qquad (3\text{-}20)$$

The transverse electric fields are found by imposing the TEM_y condition, $H_y = 0$, namely

$$\frac{\partial E_3}{\partial x} - \frac{\partial E_x}{\partial 3} = 0 , \qquad (3\text{-}21)$$

resulting in

$$E_{x1} = j\sum_{n=-\infty}^{\infty}\left(\frac{k_{x1}}{\beta_n}\right)\left[F_{n1o}\frac{\cosh k_{x1}(d+x)}{\sinh k_{x1}d} + F_{n1e}\frac{\sinh k_{x1}(d+x)}{\cosh k_{x1}d}\right]e^{-j\varphi}e^{-j\beta_n 3}, \qquad (3\text{-}22a)$$

$$E_{x2} = j \sum_{n=-\infty}^{\infty} \left(\frac{k_{x2}}{\beta_n}\right) F_{n2} \frac{\cosh k_{x2}(d+t+x)}{\sinh k_{x2}(d+t)} e^{-j\varphi} e^{-j\beta_n z}, \qquad (3\text{-}22b)$$

$$E_{x3} = j \sum_{n=-\infty}^{\infty} \left(\frac{|k_{x3}|}{\beta_n}\right) F_{n3} e^{-|k_{x3}|x} e^{-j\varphi} e^{-j\beta_n z}. \qquad (3\text{-}22c)$$

The longitudinal magnetic fields are found by dividing E_x by the intrinsic impedance of each medium; i.e. $H_{zi} = \frac{-E_{xi}}{\eta_i}$ for i = 1,2,3, yielding

$$H_{z1} = \frac{-j}{\eta_1} \sum_{n=-\infty}^{\infty} \left(\frac{k_{x1}}{\beta_n}\right) \left[F_{n1o} \frac{\cosh k_{x1}(d+x)}{\sinh k_{x1} d} + F_{n1e} \frac{\sinh k_{x1}(d+x)}{\cosh k_{x1} d}\right] e^{-j\varphi} e^{-j\beta_n z}, \qquad (3\text{-}23a)$$

$$H_{z2} = \frac{-j}{\eta_2} \sum_{n=-\infty}^{\infty} \left(\frac{k_{x2}}{\beta_n}\right) F_{n2} \frac{\cosh k_{x2}(d+t+x)}{\sinh k_{x2}(d+t)} e^{-j\varphi} e^{-j\beta_n z}, \qquad (3\text{-}23b)$$

$$H_{z3} = \frac{-j}{\eta_3} \sum_{n=-\infty}^{\infty} \left(\frac{|k_{x3}|}{\beta_n}\right) F_{n3} e^{-|k_{x3}|x} e^{-j\varphi} e^{-j\beta_n z}. \qquad (3\text{-}23c)$$

Matching E_z at $x = -d$ results in

$$F_{n1e} = F_{n2} \sinh k_{x2} t \cosh k_{x1} d \,/\, \sinh k_{x2}(d+t) . \qquad (3\text{-}24)$$

Matching H_z at $x = -d$ results in

$$F_{n1o} = F_{n2}\left(\frac{\eta_1 k_{x2}}{\eta_2 k_{x1}}\right) \cosh k_{x2} t \sinh k_{x1} d \,/\, \sinh k_{x2}(d+t) . \qquad (3\text{-}25)$$

Simultaneously solving (3-17, 3-24, 3-25) yields

$$F_{n2} = F_{n3} \sinh k_{x2}(d+t)\left[\sinh k_{x2} t \cosh k_{x1} d + \left(\frac{\eta_1 k_{x2}}{\eta_2 k_{x1}}\right) \cosh k_{x2} t \sinh k_{x1} d\right]^{-1} , \qquad (3\text{-}26)$$

$$F_{n1e} = F_{n3}\left[1 + \left(\frac{\eta_1 k_{x2}}{\eta_2 k_{x1}}\right) \frac{\tanh k_{x1} d}{\tanh k_{x2} t}\right]^{-1} , \qquad (3\text{-}27)$$

$$F_{n1o} = F_{n3}\left[1 + \left(\frac{\eta_2 k_{x1}}{\eta_1 k_{x2}}\right) \frac{\tanh k_{x2} t}{\tanh k_{x1} d}\right]^{-1} . \qquad (3\text{-}28)$$

The current flowing in the m^{th} tape in the +y direction is

$$I_m = \int_{mp-\left(\frac{p-q}{2}\right)}^{mp+\left(\frac{p-q}{2}\right)} \left(H_{z1} - H_{z3}\right)\Big|_{x=0} dz . \qquad (3\text{-}29)$$

Evaluating the magnetic fields at the tape and substituting in

(3-29) results in

$$I_m = -je^{-j\varphi}\sum_{n=-\infty}^{\infty}\left[\frac{F_{n3}|k_{x3}|}{\eta_3\beta_n}+\left(\frac{k_{x1}}{\eta_1\beta_n}\right)\left(F_{n1o}\coth k_{x1}d+F_{n1e}\tanh k_{x1}d\right)\right]\int_{mp-\left(\frac{p-q}{2}\right)}^{mp+\left(\frac{p-q}{2}\right)} e^{-j\beta_n z}\,dz \quad (3\text{-}30)$$

Performing the integration,

$$\int_{mp-\left(\frac{p-q}{2}\right)}^{mp+\left(\frac{p-q}{2}\right)} e^{-j\beta_n z}\,dz = 2e^{-jm\theta_o}\,\frac{\sin\left[\theta_n(1-R_{MET})/2\right]}{\beta_n} \quad (3\text{-}31)$$

results in

$$I_m = -2je^{-j\varphi}e^{-jm\theta_o}\sum_{n=-\infty}^{\infty}\frac{\sin\left[\theta_n(1-R_{MET})/2\right]}{\beta_n} \quad (3\text{-}32)$$

$$\cdot\left[\frac{F_{n3}|k_{x3}|}{\eta_3\beta_n}+\left(\frac{k_{x1}}{\eta_1\beta_n}\right)\left(F_{n1o}\coth k_{x1}d+F_{n1e}\tanh k_{x1}d\right)\right]$$

As previously defined $Y(\theta_o) = \dfrac{I_m}{V_m}$ which yields finally

$$Y(\theta_o) = -2\sin\left(\frac{\theta_o}{2}\right)\sum_{n=-\infty}^{\infty}(-1)^n(1-R_{MET})\,Sa\left(\frac{\theta_n R_{MET}}{2}\right)Sa\left(\frac{\theta_n(1-R_{MET})}{2}\right) \quad (3\text{-}33)$$

$$\cdot\left[\frac{|k_{x3}|}{\eta_3\beta_n}+\frac{k_{x1}}{\eta_1\beta_n}\left(\frac{1+\left(\frac{\eta_2 k_{x1}}{\eta_1 k_{x2}}\right)\tanh k_{x1}d\,\tanh k_{x2}t}{\tanh k_{x1}d+\left(\frac{\eta_2 k_{x1}}{\eta_1 k_{x2}}\right)\tanh k_{x2}t}\right)\right]\cdot$$

3.4b Fletcher's Admittance Function of a Closed - Type Planar Slow-Wave Circuit

The development of Fletcher's Admittance Function of a closed-type planar slow wave circuit follows essentially the same method as in the previous section with the addition of boundary conditions to be met at $x = + t_u$. The fields in the third medium are therefore modified to

$$E_{z3} = \sum_{n=-\infty}^{\infty} F_{n3} \frac{\sinh k_{x3}(t_u - x)}{\sinh k_{x3} t_u} e^{-j\varphi} e^{-j\beta_n z}, \tag{3-34a}$$

$$E_{x3} = -j \sum_{n=-\infty}^{\infty} \left(\frac{k_{x3}}{\beta_n}\right) F_{n3} \frac{\cosh k_{x3}(t_u - x)}{\sinh k_{x3} t_u} e^{-j\varphi} e^{-j\beta_n z}, \tag{3-34b}$$

and

$$H_{z3} = \frac{+j}{\eta_3} \sum_{n=-\infty}^{\infty} \left(\frac{k_{x3}}{\beta_n}\right) F_{n3} \frac{\cosh k_{x3}(t_u - x)}{\sinh k_{x3} t_u} e^{-j\varphi} e^{-j\beta_n z}. \tag{3-34c}$$

Evaluating the magnetic field at the tape yields:

$$H_{z3}\Big|_{x=0} = \frac{+j}{\eta_3} \sum_{n=-\infty}^{\infty} \left(\frac{k_{x3}}{\beta_n}\right) F_{n3} \coth k_{x3} t_u \, e^{-j\varphi} e^{-j\beta_n z}, \tag{3-35}$$

which when substituted in equation (3-29) results in

$$Y(\theta_0) = -2 \sin\left(\frac{\theta_0}{2}\right) \sum_{n=-\infty}^{\infty} (-1)^n (1 - R_{MET}) \, Sa\left(\frac{\theta_n R_{MET}}{2}\right) Sa\left(\frac{\theta_n (1 - R_{MET})}{2}\right) \tag{3-36}$$

$$\cdot \left[\frac{k_{x3} \coth k_{x3} t_u}{\eta_3 \beta_n} + \frac{k_{x1}}{\eta_1 \beta_n} \left(\frac{1 + \left(\frac{\eta_2 k_{x1}}{\eta_1 k_{x2}}\right) \tanh k_{x1} d \tanh k_{x2} t}{\tanh k_{x1} d + \left(\frac{\eta_2 k_{x1}}{\eta_1 k_{x2}}\right) \tanh k_{x2} t} \right) \right].$$

As $t_u \to \infty$ equation (3-36) reduces to equation (3-33) for the open type as anticipated. Since cosh x = 1.0000 to four significant figures for $x > 5$ the circuit may be considered as essentially open for $k_{x3} t_u > 5$. To evaluate k_{x3} from equation (3-15) first requires the evaluation of the effective wavelength.

3.5 Effective Intrinsic Phase Velocity of Planar Slow Wave Circuits Fabricated on Stratified Media.

The intrinsic phase velocity of a medium is given by

$$v_{pi} \triangleq \left(\eta_{eff} \epsilon_{eff}\right)^{-1}, \qquad (3\text{-}37)$$

where η_{eff} is the effective intrinsic impedance of the stratified media and ϵ_{eff} is the effective dielectric constant of the stratified media.

Without changing the geometry of the metallic boundaries the stratified media is replaced by one homogenous medium. The effective dielectric constant of this medium is chosen by equating the charge per unit length on a tape in the effective case to that in the actual case; i. e.

$$\epsilon_{eff} \triangleq \frac{\int \left(\epsilon_3 E_{x3} - \epsilon_1 E_{x1}\right)\Big|_{x=0} dS}{\int \left(E_{xB} - E_{xA}\right)\Big|_{x=0} dS}, \qquad (3\text{-}38)$$

where the integrations are carried out over the surface of the tape.

For the effective case

$$E_{zA} = \sum_{n=-\infty}^{\infty} F_{nA} \frac{\sinh \beta_n (t+d+x)}{\sinh \beta_n (t+d)} e^{-j\varphi} e^{-j\beta_n z}, \qquad (3\text{-}39a)$$

and

$$E_{zB} = \sum_{n=-\infty}^{\infty} F_{nB} \frac{\sinh \beta_n (t_u - x)}{\sinh \beta_n t_u} e^{-j\varphi} e^{-j\beta_n z} . \qquad (3\text{-}39b)$$

As before $F_{na} = F_{nb} = (-1)^n E_o R_{met} S_a (\theta_n R_{met}/2)$. Solving for E_{xa} and E_{xb}, evaluating at the surface, and substituting in (3-38) yields

$$\epsilon_{eff} = C_\epsilon \epsilon_3 , \qquad (3\text{-}40)$$

where

$$C_\epsilon = \frac{\sum_{n=-\infty}^{\infty} (-1)^n S_a\left(\frac{\theta_n R_{met}}{2}\right) S_a\left(\frac{\theta_n (1-R_{met})}{2}\right) \left[\frac{k_{x3} \coth k_{x3} t_u}{\beta_n} + \frac{\epsilon_1}{\epsilon_3} \left(\frac{1 + \left(\frac{\eta_2 k_{x1}}{\eta_1 k_{x2}}\right) \tanh k_{x1} d \tanh k_{x2} t}{\tanh k_{x1} d + \left(\frac{\eta_2 k_{x1}}{\eta_1 k_{x2}}\right) \tanh k_{x2} t} \right) \right]}{\sum_{n=-\infty}^{\infty} (-1)^n S_a\left(\frac{\theta_n R_{met}}{2}\right) S_a\left(\frac{\theta_n (1-R_{met})}{2}\right) \left[\operatorname{sgn}(n) + \coth \beta_n (t+d) \right]} . \qquad (3\text{-}41)$$

The effective dielectric constant is a function of tape geometry, the dielectric constants and the permeabilities of the various media. By extending Haddad's technique [38] an effective intrinsic impedance modeling the actual case may be obtained. This effective intrinsic impedance is not equal to $(\mu_o/\epsilon_{eff})^{1/2}$ as in Haddad's model. The effective intrinsic impedance is chosen by equating the current flowing on a tape in the effective case to that of the actual case; i. e.

$$\eta_{eff}^{-1} \triangleq \frac{\int (\eta_3^{-1} E_{x3} - \eta_1^{-1} E_{x1})\big|_{x=0} dS}{\int (E_{xB} - E_{xA})\big|_{x=0} dS} . \qquad (3\text{-}42)$$

In a similar manner,

$$\eta_{eff} = C_\eta^{-1}\eta_3 \quad , \tag{3-43}$$

where

$$C_\eta = \frac{\sum_{n=-\infty}^{\infty}(-1)^n Sa\left(\frac{\theta_n R_{MET}}{2}\right)Sa\left(\frac{\theta_n(1-R_{MET})}{2}\right)\left[\frac{k_{x3}\coth k_{x3}t_u}{\beta_n}+\frac{\eta_3}{\eta_1}\left(\frac{1+\left(\frac{\eta_2 k_{x1}}{\eta_1 k_{x2}}\right)\tanh k_{x1}d\tanh k_{x2}t}{\tanh k_{x1}d+\left(\frac{\eta_2 k_{x1}}{\eta_1 k_{x2}}\right)\tanh k_{x2}t}\right)\right]}{\sum_{n=-\infty}^{\infty}(-1)^n Sa\left(\frac{\theta_n R_{MET}}{2}\right)Sa\left(\frac{\theta_n(1-R_{MET})}{2}\right)\left[sgn(n)+\coth\beta_n(t+d)\right]} \tag{3-44}$$

This method avoids the difficulty of having to choose between an effective dielectric constant derived from either an equal current or equal charge approximation [39] that are different. If one were to seek an effective dielectric constant based on an equal current approximation and an effective intrinsic impedance based on an equal charge approximation, the converse of the preceeding derivation, one obtains exactly the same result; i. e. The ϵ_{eff} and η_{eff} are unique.

The effective wavelength is found from

$$\lambda_{eff} = \left(\frac{v_{pi}}{c_3}\right)\lambda_3 = \left(\frac{C_\eta}{C_\epsilon}\right)\lambda_3 \quad . \tag{3-45}$$

To evaluate the reduction factor C_η / C_ϵ requires simultaneously solving equations (3-15, 3-41, 3-44, 3-45). This difficulty may be avoided by utilizing the properties of slow waves. Since the wave is slow, it is reasonable to assume

$$|\beta_n|^2 \gg \left|\left(\frac{2\pi}{\lambda_{eff}}\right)^2 - \left(\frac{2\pi}{\lambda_i}\right)^2\right| \quad . \tag{3-46}$$

Equation (3-15) therefore becomes

$$k_{xi}^2 \approx \beta_n^2 \qquad (3\text{-}47)$$

thus allowing the direct evaluation of equations (3-41, 3-44, and 3-45).

The ratio of effective to intrinsic wavelength, λ_{eff}/λ_3 is plotted in Figure 3.5 for the case $\epsilon_2 = \epsilon_3 = 10\epsilon_1$ with the geometrical dimension stated in the figure. It is seen that the effective wavelength decreases monotonically with θ_0 . Physically this may be interpreted in the following manner. At higher θ_0 the fields decay away from the tape more rapidly with more of the energy being stored in the high dielectric constant medium 3. It is noted that the metallation ratio has little if any effect in determining λ_{eff}/λ_3 . The effects of increasing the dielectric plate thickness to period ratio are shown in Figure 3.5. Increasing the plate thickness increases the effective wavelength.

3.6 Evaluation of Fletcher's Admittance Function

Fletcher's Admittance Function, $Y(\theta_0)$, is plotted in Figure 3.6 for the case $\epsilon_2 = \epsilon_3 = 10\epsilon_1$, with the geometrical dimensions stated in the figure. The metallization ratio, R_{met}, markedly effects $Y(\theta_0)$, $Y(\theta_0)$ decreasing with increasing R_{met} as anticipated. It is also noted that $Y(\theta_0)$ increases monotonically with θ_0 .

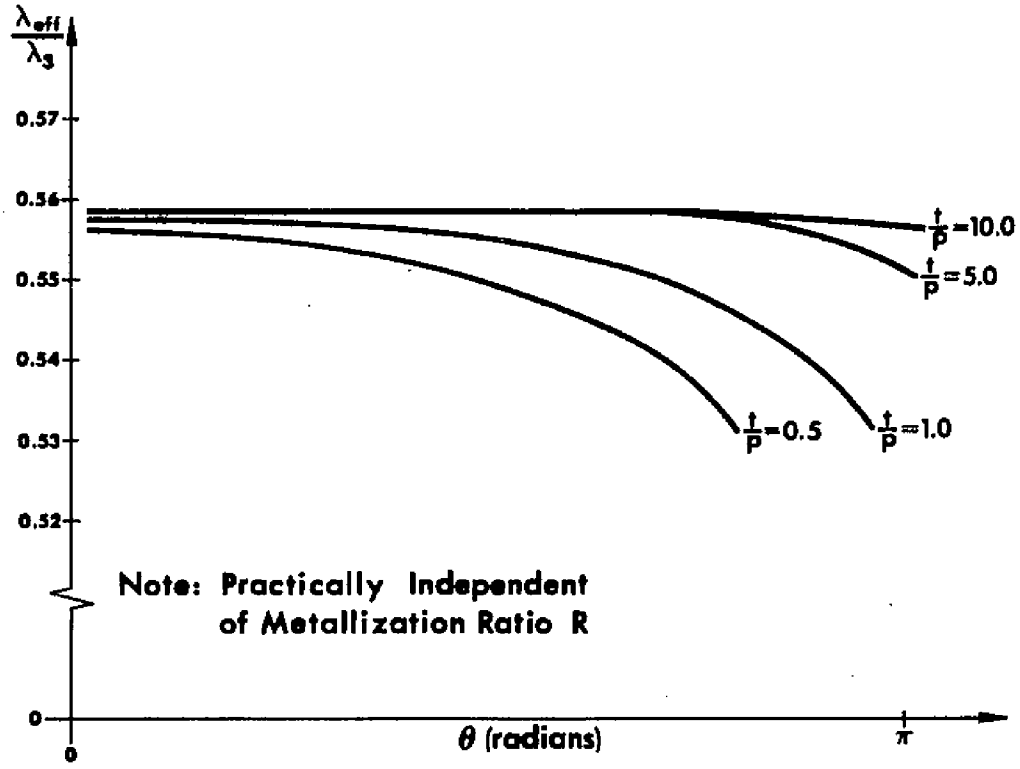

Figure 3.5 Effective Wavelength.
(d=62.5 mils; t=125 mils, $t_u \rightarrow \infty$)

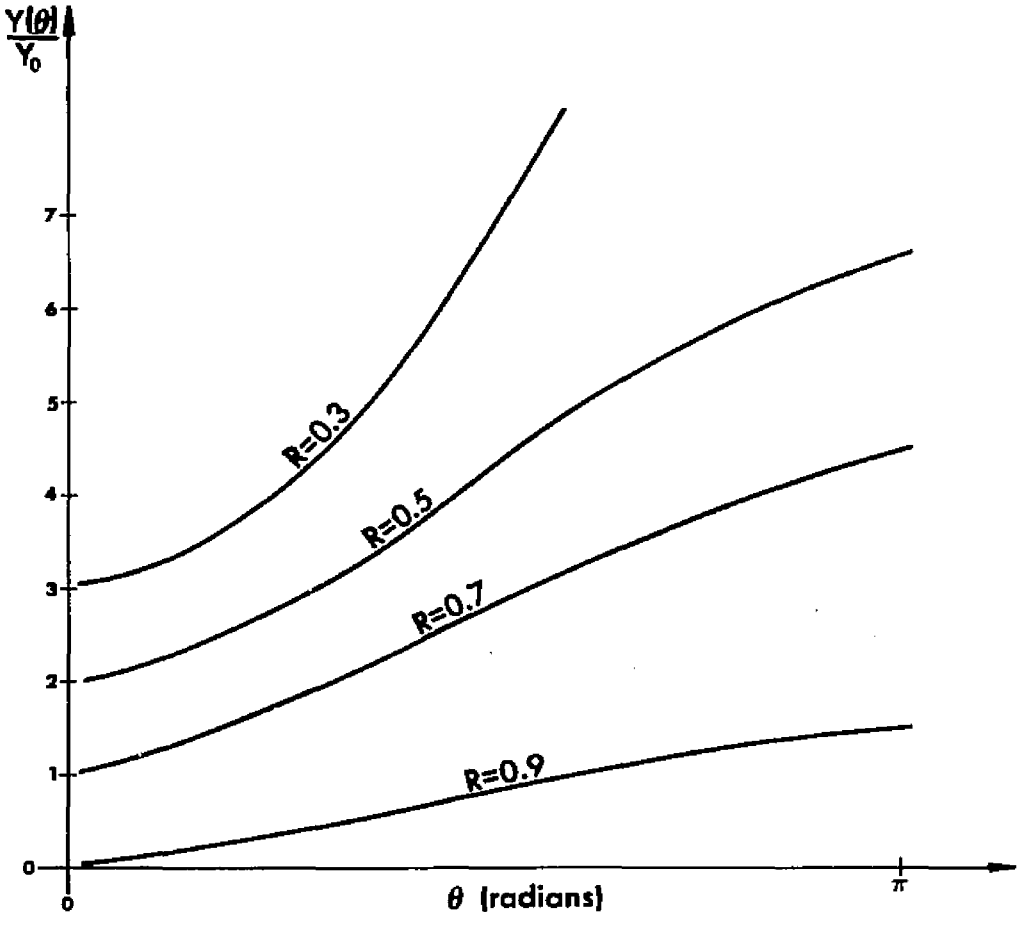

Figure 3.6 Fletcher's Admittance Function.
(d=62.5 mils; t=125 mils; $t_0 \rightarrow \infty$)

$X(\theta_o) = Y(\theta_o)/Y(\theta_o+\pi)$ vs. θ_o is plotted in Figure 3.7 for the above case. It is noted that $X(\theta_o)$ is independent of R_{met}. Hence the dispersion equation is independent of R_{met}.

3.7 Solution of the Determinantal Equation

The methods for evaluating the parameters of the determinantal equation have been discussed in the previous sections. The interval-halving method [40] is particularly well suited for solving the determinantal equation because convergence to a solution within one degree is assured in eight iterations.

The solutions to the determinantal equation so found are plotted in Figure 3.8 for several aspect ratios, a/b. It is noted that increasing the aspect ratio decreases the phase velocity, the slope of a radius vector to a point on the curve, for a given frequency. Near cutoff, $\lambda_{eff} = 4b$, or alternately, $f_c = v_{eff}/4b$, the group velocity (the slope of the curve) is non-zero. This error occurs because the assumption of uniform inter-tape electric field is not valid at high phase shift per unit length.

3.8 Interaction Impedance of the Stub-Loaded Meander Line

The interaction impedance, Z_n, of the n^{th} space harmonic of the longitudinal electric field is defined by equation (2-40)

$$Z_n \triangleq \frac{|E_{zn}|^2}{2\beta_n^2 P} \qquad (2\text{-}40)$$

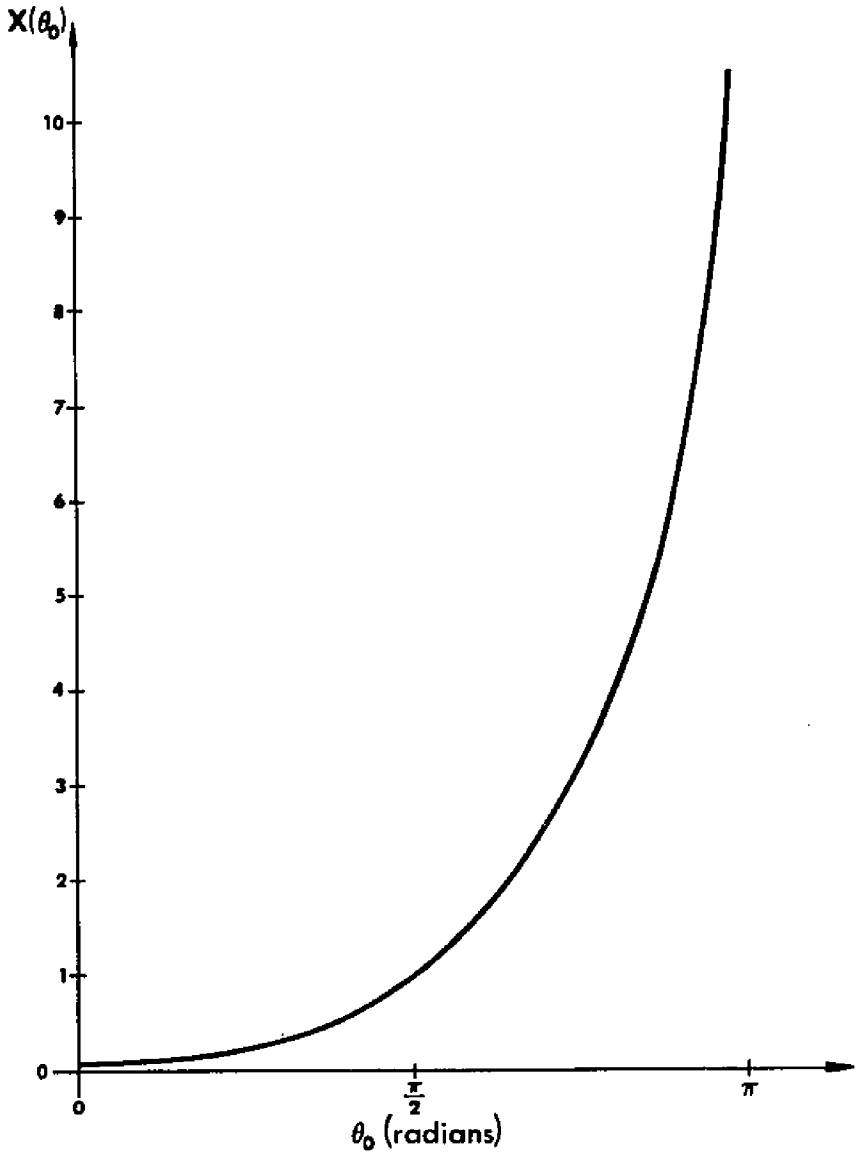

Figure 3.7 $X(\theta_0)$ vs. θ_0.
(d=62.5 mils; t=125 mils; $t_u \rightarrow \infty$)

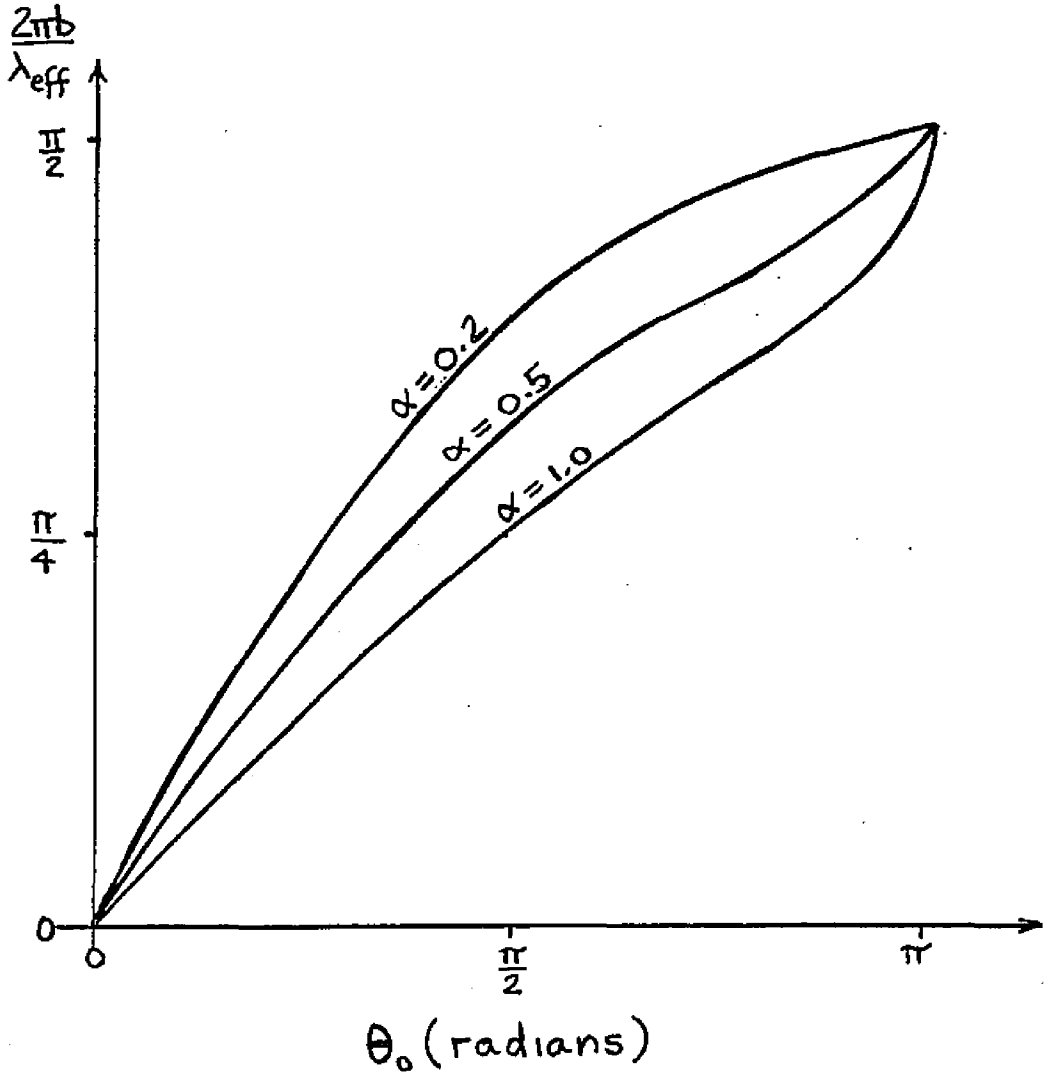

FIGURE 3.8 DISPERSION EQUATION
(d = 62.5 mils, t = 125 mils, $t_u \to \infty$)

where P is the power flowing along the line. As previously stated, the power flowing along the line is found by multiplying the stored energy per unit length by the group velocity. Hence, the evaluation of the interaction impedance additionally requires the calculation of the stored energy per unit length of a planar tape slow wave circuit and the calculation of the space harmonic amplitudes.

3.8a) Stored Energy per Period of a Planar Tape Slow Wave Circuit

Consider the power flowing in the transverse direction along the m^{th} tape, ,

$$P_M = \frac{1}{2} V_M I_M^* = \frac{1}{2} V_M Y(\theta_o) V_M^* = W_{SM} V_e = W_{SM} V_g \qquad (3\text{-}48)$$

Hence, the time average energy stored per unit transverse length on one tape, W_{sm}, is

$$W_{SM} = \frac{Y(\theta_o) V_m V_m^*}{2 V_g} . \qquad (3\text{-}49)$$

Of interest is the total average stored energy for one tape, $\overline{W}_{SM}$, where

$$\overline{W}_{SM} = \sum_{i=1}^{3} \frac{Y_i(\theta_o)}{2 V_g} \int_{\ell_{i1}}^{\ell_{i2}} V_{im} V_{im}^* \, d\ell \qquad (3\text{-}50)$$

For the line under consideration,

$$V_{im} = \left(A_{i1}\cos\varphi + A_{i2}\sin\varphi\right)e^{-jm\theta_0} + \left(A_{i3}\sin\varphi + A_{i4}\cos\varphi\right)e^{-jm(\theta_0+\pi)} \quad (3\text{-}51)$$

It is shown in the second appendix that $V_{im}V_{im}^*$ is independent of m and is given by

$$V_i V_i^* = \cos^2\varphi\left(A_{i1}A_{i1}^* - f_{i4}^2 A_{i2}A_{i2}^*\right) + \sin^2\varphi\left(A_{i2}A_{i2}^* - f_{i3}^2 A_{i1}A_{i1}^*\right), \quad (3\text{-}52)$$

where f_{i3} and f_{i4} are pure imaginary relational coefficients that are known functions of line geometry and phase shift per unit length. As required $V_i V_i^* \geq 0$. Defining

$$C_{i1} \triangleq A_{i1}A_{i1}^*\left(1 - k_i^2 f_{i4}^2\right), \quad (3\text{-}53a)$$

$$C_{i2} \triangleq A_{i4}A_{i1}^*\left(k_i^2 - f_{i3}^2\right), \quad (3\text{-}53b)$$

where

$$k_i \triangleq \frac{A_{i2}}{A_{i1}}, \quad (3\text{-}54)$$

results in

$$\overline{W}_{SM} = \overline{W}_S = \sum_{i=1}^{3} \frac{Y_i(\theta_0)}{2\omega} \int_{\varphi_{i1}}^{\varphi_{i2}} \left(C_{i1}\cos^2\varphi + C_{i2}\sin^2\varphi\right) d\varphi . \quad (3\text{-}55)$$

Since the circuit is biperiodic, the stored energy per period $\overline{W}_{ST}$

equals twice the stored energy per tape. Evaluating (3-55) yields

$$\overline{W}_{ST}=\sum_{i=1}^{3}\frac{Y_i(\theta_o)}{4\omega}\left[2(C_{i1}+C_{i2})(\varphi_{i2}-\varphi_{i1})+(C_{iu}-C_{i2})(\sin 2\varphi_{i2}-\sin 2\varphi_{iu})\right]. \quad (3\text{-}56)$$

The stored energy per period, $\overline{W}_{ST}$, is plotted vs. θ_o for the case $\epsilon_2 = \epsilon_3 = 10\epsilon_1$, in Figure 3.9 for several different aspect ratios a/b. The stored energy per period is seen to decrease with increasing aspect ratio or phase shift per unit length and hence with increasing frequency.

3.8b Stub-Loaded Meander Line Space Harmonic Amplitudes

Assuming that the intertape electric field is uniform results in

$$E_z\Big|_{\substack{x=0\\y=0}} = -\frac{\left[(V_{1(m+1)}-V_{1m})\Big|_{\substack{x=0\\y=0}}\right]}{q} \quad (3\text{-}57)$$

Substitution of equation (3-6) in (3-57) yields

$$E_z\Big|_{\substack{x=0\\y=0}} = \frac{e^{-j(m+\frac{1}{2})\theta_o}\left[2jA_1\sin\left(\frac{\theta_o}{2}\right)\right]+e^{-j(m+\frac{1}{2})(\theta_o+\pi)}\left[2jA_4\sin\left(\frac{\theta_o+\pi}{2}\right)\right]}{q} \quad (3\text{-}58)$$

Expanding in Fourier Series form,

$$E_z=\sum_{n=-\infty}^{\infty}E_{zn}e^{-j\beta_n z}, \quad (3\text{-}59)$$

such that

$$E_{zn}=\frac{(-1)^n 2j}{p}\left[A_1 g_1(\theta_o)+A_4 g_4(\theta_o)\right], \quad (3\text{-}60)$$

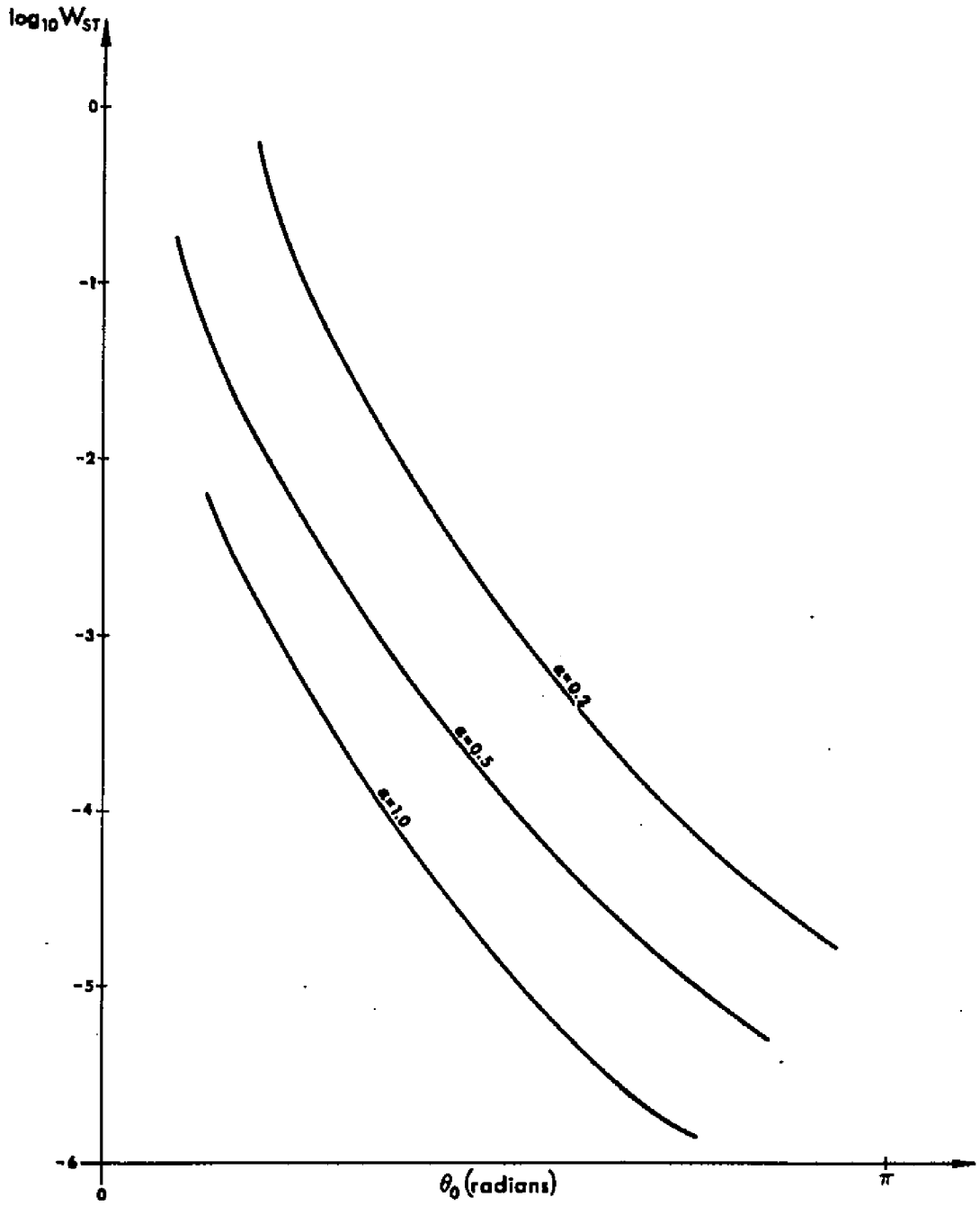

Figure 3.9 Stored Energy per Period vs. θ_0.
(d= 62.5 mils; t=125 mils; $t_u \rightarrow \infty$)

where $$g_1(\theta_o) \triangleq \sin\left(\frac{\theta_o}{2}\right) Sa\left(\frac{\theta_o R_{MET}}{2}\right) , \tag{3-61a}$$

and

$$g_4(\theta_o) \triangleq \sin\left(\frac{\theta_o+\pi}{2}\right) Sa\left[\left(\theta_o+(2n+1)\pi\right)\frac{R_{MET}}{2}\right] . \tag{3-61b}$$

It is noted that $g_1(\theta_o)$ and $g_4(\theta_o)$ are real while A_1 and A_4 are in general complex. As a consequence of the properties of the relational coefficients, f_i , the space harmonic amplitudes are found to be

$$|E_{zn}|^2 = \frac{4}{p^2} A_1 A_1^* \left[g_1^2(\theta_o) - f_{14}^2 k_1^2 g_4^2(\theta_o)\right] . \tag{3-62}$$

3.8c Evaluation of Interaction Impedance

The interaction impedance is evaluated from equations (2-24), (3-48), (3-56), and (3-62) at the surface of the tape. The interaction impedance, Z_n, is plotted vs. θ_o for the case $\epsilon_2 = \epsilon_3 = 10\,\epsilon_1$, in Figure 3.10 for several different aspect ratios $\frac{a}{b}$. It is seen that Z_n decreases monotonically over five orders of magnitude for $0 < \theta_o < \pi$ for all aspect ratios. As anticipated decreasing the aspect ratio increases the interaction impedance. When compared with Figure 3.8 it is seen that the increase in interaction impedance is unfortunately accompanied by an increase in phase velocity.

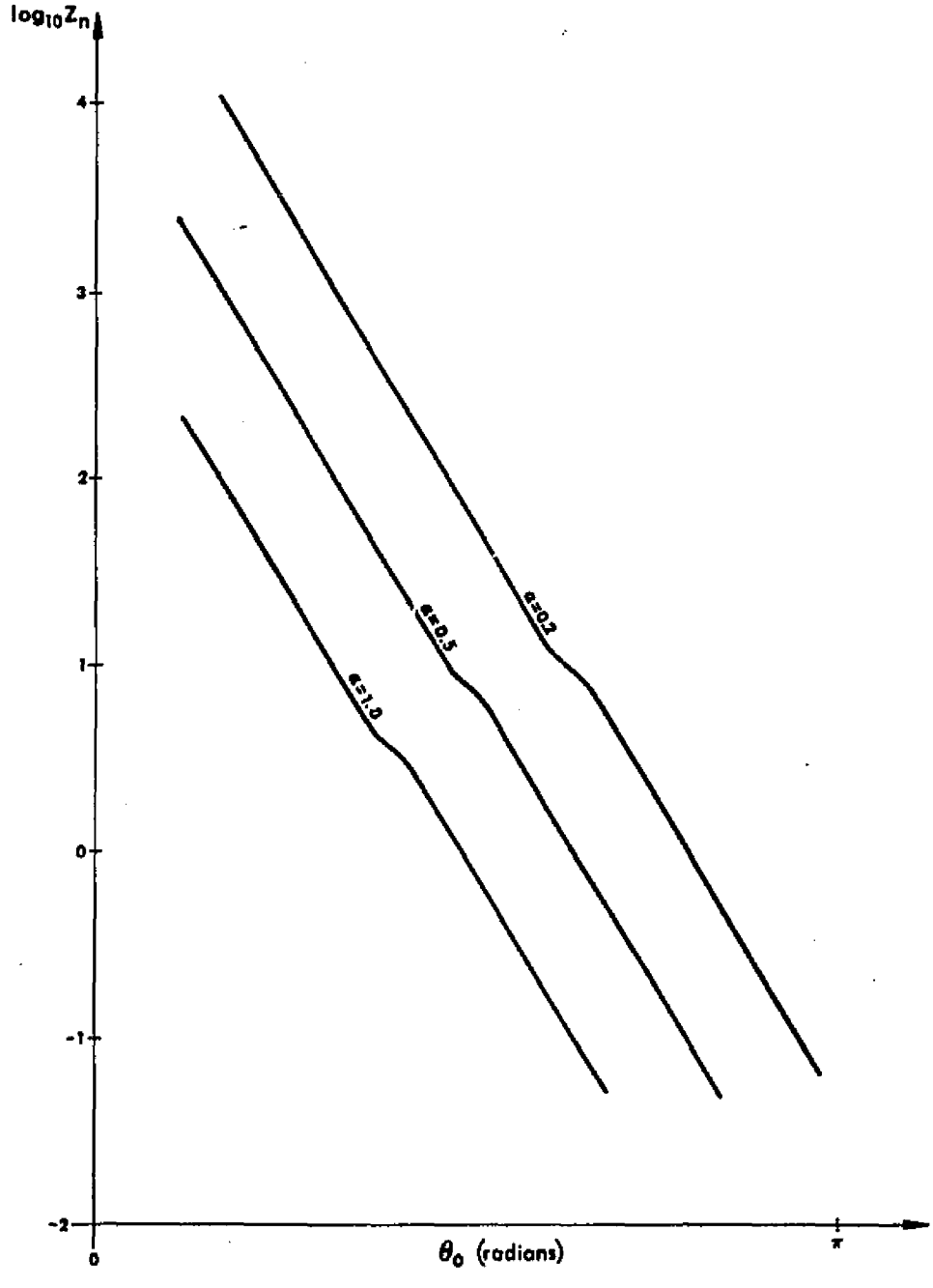

Figure 3.10 Interaction Impedance vs. θ_0.
(d=62.5 mils; t=125 mils; $t_v \rightarrow \infty$)

3.9 Conclusions

A slow wave circuit suitable for use in experimentally studying the interaction between drifting carriers in a semiconductor and slow electromagnetic waves has been investigated. The dispersion characteristics and interaction impedance of this planar type slow wave circuit, the stub loaded meander line, have been obtained using a modification of Fletcher's method of analysis. The unique effective intrinsic phase velocity of this circuit fabricated on stratified media has been derived.

Examination of the stub loaded meander line analysis, keeping in mind the required circuit construction technology, reveals that a minimum phase velocity of 10^7 cm/sec is possible with dielectric materials having $\epsilon_r = 25$. Lower velocities will be attainable by utilizing higher permittivity materials, when they become available, and by improving the photolithographic technology. Interaction impedances greater than one hundred ohms are anticipated because of the very low group velocity.

CHAPTER FOUR - THE STUB LOADED MEANDER LINE SLOW WAVE CIRCUIT - MEASUREMENTS

The purpose of this chapter is to synopsize the methods available to measure two parameters characterizing the stub loaded meander line; namely, the cold circuit propagation constant, γ_0 , and the interaction impedance of the n^{th} space harmonic, Z_n. The design and instrumentation of experiments will be discussed and results will be compared to the theoretically predicted values as developed in chapter three.

4.1 Measurement of the Cold Circuit Propagation Constant

The measurement of the real part of the propagation constant, α_0 , is accomplished by terminating the circuit with its characteristic impedance and determining its insertion loss, and will therefore not be discussed further. The measurement of β_0 is more difficult and leads directly to a knowledge of the circuit phase and group velocities; i.e. $v_p = \omega/\beta_0$, and $v_g = \partial\omega/\partial\beta_0$.

There are three common techniques for measuring β_0 . The first and simplest is to construct a resonant section of the circuit N periods long [41] by placing electric field shorts [or opens] at planes of mirror symmetry. The circuit is then weakly coupled at both ends (to maintain high-Q for the resonant cavity) and transmission measurements through the cavity are made while varying the excitation frequency.

The points of relative maximum transmission occur when the cavity is resonant, a condition corresponding to the cavity being an integral number of half wavelengths long. The equation for β_0 is found to be

$$\beta_0 = \frac{n\pi}{NP} \,, \tag{4-1}$$

where n is the resonance index (n = 1,2,3, ... N-1), and P is the period of the circuit.

In practice there are three major difficulties in utilizing this method. First, to minimize end effects, i. e. non - perfect short and/or placement at planes of non - mirror symmetry, a large number of sections should be chosen. Second, the index of a resonance has to be determined by field probing and/or by the sequential observation of all resonances. Third, the resonances must be sharp and distinct. This latter requirement may be achieved only when low loss circuits with sufficiently high unloaded Q_o may be constructed. Additionally, coupling to the cavity has to be weak to insure that external loading does not lower the unloaded Q_o.

For the high slowing factor circuits under consideration distinct resonances were obtainable only when the geometric slowing factors were less than twenty-five. Experiments were conducted on a circuit with aspect ratio = 0.5, line width = 250 mils and circuit width = 5000 mils, constructed on a 500 mil thick styrofoam slab, as shown in Figure 4-1. The input and output couplers were empirically

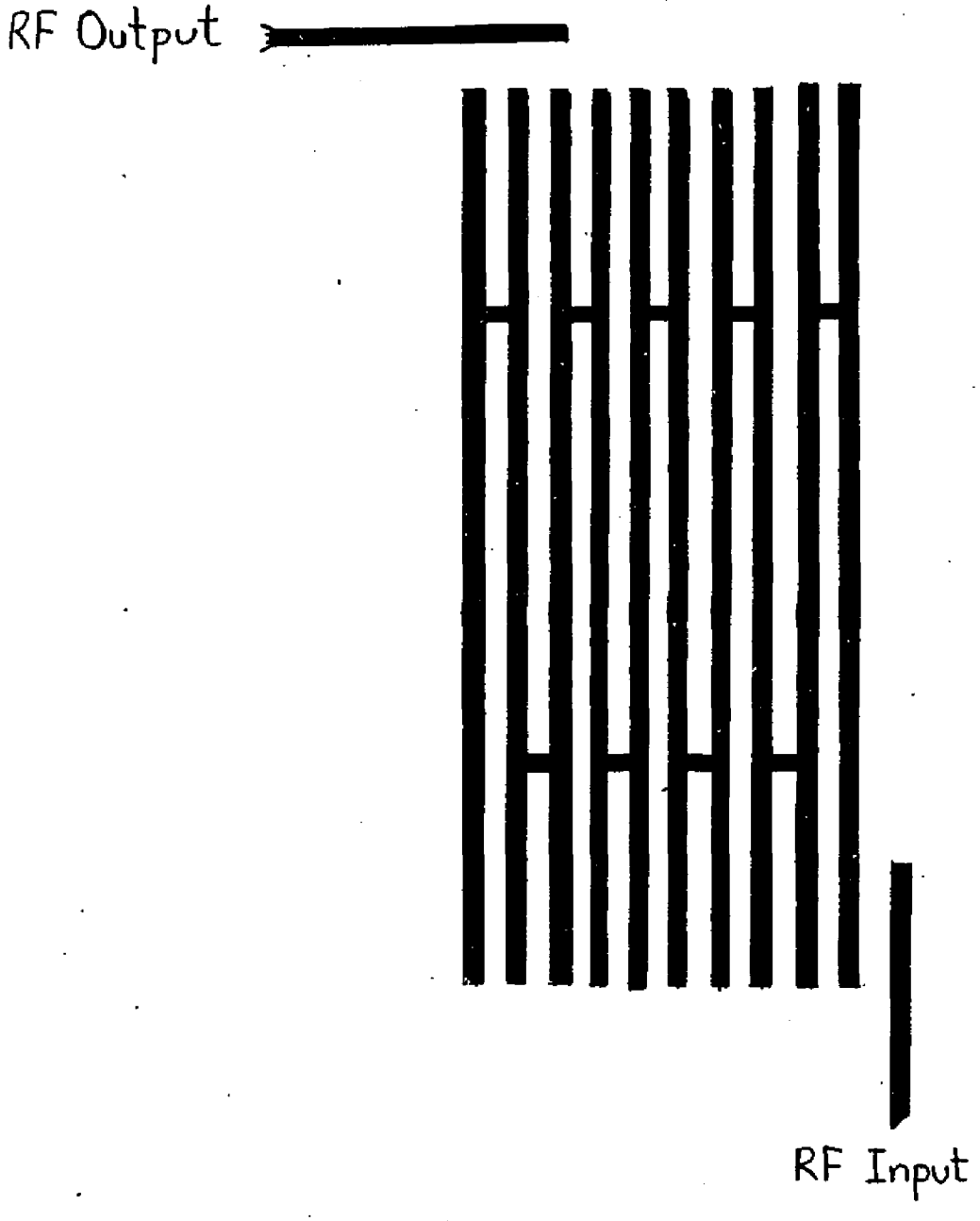

Figure 4-1 Resonant Experiment on the Stub-Loaded Meander Line (line width = 250 mils, circuit width = 5000 mils)

designed to give sharp resonances with adequate output level. Distinct resonances were obtainable only at frequencies below 150 MHz. Thus limiting the maximum measureable β_o. The results of this experiment are shown in Figure 4-2. The resonance indices were obtained by the observation of successive resonances. It is seen that there is good agreement between the experimental and theoretical curve for the frequency range covered.

The second technique for measuring β_o is to employ time domain reflectometer techniques to measure the "effective distance" between obstacles on the circuit. Unfortunately, this method does not correspond to single frequency excitation and requires involved techniques [42] (too involved in this case to justify their performance) to find β_o (w). It does however reveal the existence of either "slow" or "fast" waves along the circuit. In one test, performed on a circuit with line width = 25 mils and circuit width = 10,000 mils, an obstacle one inch from the source appeared ten meters away on the time domain reflectometer indicating a slowing of approximately four hundred. (Note: 2 a/p in this case is four hundred.)

The third technique for measuring β_o is to probe the field of the slow wave circuit that is terminated by a short circuit. The reflected wave interfers with the incident field to form a standing wave pattern even in the presence of moderate attenuation due to circuit loss; the distance between successive minima or maxima being

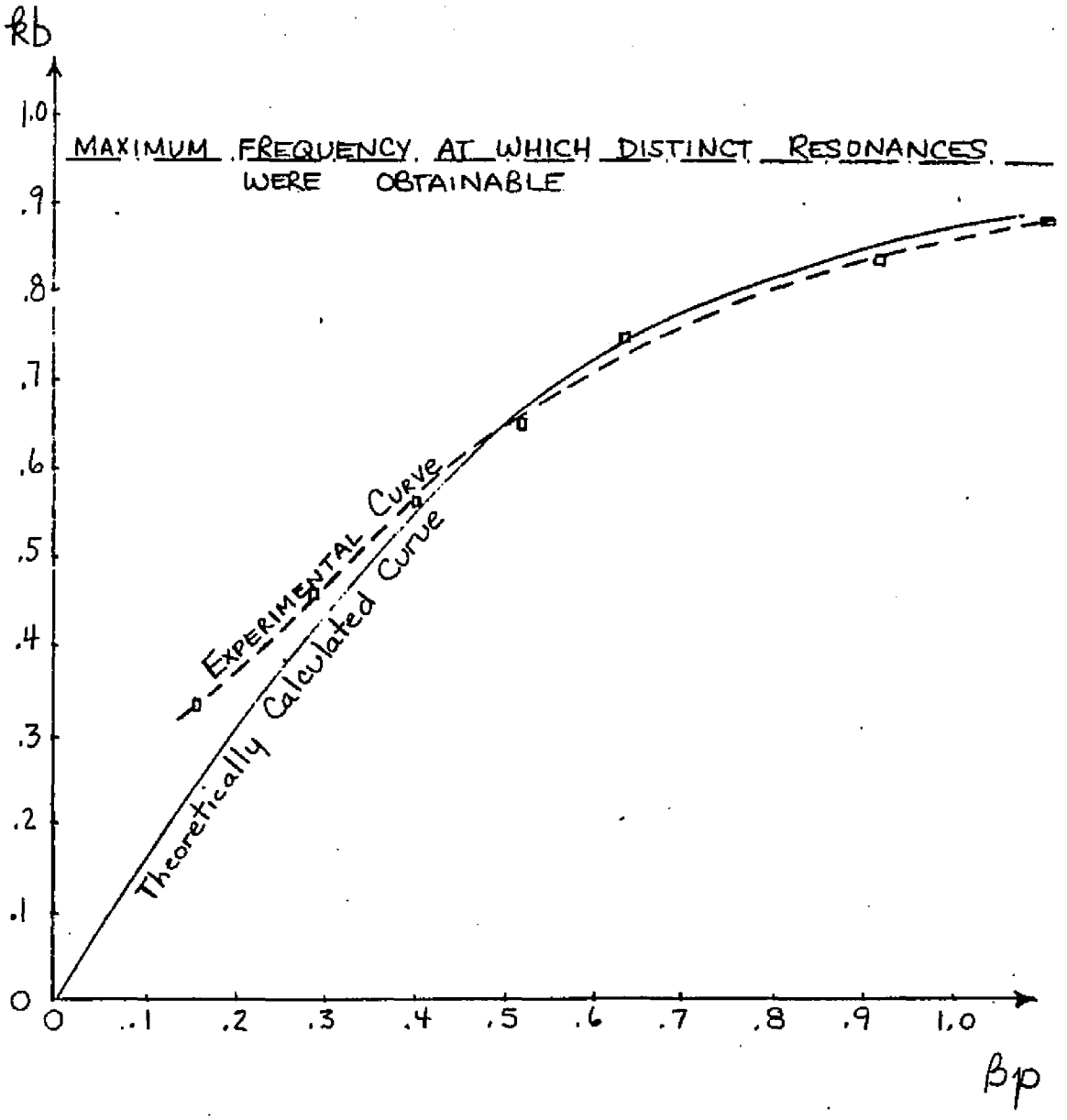

Figure 4.2 Dispersion Characteristics Obtained from Resonance Experiment

$\lambda_g/2$. This technique may be instrumented by either a movable probe or movable short [43, 44] . For the case at hand it was simpler to construct the movable probe technique.

The circuit assembled for test is shown in Figure 4-3 and consists of a HP model 809B slotted line carriage modified to accept a specially designed probe. The probe is a magnetic field loop approximately 1000 mils-square cross sectional area and 40 mils thick as shown in Figure 4-4. The maximum sensitivity direction could be changed by rotating the supporting jig. The circuit has aspect ratio = 1.0, line width = 25 mils, and circuit width = 10,000 mils. The circuit board is photolithographically etched REXOLITE 2200, 62.5 mils thick with 1 oz. copper one side and a relative dielectric constant of 2.53. It is mounted above a 125 mils dielectric plate, Custom Materials Hi-K 707, with relative dielectric constant 25.0 to give additional non-geometric slowing. This experiment therefore also tests the theory developed for calculating the effective intrinsic velocity of layered media chapter 3, section 3.5.

Field plots obtained at various frequencies are shown in Figure 4-5. The probe was oriented to detect H_z at the center of the circuit. This data is processed to obtain wavelength vs. excitation frequency, Figure 4-6, and phase shift per unit length vs. frequency, Figure 4-7. At low frequency the agreement between experiment and theory is good. At higher frequency the forward mode is not excited,

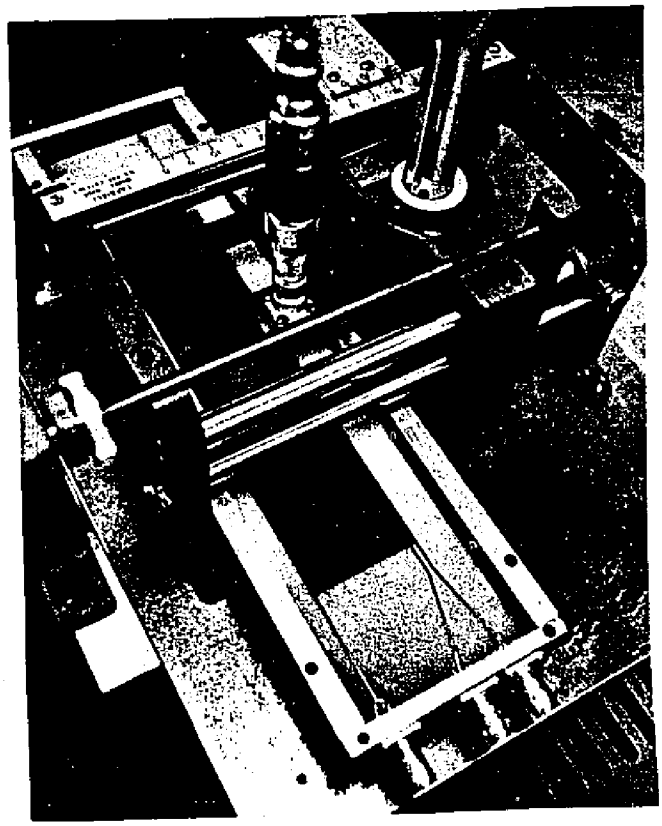

Figure 4.3 Circuit Under Test

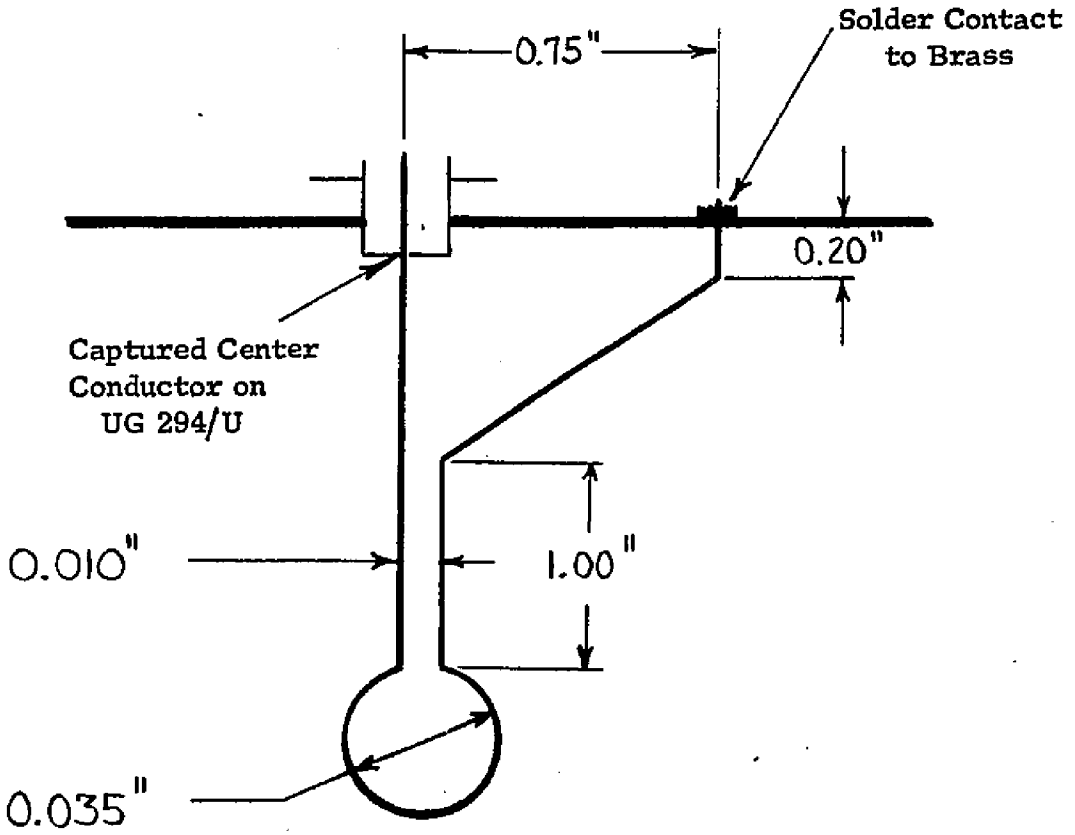

Figure 4.4. Probe Details for test jig

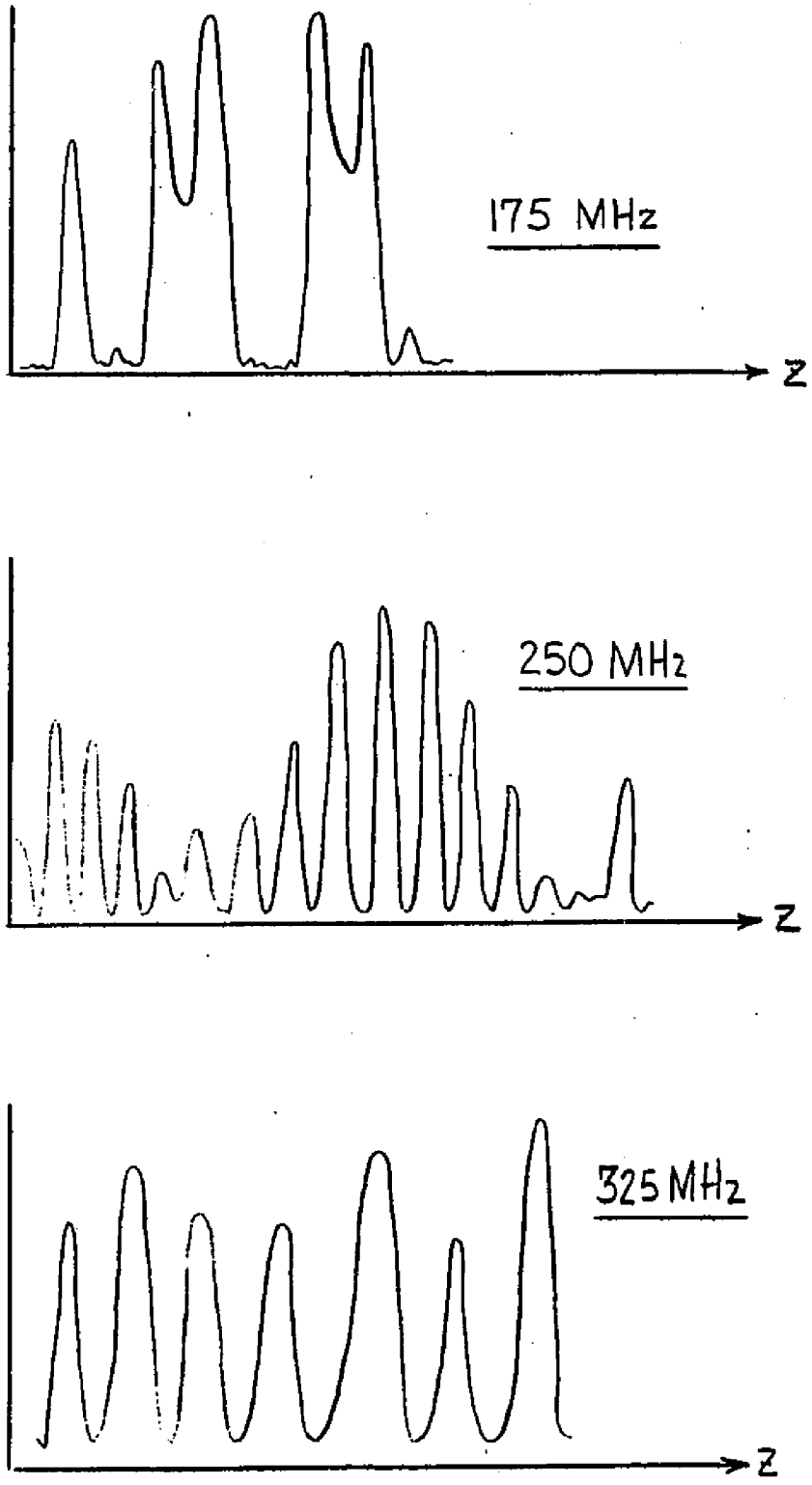

Figure 4.5 Meander Line Field Plots

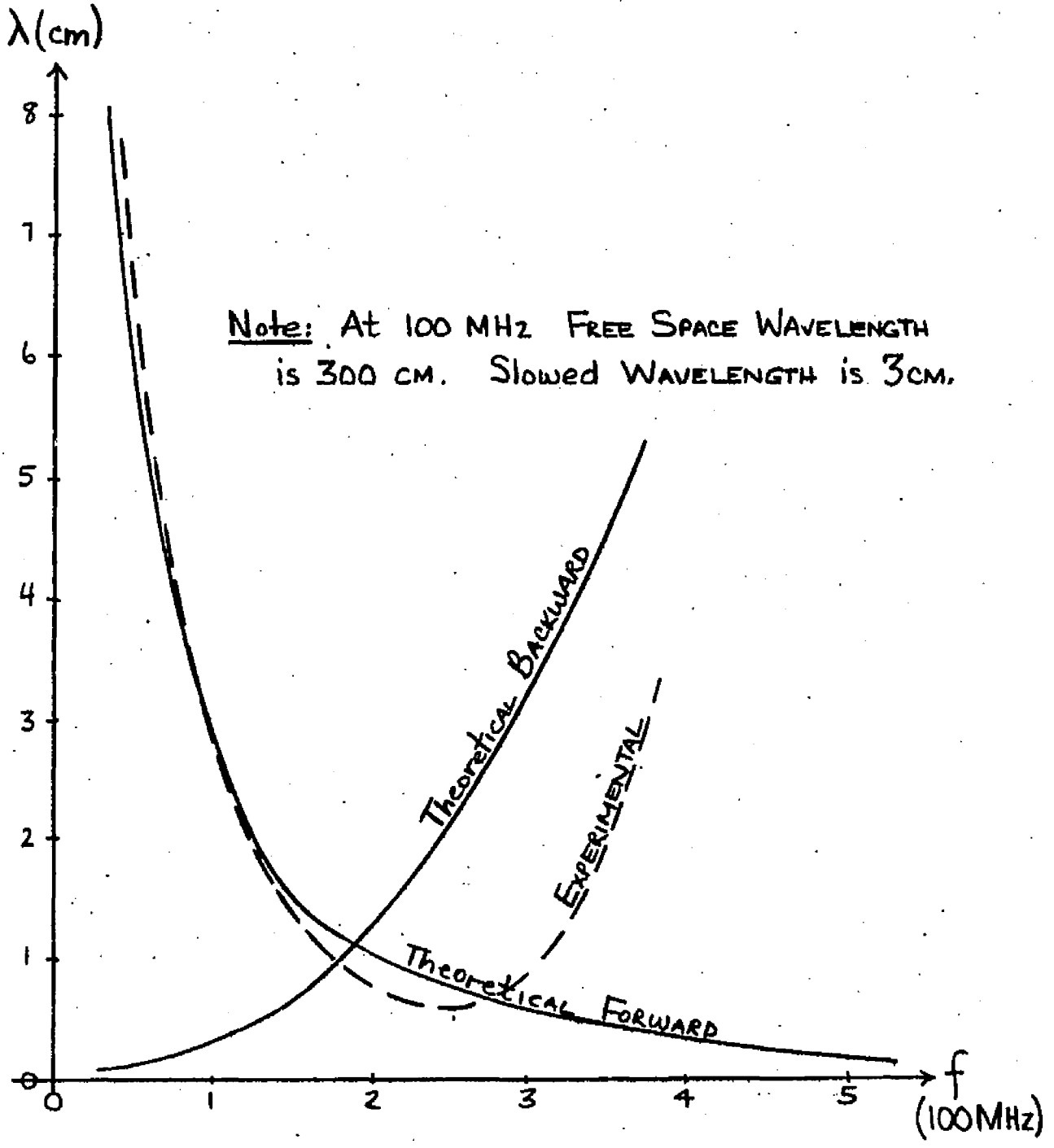

Figure 4.6 Wavelength vs. Excitation Frequency

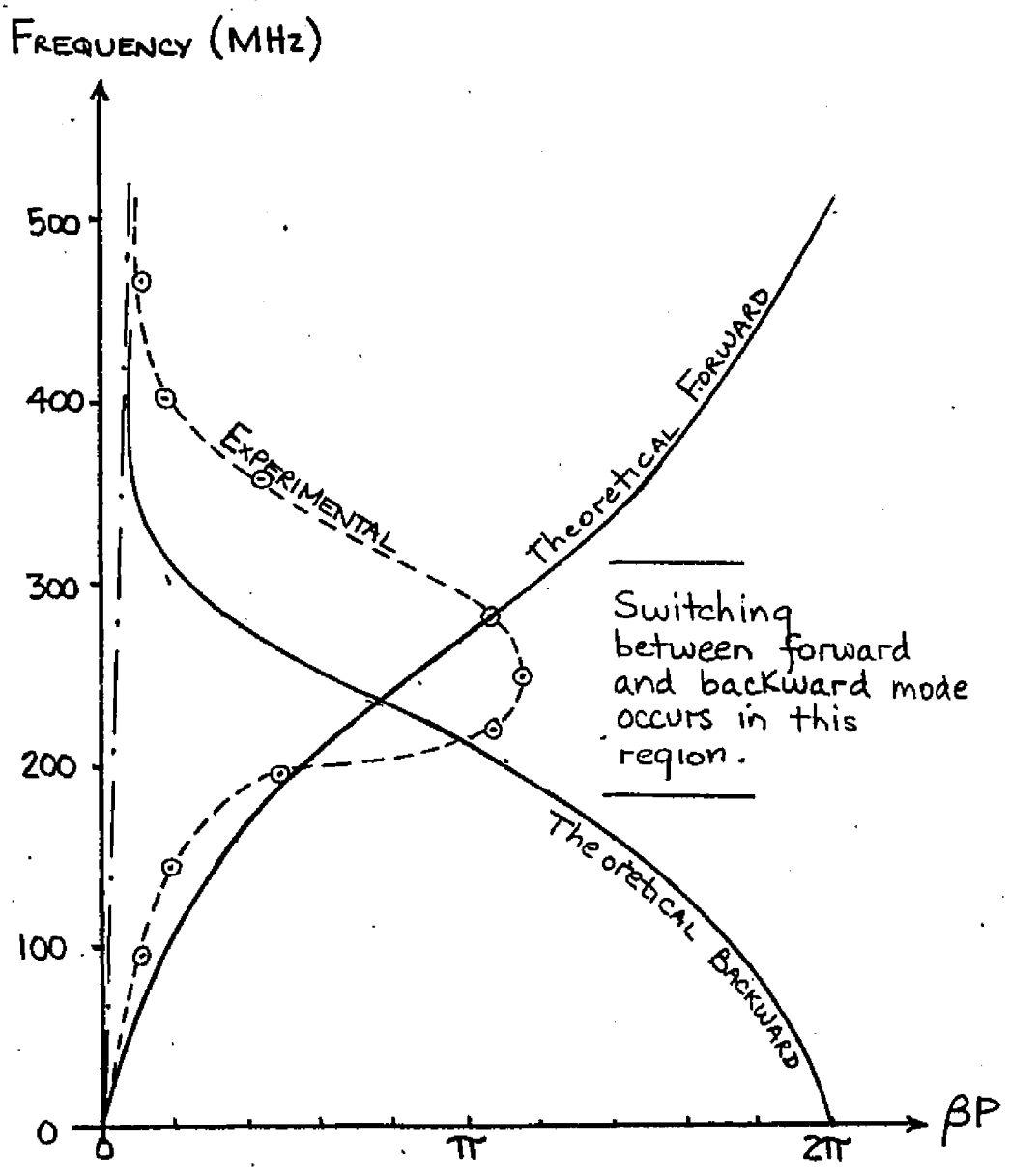

Figure 4.7 Phase Shift vs. Frequency

the detected field being attributable to the excitation of the n = + 1 backward mode. This is unavoidable since no precaution was taken in this experiment regarding the relative amplitudes of mode excitation. Even at lower frequencies the field patterns reveal the existence of other modes. The effect of having two nearly equal wavelength modes propagating on a loss less circuit is shown in Figure 4-8. The resultant field pattern is most similar to the experimental plot taken at 250 MHz, the point at which the two modes have nearly equal wavelength.

The discrepancy between the predicted and measured backward mode at higher frequency is caused by the uniform electric field assumption used in calculating λ_{eff} and $Y(\theta_o)$. This assumption is poorest at large θ_o necessary to produce the small $\theta_1 = -\theta_o + \pi$.

The zero transverse magnetic field assumption TEM_y, (or $|H_y| \approx 0$) was tested using the same experimental apparatus. The probe was rotated 90^o to make the y direction sensitivity maximum. The various plots were repeated for different transverse positions. It was found that the magnitude of H_y was greater than 60 db down from the magnitude of H_z at all positions (except directly over the interline shorting link) and frequencies tested thus confirming the intuitive assumption made in the theoretical analysis.

4.2 Empirical Matching Techniques

Two experiments were performed in an attempt to improve the

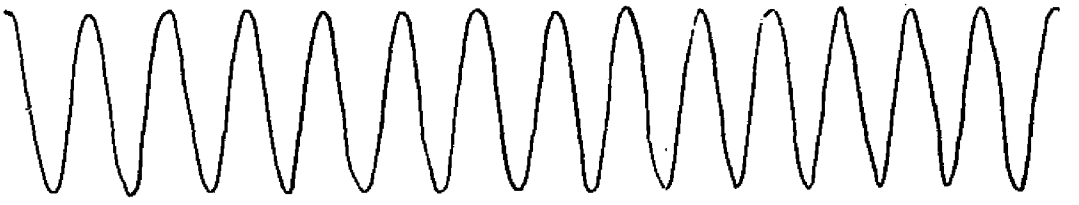

(a) wave number one - cos ω t

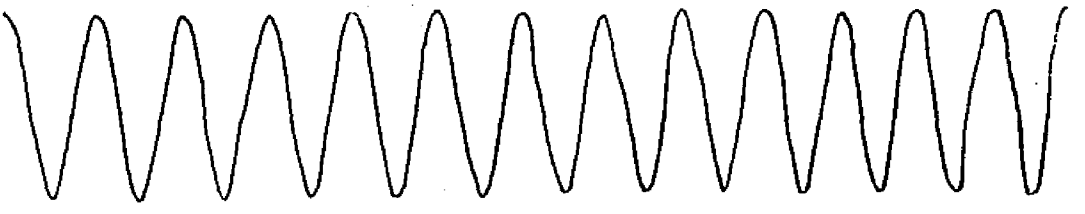

(b) wave number two - cos kωt , k = 0.9

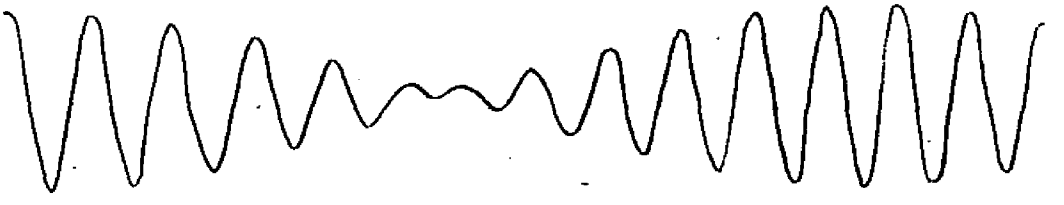

(c) wave number one + two - 0.5 (cos ωt + cos kωt)

(d) detected field - $\left| 0.5 \left(\cos \omega t + \cos k\omega t \right) \right|$

Figure 4.8 Standing Wave Pattern for Double Mode Excitation

input VSWR and to favor the excitation of the forward wave at higher frequencies. The idea behind these experiments was to excite more than one line and to adjust the relative phases such that the proper β_o for a given (ω) was attained. The two configurations tried are shown in Figure 4-9. The results of these experiments were disappointing since there was no appreciable improvement in the forward wave excitation.

4.3 Measurement of Interaction Impedance

The interaction impedance of the n^{th} space harmonic was defined in chapter two as $Z_n \triangleq |E_{zn}|^2 / 2\beta_n^2 P$ and may be rewritten as

$$Z_n = \left(\frac{1}{2\beta_n^2 v_g}\right)\left(\frac{|E_{zn}|^2}{\bar{E}^2}\right)\left(\frac{\bar{E}^2}{\bar{W}}\right) \qquad (4\text{-}2)$$

where $\bar{W}$ is the time average stored energy per unit length. The direct measurement of Z_n involves determing the above three quantities by cavity perturbation techniques [45]. The first quantity is evaluated from the measurement of the cold circuit propagation constant as previously outlined whereas the second and third are found by perturbing the resonant frequency of a cavity formed from the slow wave circuit. It has been shown [46] that the relative change in resonant frequency is given by

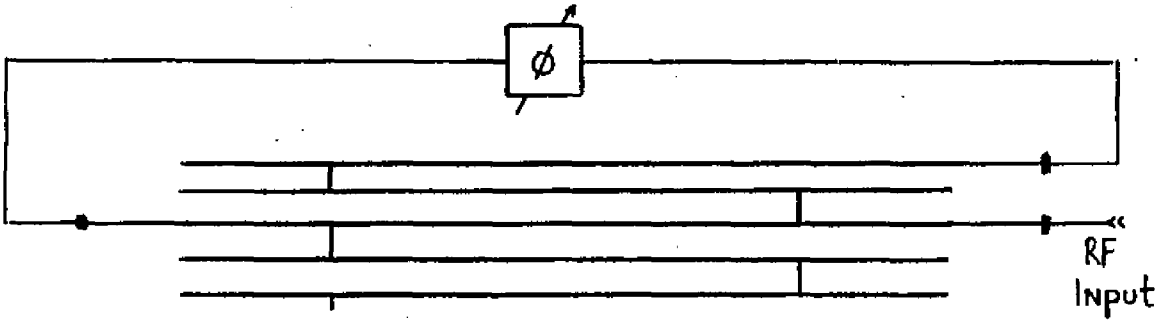

(a) Method Number One

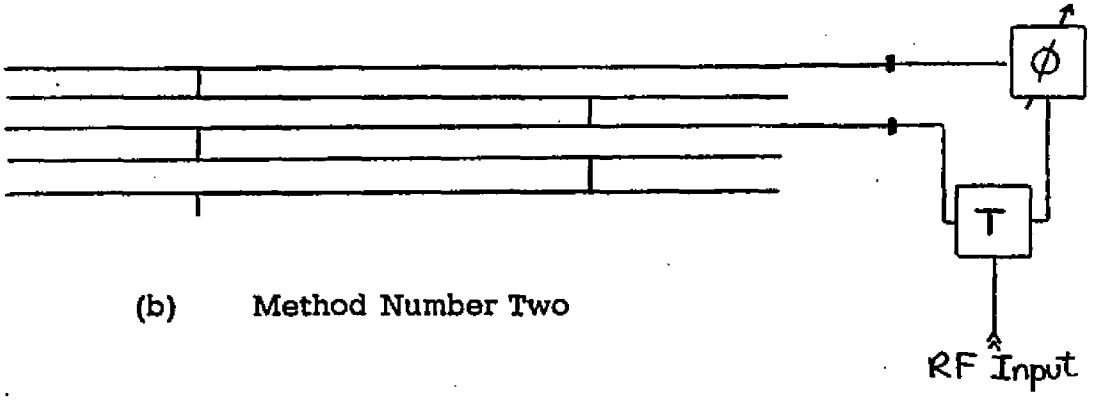

(b) Method Number Two

Figure 4.9 Empirical Matching Experiments

$$\frac{\delta\omega}{\omega_a} = \frac{-\int_\tau (\vec{P}^* \cdot \vec{E}_a + \vec{M}^* \cdot \vec{B}_a)\, dv}{2NL\bar{W}} \qquad (4\text{-}3a)$$

which for a small metallic circular bead reduces to

$$\frac{\delta\omega}{\omega_a} = \frac{-3\epsilon_0 \tau}{2NL}\left(\frac{E_a^2}{\bar{W}}\right) \qquad (4\text{-}3b)$$

where τ is the volume of the volume of the bead and E_a is the unperturbed electric field at the position of the bead. A plot of $E_a(\gamma)$ may thus be obtained from which $\bar{E}^2$ and $|E_{zn}|^2$ are found by Fourier analysis. As previously mentioned, however, any cavity technique depends upon the ability to obtain sharp distinct resonances. For the circuits being studied sufficiently sharp resonances were not obtainable due to large circuit loss. It was not possible, therefore, to measure the interaction impedance by this method.

There is, however, another technique for measuring interaction impedance that has been employed for high slowing factor circuits [47]. This technique, essentially a substitution method, consists of constructing a variable low voltage vacuum traveling wave tube with a controllable beam cross section. Gain frequency measurements are taken with a standard (e. g. a helix) and then the text circuit. The interaction impedance of the test circuit may then be calculated from the gain-frequency measurements.

This latter method is both costly and time consuming. It was felt that since the gain varies approximately as $Z_n^{1/3}$, and the calculated values and frequency dependence were within reasonably expected values of known structures (e.g. the helix) that this experiment was unwarranted. It was therefore not undertaken.

4.4 Conclusions

The theoretically predicted dispersion characteristics of the stub-loaded meander line were experimentally verified with good agreement. The required slowing factors for studying the interaction between slow electromagnetic waves and drifting carriers in a semiconductor are marginally obtainable for the fundamental space harmonic.

Difficulties encountered in obtaining distinct resonances, due to circuit loss, prevented the measurement of the interaction impedance by a perturbation of resonant frequency technique. Discrepancy between experiment and theory at high phase shift per unit length indidicates the need for higher order field approximation. Techniques investigated for the preferential excitation of the forward wave have proved unsatisfactory and thus limit the excitation frequency to approximately one third the cutoff frequency; i.e. the forward wave is excited strongly for $f < \frac{f_c}{3} = \frac{v_{eff}}{12b}$.

CHAPTER FIVE - TOPICS PRELIMINARY TO THE CALCULATION OF THE GAIN OF DEVICES UTILIZING THE INTERACTION BETWEEN SLOW ELECTROMAGNETIC WAVES AND DRIFTING CARRIERS IN A SEMICONDUCTOR

The purpose of this chapter is the consideration of topics preliminary to the calculation of the gain of devices utilizing the interaction between slow electromagnetic waves and drifting carriers in a semiconductor.

As the mean carrier velocity is varied to calculate the gain-voltage characteristics, the perturbational assumption $|h| \ll |\beta_e|$ is very often not satisfied. The range of validity of the perturbational solution of the dominant carrier dispersion equation will be extended to include highly asynchronous operation. The simultaneous interaction with more than one space harmonic is investigated using this solution.

The calculation of the gain of a device requires the knowledge of the excitation amplitudes and phases of the various modes as well as their growth rates. The effects of collisions and space charge on the modal excitations are determined.

The development of a growing mode criterion allowing one to determine the existence of a convective instability without having to calculate its growth rate is of interest. An expression for the maximum allowable carrier density for which a convective instability exists is found as a function of the device parameters using the analytic theory of continued fractions.

5.1 Asynchronous Perturbational Solution of the Dominant Carrier Dispersion Equation.

The dominant carrier dispersion equation, (2-48), is developed in the second chapter. Substitution of equations (2-50, 2-51) into (2-48) without using

the condition $|h_A| << |\beta_{eA}|$ results in

$$S^3 + (\beta_{CA} + \beta_{RA} + \alpha_o + jh_A)S^2 + [(\beta_{CA} + \beta_{RA})(\alpha_o + jh_A) + \beta_{CA}\beta_{RA} + \beta_{QA}^2(1 + \lambda_{DA}^2\beta_{eA}^2)]S + [\beta_{CA}\beta_{RA} + \beta_{QA}^2(1 + \lambda_{DA}^2\beta_{eA}^2)] \cdot [\alpha_o + jh_A] + jP(h_A) = 0 , \quad (5\text{-}1)$$

where $P(h_A)$ is a synchronization function defined as

$$P(h_A) = \frac{2(1 + h_A C)}{(2 + h_A C)} = \frac{2\left(\frac{V_{oA}}{v_p}\right)}{\left(1 + \frac{V_{oA}}{v_p}\right)} , \quad (5\text{-}2)$$

and is plotted in Figure 5.1. For the synchronous case, $v_{oA} = v_p$ (or $h_A = 0$), $P(h_A) = 1$ and equation (5-1) reduces to (2-53). The synchronization function has a pole at $\frac{v_{oA}}{v_p} = -1$ that does not correspond to any physical condition but rather is a result of the perturbational assumption $|\delta| << |\beta_{eA}|$ not being met.

Of interest is the interaction with space harmonics of the circuit wave. As the drift velocity is decreased from synchronism with the fundamental mode a point is reached where interaction with a space harmonic is possible. Since the interaction impedance of the space harmonic is smaller than the fundamental mode interaction impedance, the overall space harmonic growth rate will be smaller (if growth at all occurs). The growth rate vs. drift velocity is plotted in Figure 5.2 as the drift velocity is varied such that interaction with the first two space harmonics occurs. It is noted that in obtaining the above results a linearizing assumption was made; i.e., it was assumed that the interaction with the n^{th} space harmonic occurs independently of the interaction with the $(n+1)^{th}$ space harmonic. This is justified

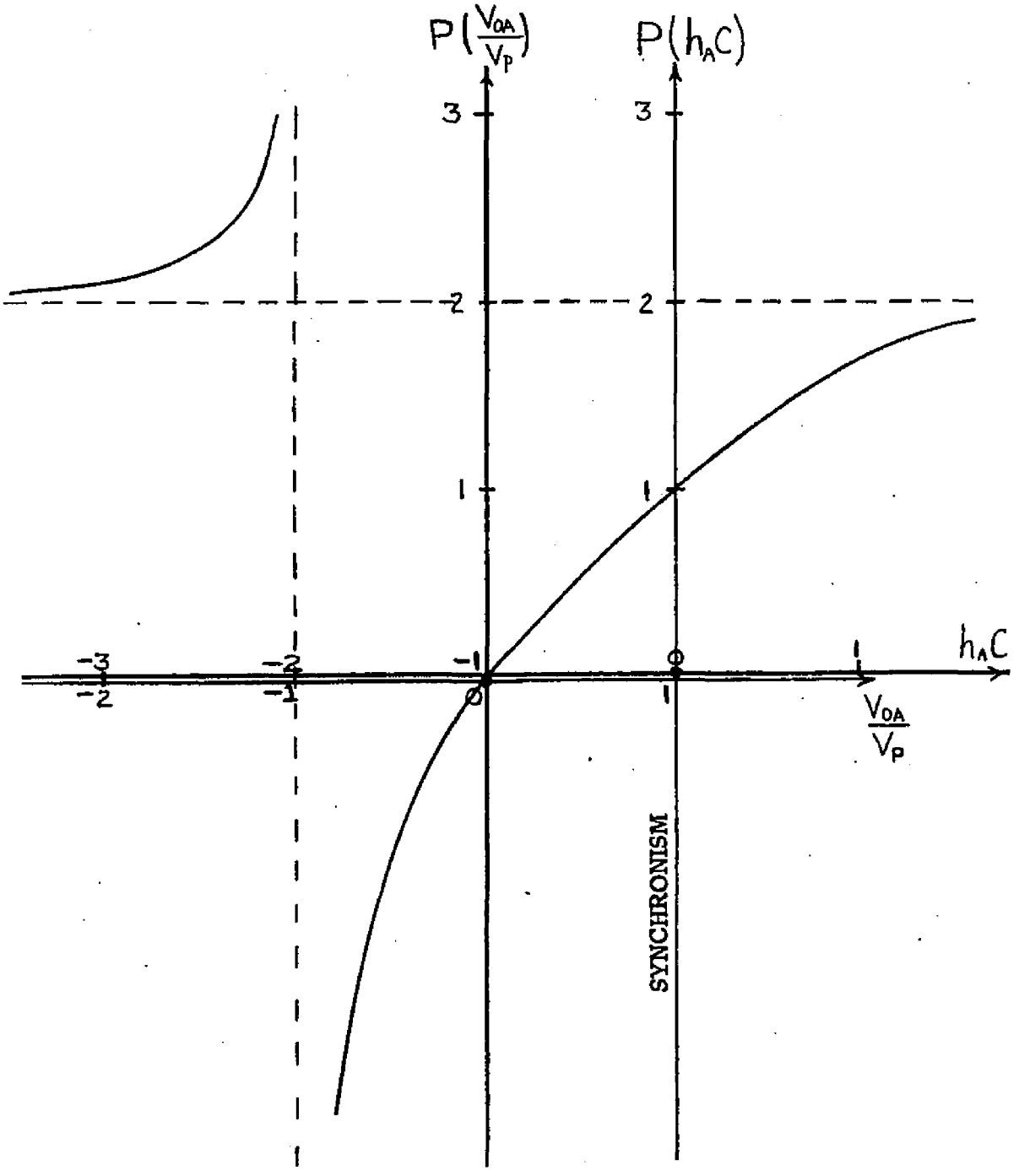

Figure 5.1 Synchronization function

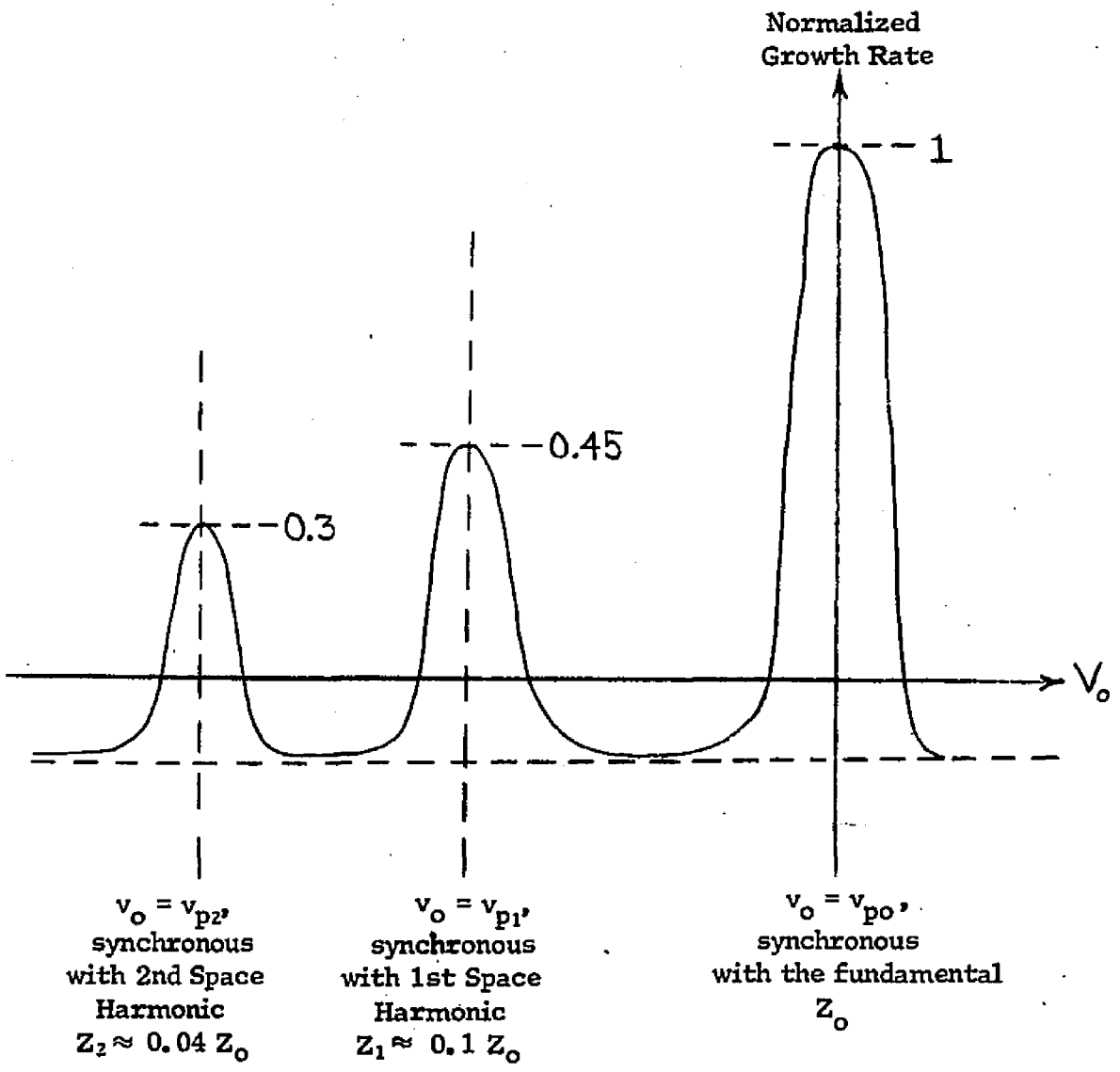

Figure 5.2 Illustrating the effect of space harmonic interaction as the mean drift velocity is varied

since the synchronization function is much smaller than one thus reducing the n^{th} space harmonic growth rate when v_{oA} is in near synchronism with the $(n+1)^{th}$ space harmonic.

5.2 Growing Mode Criteria

It is useful to determine the necessary and sufficient conditions for a convective instability (growing mode) to occur. This is done by applying several theorems from the analytic theory of continued fractions to the problem at hand.

Consider the polynomial

$$P(z) = Z^n + \delta_1 Z^{n-1} + \delta_2 Z^{n-2} + \cdots + \delta_n \,, \qquad (5\text{-}3)$$

where the complex coefficients are

$$\delta_k = p_k + j q_k \qquad (5\text{-}4)$$

The alternant of P(Z) is defined as

$$Q(z) = p_1 Z^{n-1} + j q_2 Z^{n-2} + p_3 Z^{n-3} + \cdots \qquad (5\text{-}5)$$

In general, the quotient of $\frac{Q(Z)}{P(Z)}$ has a J-fraction expansion of the form

$$\frac{Q(Z)}{P(Z)} = \cfrac{1}{C_1 Z + 1 + k_1 + \cfrac{1}{C_2 Z + k_2 + \cfrac{1}{C_3 Z + k_3 + \ddots + \cfrac{1}{C_n Z + k_n}}}} \qquad (5\text{-}6)$$

called the test fraction of P(Z). The coefficients of the test fraction, C_p and k_p, are listed in Table 5.1 as functions of p_k and q_k for the case n = 3 and may in general be found by an algorithm[48]. Stating a theorem due to Wall[49]

$$C_1 = \frac{a_{00}}{a_{01}}$$

$$C_2 = \frac{a_{11}^3}{\left[a_{11}\left(a_{02}a_{11} - a_{00}a_{13} - a_{01}a_{12}\right) + a_{00}a_{12}^2\right]}$$

$$C_3 = \frac{a_{11}}{C_2}\left(a_{13} + \left[\frac{a_{01}a_{11}a_{13} - a_{00}a_{12}a_{13} - a_{03}a_{11}^2}{a_{11}^2}\right] \cdot \left[\frac{a_{11}^2 a_{12} + C_2\left[a_{11}\left(a_{01}a_{13} - a_{03}a_{11}\right) - a_{00}a_{12}a_{13}\right]}{a_{11}\left(a_{02}a_{11} - a_{00}a_{13} - a_{01}a_{12}\right) + a_{00}^2 a_{12}}\right]\right)^{-1}$$

where $a_{00} = 1$

$a_{01} = jq_1$ $\quad a_{11} = p_1$

$a_{02} = p_2$ $\quad a_{12} = jq_2$

$a_{03} = jq_3$ $\quad a_{13} = p_3$

Table 5.1

Coefficients of the Test Fraction of P(Z)

Theorem: If P(Z) has a test fraction in which m of the C_p are negative and (n-m) of the C_p are positive, then m of the roots of P(Z) = 0 have positive real part and (n-m) have negative real part.

Therefore, the growing mode criterion is that there exist at least one negative C_p in the test fraction expansion of the dispersion equation.

5.3 Dominant Carrier Growing Mode Criterion

The growing mode criterion for the dominant carrier dispersion equation is too involved to study by hand; rather, several simpler cases will be studied. The first example, a trivial one that is presented in the second chapter, illustrates the method used. Consider the case when recombination lifetime is arbitrarily large, cold circuit attenuation is zero and the interaction is synchronous. Under these conditions equation (5-1) reduces to

$$S^3 + \beta_{CA} S^2 + \beta_{QA}^2 (1 + \lambda_{DA}^2 \beta_{eA}^2) S + j = 0 . \tag{5-7}$$

The coefficients of the test fraction are calculated to be

$$C_1 = \beta_{CA}^{-1} , \tag{5-8a}$$

$$C_2 = \frac{\beta_{CA}}{\beta_{QA}^2 (1 + \lambda_{DA}^2 \beta_{eA}^2)} , \tag{5-8b}$$

$$C_3 = - \frac{\beta_{QA}^6 (1 + \lambda_{DA}^2 \beta_{eA}^2)^3}{\beta_{CA}} . \tag{5-8c}$$

Inspection of the coefficients reveals that since β_{CA}, β_{qA}, λ_{DA}, and β_{eA}^2 are all positive real, two of the coefficients are always positive and the third is always negative. It is therefore concluded that for all possible values of the coefficients of equation (5-7) there are two roots with negative real part and one with positive real part as shown in Figure 2.5, for $\alpha_o = 0$.

The next case considered is that of the high resistivity semiconductor in which recombination lifetime is negligible. Under these conditions

equation (5-1) reduces to

$$S^3 + (\beta_{CA} + \alpha_o + j h_A) S^2 + \beta_{CA}(\alpha_o + j h_A) S + j P(h_A) = 0 . \quad (5\text{-}9)$$

The coefficients of the test fraction are calculated to be

$$C_1 = (\beta_{CA} + \alpha_o)^{-1} \quad (5\text{-}10a)$$

$$C_2 = \frac{\beta_{CA} + \alpha_o}{\beta_{CA}\alpha_o\left[1 + \left(\frac{h_A}{\beta_{CA}+\alpha_o}\right)^2\right]} , \quad (5\text{-}10b)$$

and

$$C_3 = \frac{\beta_{CA}\alpha_o\left[h_A^2 + (\beta_{CA}+\alpha_o)^2\right]}{P(h_A)C_2(\beta_{CA}+\alpha_o)\left[\beta_{CA}h_A - P(h_A)C_2\right]} . \quad (5\text{-}10c)$$

Inspection of the coefficients reveals that two of the roots always have negative real part and the third can have positive real part, if and only if

$$P(h_A)\, C_2 > \beta_{CA}\, h_A . \quad (5\text{-}11)$$

Since maximum gain is anticipated near synchronism it is reasonable to assume that $|h_A| << |\beta_{CA} + \alpha_o|$ which allows C_2 to be approximated as

$$C_2 \approx \frac{\beta_{CA} + \alpha_o}{\beta_{CA}\alpha_o} \quad (5\text{-}12)$$

resulting in the growing mode criterion

$$\frac{h_A}{P(h_A)} \leq \frac{\beta_{CA} + \alpha_o}{\beta_{CA}^2 \alpha_o} . \tag{5-13}$$

Below synchronism, $h_A < 0$, the condition is satisfied subject to the above approximation since $P(h_A) \approx 1$; however, above synchronism, $h_A > 0$, the condition is very severe and limits the maximum mean drift velocity for which a growing mode may exist to slightly above synchronism.

The last case considered is that of a semiconductor with negligible recombination lifetime operating under synchronous conditions. Equation (5-1) becomes

$$S^3 + (\beta_{CA} + \alpha_o)S^2 + \left[\beta_{CA}\alpha_o + \beta_{QA}^2(1 + \lambda_{DA}^2\beta_{eA}^2)\right]S + \alpha_o\beta_{QA}^2(1 + \lambda_{DA}^2\beta_{eA}^2) + j = 0. \tag{5-14}$$

The coefficients of the test fraction are calculated to be

$$C_1 = (\beta_{CA} + \alpha_o)^{-1}, \tag{5-15a}$$

$$C_2 = \frac{\beta_{CA} + \alpha_o}{\beta_{CA}\left[\alpha_o^2 + \beta_{CA}\alpha_o + \beta_{QA}^2(1 + \lambda_{DA}^2\beta_{eA}^2)\right]}, \tag{5-15b}$$

and

$$C_3 = \frac{\beta_{CA}(\beta_{CA} + \alpha_o)\left[\alpha_o^2 + \beta_{CA}\alpha_o + \beta_{QA}^2(1 + \lambda_{DA}^2\beta_{eA}^2)\right]}{\alpha_o\beta_{CA}\beta_{QA}^2(1 + \lambda_{DA}^2\beta_{eA}^2)\left[\alpha_o^2 + \beta_{CA}\alpha_o + \beta_{QA}^2(1 + \lambda_{DA}^2\beta_{eA}^2)\right] - C_2(\beta_{CA} + \alpha_o)} \tag{5-15c}$$

Inspection of the coefficients reveals that only C_3 may be negative under the condition

$$\alpha_0 \beta_{CA}^2 \beta_{QA}^2 (1+\lambda_{DA}^2 \beta_{CA}^2)\left[\alpha_0^2+\beta_{CA}\alpha_0+\beta_{QA}^2(1+\lambda_{DA}^2\beta_{CA}^2)\right]^2-(\beta_{CA}+\alpha_0)^2<0 . \quad (5\text{-}16)$$

Equation (5-16) relates the maximum carrier density, β_{QAM}^2 , for a growing mode to exist under synchronous conditions to the other semiconductor and circuit parameters. For most semiconductors and circuits

$$|\beta_{QA}^2| >> |\alpha_0^2 + \beta_{CA}\alpha_0| , \quad (5\text{-}17)$$

thus allowing equation (5-16) to be rewritten approximately as

$$\alpha_0 \beta_{CA}^2 \beta_{QA}^6 - (\beta_{CA}+\alpha_0)^2 < 0 \quad (5\text{-}18)$$

resulting in

$$\beta_{QAM} = \sqrt[6]{\frac{(\beta_{CA}+\alpha_0)^2}{\beta_{CA}^2\alpha_0}} . \quad (5\text{-}19)$$

Since maximum gain generally does not occur at synchronism equation (5-19) may be interpreted as giving an order of magnitude approximation for the maximum carrier density for a growing mode to exist.

Although only simplified cases have been presented, the general case may be calculated on the digital computer.

5.4 Excitation Matrix

In addition to knowing the exponential behavior of all the traveling waves one must know the excitation amplitudes and phases to be able to calculate the RF output. The RF amplitudes and phase of these waves are determined by

boundary conditions at the input; the output being considered perfectly terminated thus not exciting reflected waves. Most frequently these boundary conditions are: the sum of the electric field traveling waves at the input equals the applied electric field, there exist no RF current modulation at the input, and there exist no RF velocity modulation at the input. These conditions are

$$\sum_{i=1}^{n} E_i = E_{applied} \,, \tag{5-20a}$$

$$\sum_{i=1}^{n} J_i = 0 \,, \tag{5-20b}$$

and

$$\sum_{i=1}^{n} V_i = 0 \,. \tag{5-20c}$$

Since strong interaction occurs with only one space harmonic (linearized model) and assuming that the circuit is properly terminated thus not exciting a reflected wave allows n to be taken as three.

Each of the J_i and V_i may be expressed as functions of δ_i and E_i. From the electronic admittance of the dominant carrier case it is found that neglecting recombination lifetime

$$J_i = \frac{j\omega\epsilon\beta_{QA}^2 E_i}{\delta_i(\delta_i+\beta_{CA}) + \beta_{QA}^2(1+\lambda_{DA}^2\beta_{eA}^2)} \,. \tag{5-21}$$

Reducing equation (2-35) to the dominant carrier case results in

$$V_i = \frac{\eta_A^* \delta_i E_i}{V_{0A}\left[\delta_i(\delta_i+\beta_{CA}) + \beta_{QA}^2(1+\lambda_{DA}^2\beta_{eA}^2)\right]} \,. \tag{5-22}$$

The boundary condition equations (5-20) may be rewritten as

$$\begin{pmatrix} 1 & 1 & 1 \\ \left[\delta_1(\delta_1+\beta_{CA})+\beta_L^2\right]^{-1} & \left[\delta_2(\delta_2+\beta_{CA})+\beta_L^2\right]^{-1} & \left[\delta_3(\delta_3+\beta_{CA})+\beta_L^2\right]^{-1} \\ \delta_1\left[\delta_1(\delta_1+\beta_{CA})+\beta_L^2\right]^{-1} & \delta_2\left[\delta_2(\delta_2+\beta_{CA})+\beta_L^2\right]^{-1} & \delta_3\left[\delta_3(\delta_3+\beta_{CA})+\beta_L^2\right]^{-1} \end{pmatrix} \begin{pmatrix} E_1 \\ E_2 \\ E_3 \end{pmatrix} = \begin{pmatrix} E_{app} \\ 0 \\ 0 \end{pmatrix} \quad (5\text{-}23)$$

where

$$\beta_L^2 \triangleq \beta_{QA}^2\left(1+\lambda_{DA}^2\beta_{eA}^2\right). \quad (5\text{-}24)$$

5.4a Low Density Excitation Matrix

At low density, e.g., high resistivity semiconductor, such that $|\beta_L^2| \ll |\delta_1(\delta_1+\beta_{CA})|$, the excitation matrix reduces to

$$\text{E.M.} = \begin{pmatrix} 1 & 1 & 1 \\ \left[\delta_1(\delta_1+\beta_{CA})\right]^{-1} & \left[\delta_2(\delta_2+\beta_{CA})\right]^{-1} & \left[\delta_3(\delta_3+\beta_{CA})\right]^{-1} \\ (\delta_1+\beta_{CA})^{-1} & (\delta_2+\beta_{CA})^{-1} & (\delta_3+\beta_{CA})^{-1} \end{pmatrix} \quad (5\text{-}25)$$

Since each column of the matrix is a function of a single variable the determinant of the matrix may be written as

$$|\text{E.M.}| = \frac{(\delta_1-\delta_3)(\delta_2-\delta_3)(\delta_3-\delta_1)}{\delta_1\delta_2\delta_3(\delta_1+\beta_{CA})(\delta_2+\beta_{CA})(\delta_3+\beta_{CA})}. \quad (5\text{-}26)$$

Letting $\chi_i \triangleq \delta_i^{-1}$ and solving equations (5-23) for this case results in

$$E_i = \frac{\chi_j \chi_k (1+\chi_i \beta_{CA}) E_{app}}{(\chi_i - \chi_j)(\chi_i - \chi_k)} , \qquad (5\text{-}27)$$

for cyclic interchange of i, j, k = 1, 2, 3. E. G., consider the well known synchronous lossless case for which the roots of the dispersion equation (2-49) are $S_1 = +j$, $S_2 = 0.5(\sqrt{3} - j)$, and $S_3 = -0.5(\sqrt{3}+j)$. Substitution in equation (5-27) yields

$$E_1 = E_2 = E_3 = \frac{1}{3} E_{app} , \qquad (5\text{-}28)$$

i.e., the three traveling waves are excited equally and in-phase.

The solutions to the boundary condition equations (5-25) are not in general expressible in simple algebraic form as is the collisionless case result, equation (5-27). The effects of collision on the excitation amplitudes and phases have been determined by digital computer solution of equations (5-25) by Cramer's rule for a wide range of the parameters β_{CA} and α_0 . These results are plotted in Figures 5.3 and 5.4 for the synchronous case. The three waves are denoted by encircled numbers, one referring to the gaining wave, two referring to the slightly attenuating wave, and three referring to the strongly attenuating wave. At low collision frequency (the inertia dominated limit), $\log_{10}(\beta_{CA}) = -5$, each wave is equally excited, 1/3 E app, and they are in phase. As the cold circuit attenuation increases there is a slight difference in amplitude even at low β_{CA} . Increasing the collision wave number to 10^0 results in increased excitation of the gaining wave (one) and the circuit wave (two) while the strongly attenuating wave (three) is not excited. There is a wide range of collision frequencies for which the growing wave is

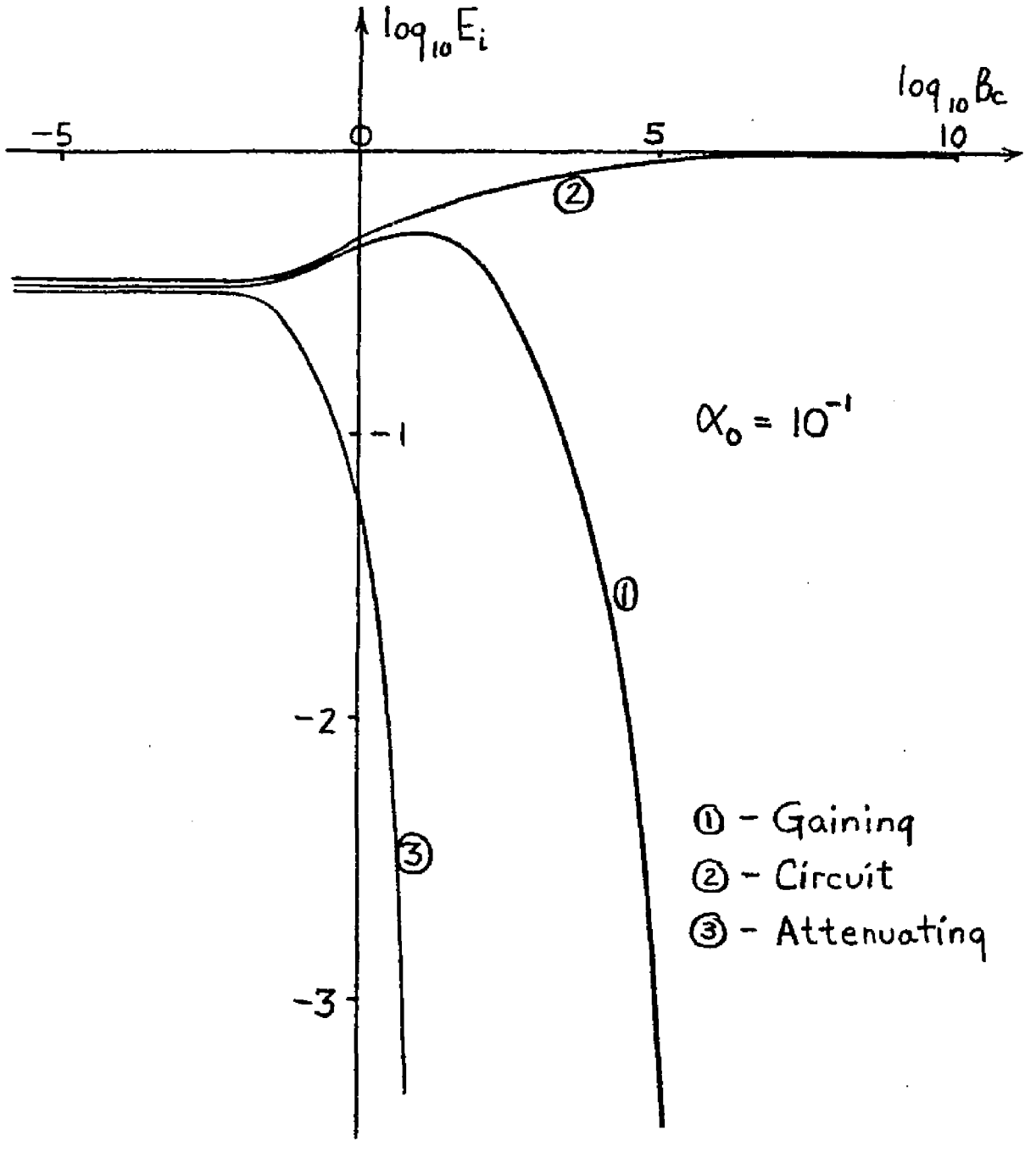
log10 Ei
log10 Bc
-5
0
5
10
-1
-2
-3
α0 = 10^-1
①
②
③
① - Gaining
② - Circuit
③ - Attenuating

Figure 5.3a

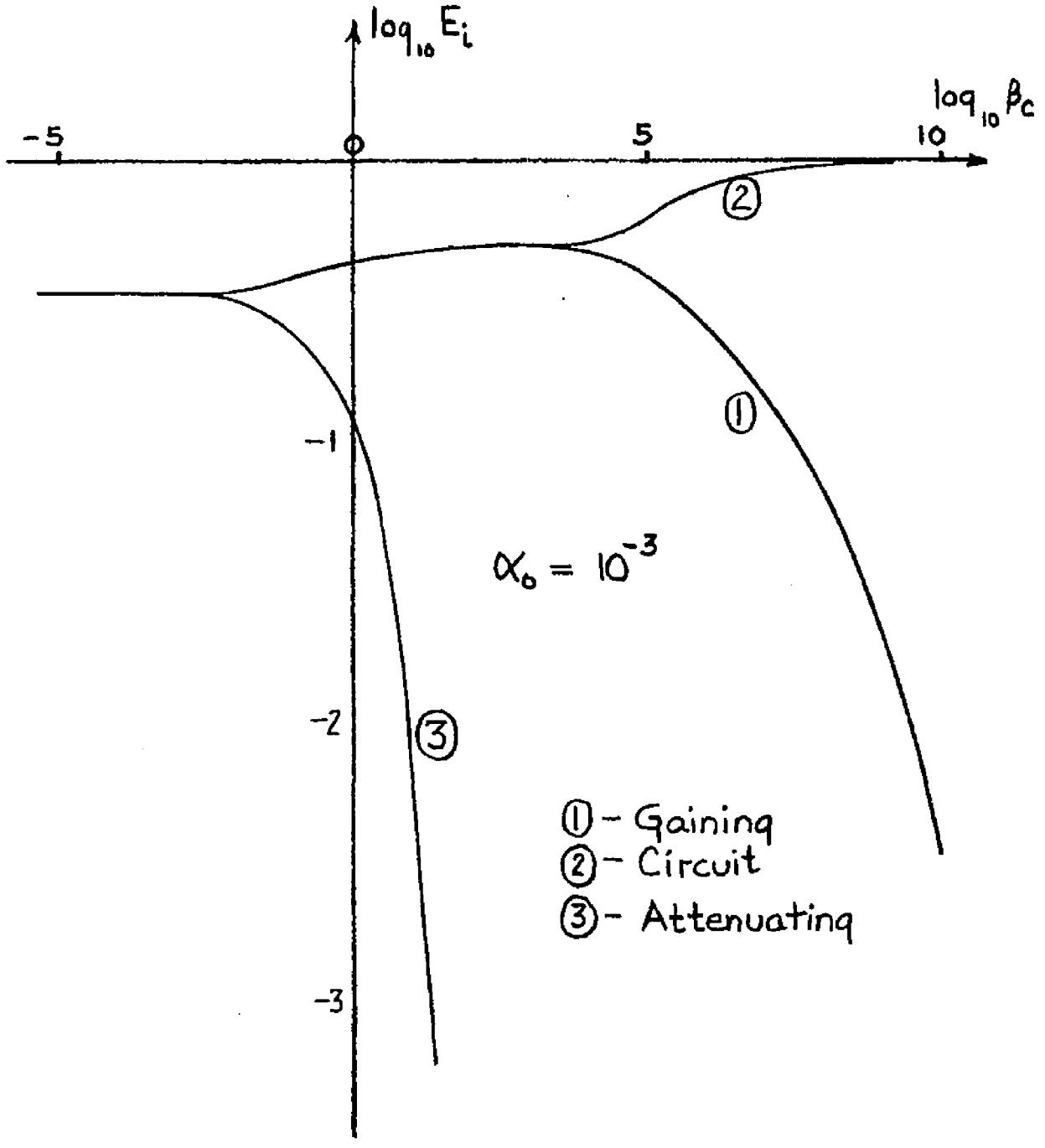
log10 Ei
log10 βc
-5
0
5
10
-1
-2
-3
②
①
③
α0 = 10^-3
① - Gaining
② - Circuit
③ - Attenuating

Figure 5.3b

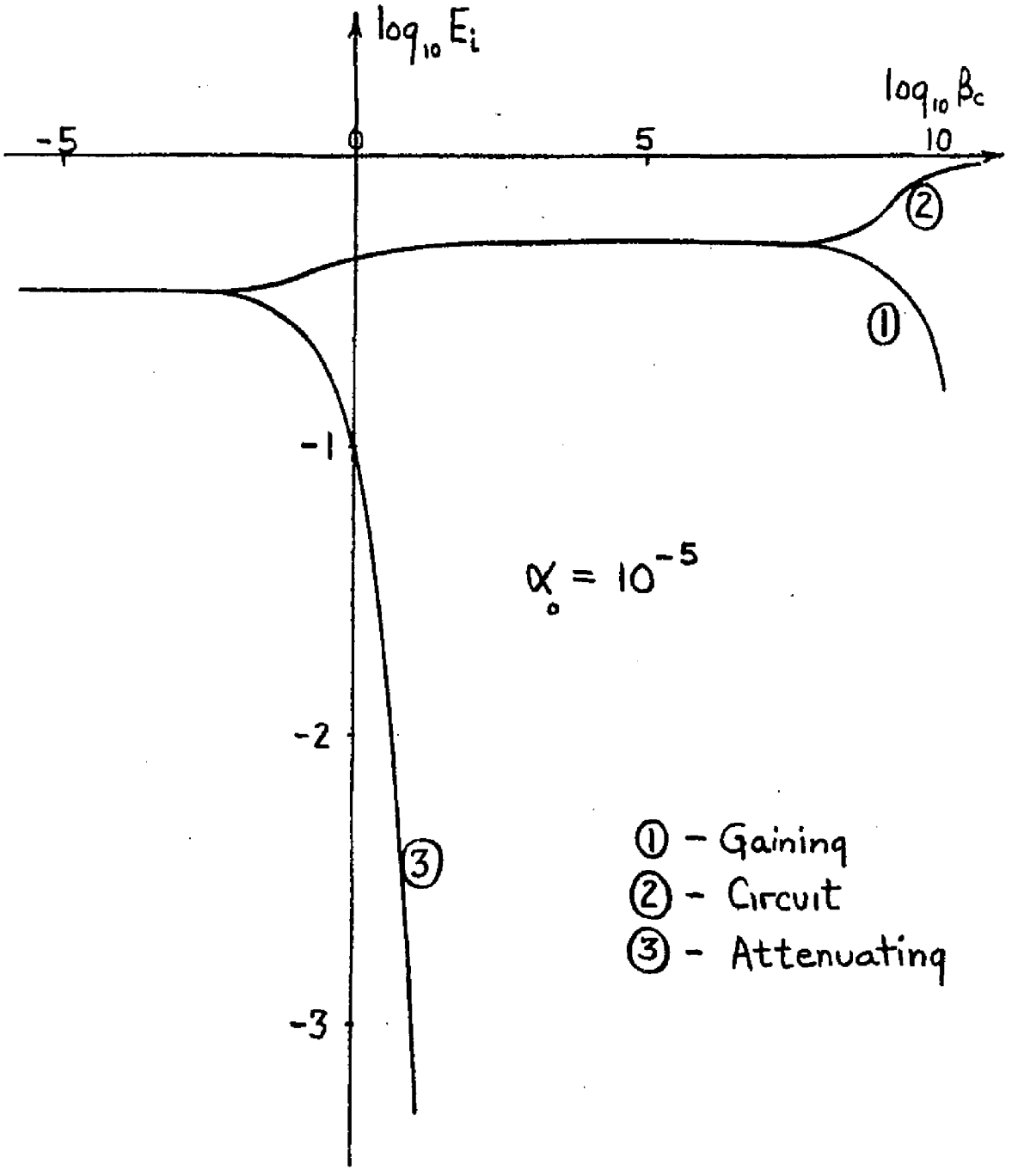
log10 Ei
log10 Bc
-5
0
5
10
-1
-2
-3
α0 = 10^-5
① - Gaining
② - Circuit
③ - Attenuating

Figure 5.3c

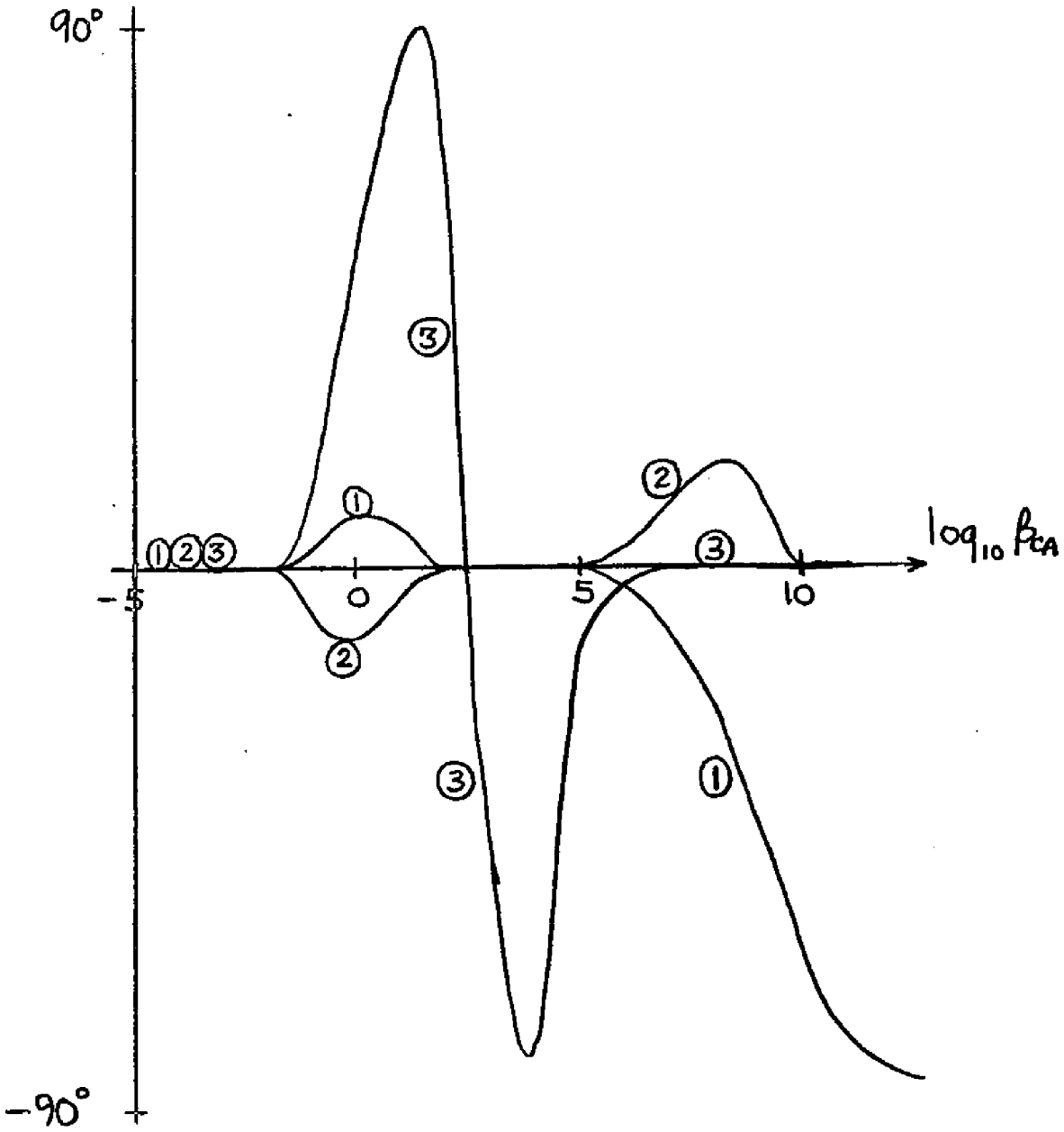

Figure 5.4 Excitation Phase

excited with larger amplitude, approximately 0.5 Eapp, than in the collisionless case, approximately 0.33 Eapp. In the collision dominated limit, $\log_{10}(\beta_{CA}) > 6$, only the circuit wave is strongly excited.

Study of asynchronous cases results in very much the same format and is therefore not presented.

5.4b High Density Excitation Matrix

At high density, low resistivity semiconductor, such that $|\beta_L^2| >> |\delta_i(\delta_i + \beta_{CA})|$ the excitation matrix reduces to

$$E.M. = \begin{pmatrix} 1 & 1 & 1 \\ \beta_L^{-2} & \beta_L^{-2} & \beta_L^{-2} \\ \delta_1\beta_L^{-2} & \delta_2\beta_L^{-2} & \delta_3\beta_L^{-2} \end{pmatrix} \qquad (5\text{-}29)$$

where because of the approximation made the determinant of the excitation matrix is non-zero, i.e., row two of the matrix is not identically but rather approximately a multiple of row one. The magnitude of the strongly attenuating root (three) usually far exceeds the magnitude of either the gaining wave root or the slightly attenuating wave, resulting in the amplitudes of one and two far exceeding the amplitude of three. Equation (5-29) therefore reduces to the 2x2 matrix yielding $E_1 = E_2 = 1/2$ Eapp, all in phase. This behavior is very similar to the low density case where the collision wave number is in the range 10^1 to 10^5.

5.5 Conclusion

The range of validity of the perturbational solution to the dominant carrier dispersion equation was extended to include highly asynchronous operation. Topics from the analytic theory of continued fractions were

reviewed and used to derive a growing mode criterion for several simplified cases indicating that high resistivity materials (resistivity dependent on collision frequency and cold circuit attenuation) should be studied numerically. The effects of collisions, cold circuit attenuation and carrier number density on the relative excitations of the traveling waves were studied revealing the necessity of not making the collision dominated assumption. For high resistivity materials it was shown that the modal excitation is predominantly determined by the collision frequency. For low resistivity materials the strongly attenuating mode is not excited while the growing and slightly attenuating modes are equally excited in phase.

Having considered these topics the numerical evaluation of device gain may now be undertaken.

CHAPTER SIX - NUMERICAL EVALUATION OF THE GAIN OF DEVICES UTILIZING THE INTERACTION BETWEEN SLOW ELECTROMAGNETIC WAVES AND DRIFTING CARRIERS IN A SEMICONDUCTOR

The purpose of this chapter is to outline numerical methods used in studying the interaction between slow electromagnetic waves and drifting carriers in semiconductors, present numerical results and compare them with the analysis of Sumi [50], Zotter [51], and Vural and Steele [52]. Numerical results will be compared with a recent experiment performed by Sumi [53] using Indium Antimonide at liquid nitrogen temperature.

A new numerical method, based upon the analytic theory of continued fractions, will be developed to circumvent difficulties encountered with roundoff error in present methods.

6.1 Numerical Methods

Equations developed in the previous chapters were solved by digital computer as outlined in Figure 6.1, a flow chart of the programs used. The detailed programs are listed in Appendix Three. The program is divided into three main sections; evaluation of slow wave circuit dispersion characteristics, evaluation of the dominant carrier dispersion equation coefficients from both semiconductor data and circuit dimension, and calculation of device gain vs. frequency and mean carrier velocity.

The determinantal slow wave circuit dispersion equation (3-10) is solved using the interval halving method. It is known that the solution, if it exists, must be bounded by 0+ and π- therefore, a trial value equal $(\frac{\pi}{2})$ is tested as a possible solution to (3-10). Since the terms in the series expression for $\chi(\theta_{TEST})$ decrease as fast as $Sa^2(x)$ forty terms were

COMPUTER PROGRAM FLOW CHART

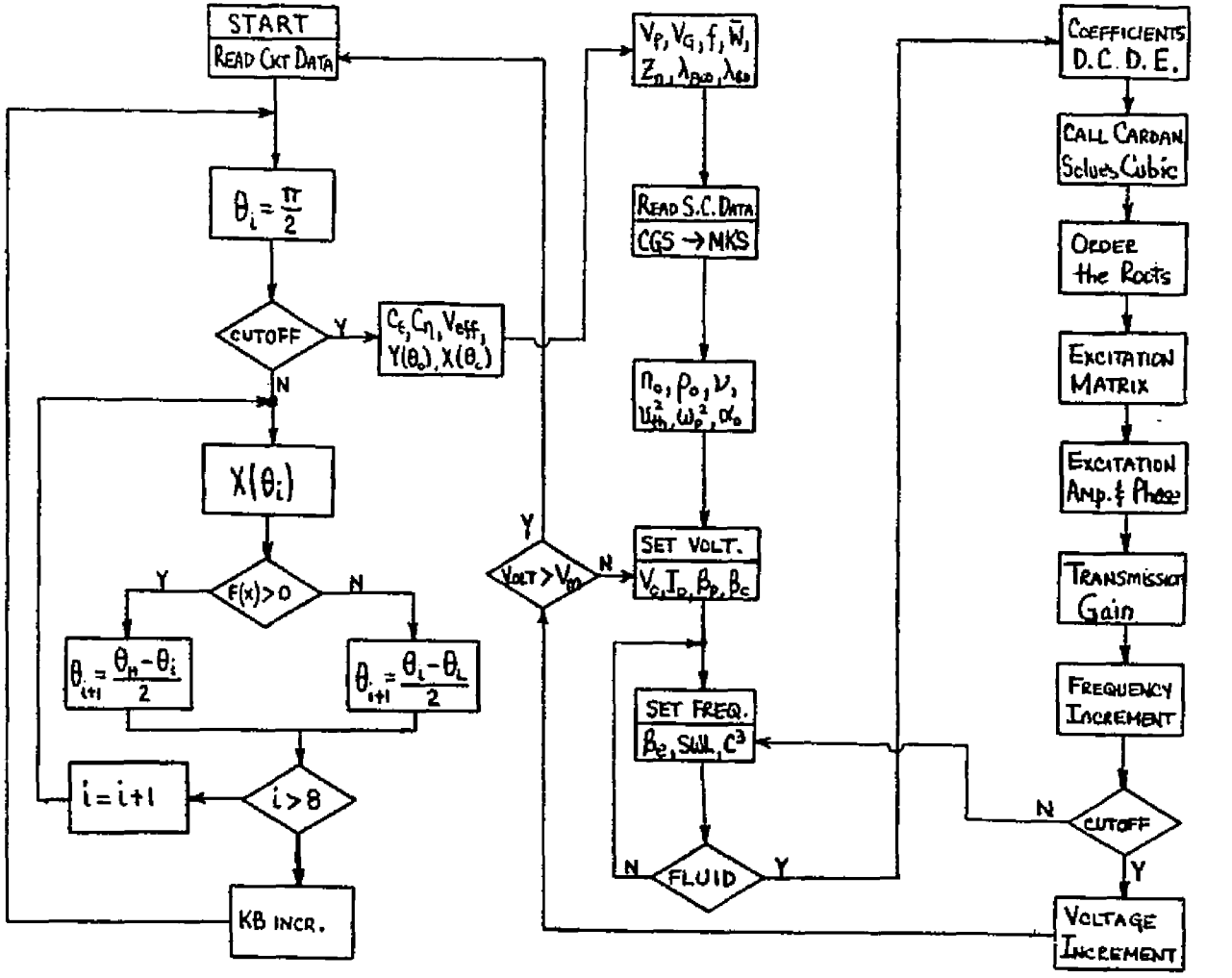

Figure 6.1

required to insure correct evaluation of $X(\theta_{TEST})$ to eight significant figures. The function $f(k,\theta_{TEST}) = \tan(ka)\tan(kb)X(\theta_{TEST}) - \tan^2\left(\frac{\theta_{TEST}}{2}\right)$ was tested to determine its sign. Two points were then selected, either $\theta_1 = 0+$ and $\theta_2 = \theta_{TEST}$ or $\theta_1 = \theta_{TEST}$ and $\theta_2 = \pi-$, such that $f(k,\theta_1)f(k,\theta_2) < 0$. The process was then repeated eight times until θ_o was known within one degree. This process required 2.6 seconds of machine $f(k,\theta_1)f(k,\theta_2)$ the IBM 360/50. The effective dielectric constant, effective intrinsic impedance, and the effective intrinsic velocity were then evaluated at θ_o.

The coefficients of the dominant carrier dispersion equation were then evaluated. The phase velocity, group velocity, frequency, stored energy per period and the interaction impedance were calculated utilizing the results of the first part of the program. Data regarding the semiconductor was read and used to calculate the remaining coefficients.

For each data point the density was checked to insure fluid behavior; i.e. the slow wavelength was compared to the Debye wavelength. The roots of the dominant carrier dispersion equation were calculated using Cardan's method due to Tartaglia [54]. It was necessary to rewrite this method to avoid excessive roundoff error. The roots were then ordered by descending real parts and used to evaluate the elements of the excitation matrix. The amplitude and phase of excitation of each wave were calculated and used to compute the overall device gain which was printed in table form.

Modifications of the above program were written to allow the computation of individual sections of the main program. The results of such a program are presented in the next section.

6.2 Numerical Solutions of the Perturbed Dominant Carriers Dispersion Equation

Equation (2-55) was solved as outlined above. The results are presented graphically in Figures 6.2a and 6.2b. It is seen that the effects of space charge and cold circuit attenuation are to appreciably reduce the overall growth rate. When the carrier velocity is optimized the growth rate increases as shown in Figures 6.3a. b amd c while maintaining basically the same behavior. It is seen that in the collision dominated limit the optimum velocity is near synchronism.

6.3 A Numerical Example

The usefulness of the growing mode criteria is demonstrated by the following numerical example. Consider the following device; 10^{12} collisions/second, 10db/sec cold circuit attenuation, 10 cm/sec phase velocity, 1 ohm interaction impedance such that C=1.0, and 10^{8} sec^{-1} excitation frequency. Equation (5-1) is solved by digital computer as the drift velocity is varied from one to twice the phase velocity and is plotted in Figure 6.4. It is noted that the net growth rate changes very rapidly about synchronism. Applying the growing mode criterion (5-13) to the problem at hand it is seen that net growth is possible for $h \leq .0376$.

Furthermore, although the net growth rate becomes exceedingly small it does extend to velocities well below synchronism; e.g. in the above case to $V_o = 0.5\ V_p$.

6.4 Comparison With Other Analytical Results

In a recent paper Sumi [55] performs a two dimensional analysis revealing the possibility of microwave amplification by the interaction of slow electromagnetic waves and drifting carriers in a semiconductor. His approach is to make a collision dominated assumption for a semiconductor

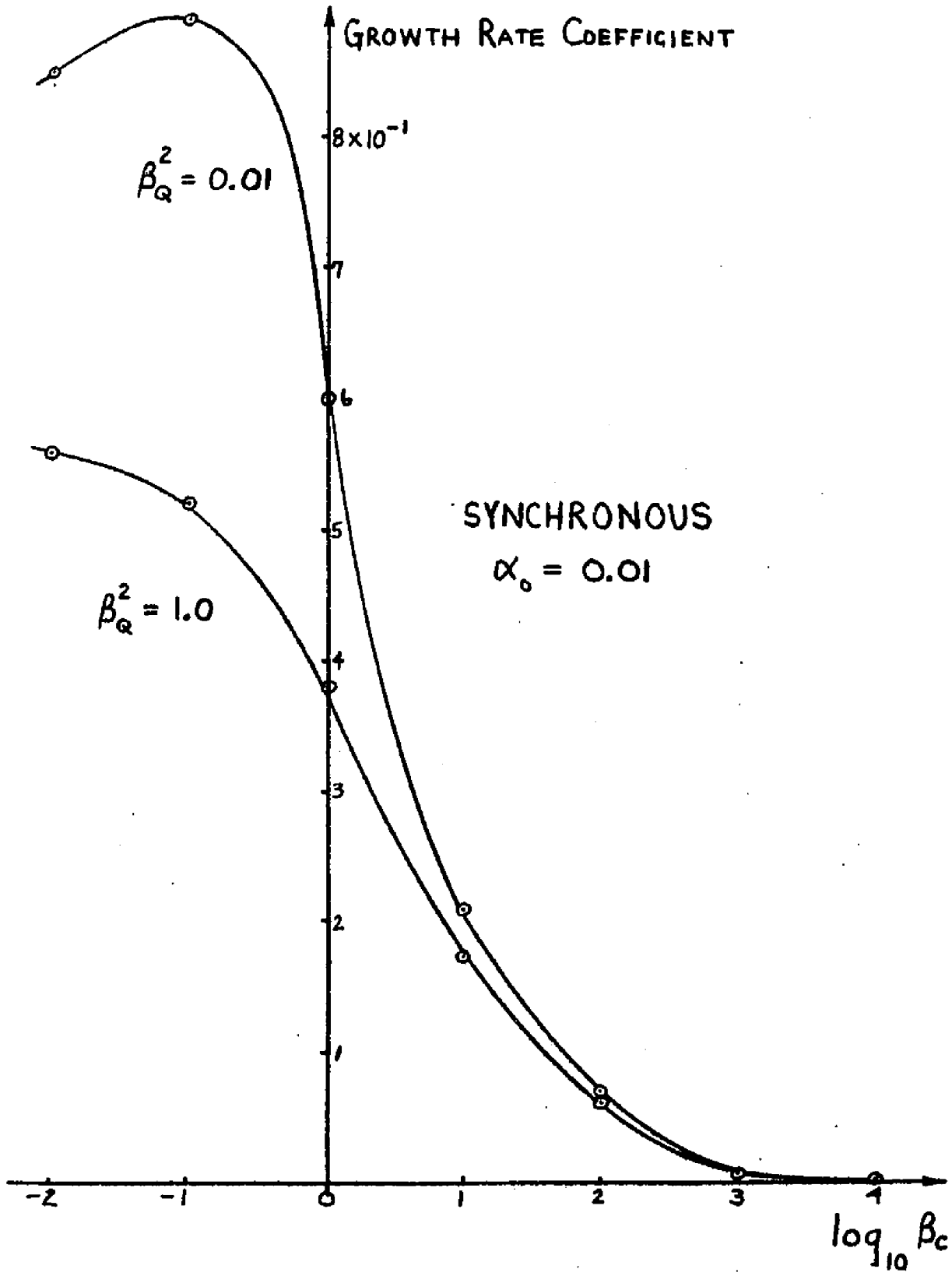
GROWTH RATE COEFFICIENT
8×10^{-1}
7
6
5
4
3
2
1
$\beta_Q^2 = 0.01$
$\beta_Q^2 = 1.0$
SYNCHRONOUS
$\alpha_0 = 0.01$
-2
-1
0
1
2
3
4
$\log_{10}\beta_c$

FIGURE 6.2a

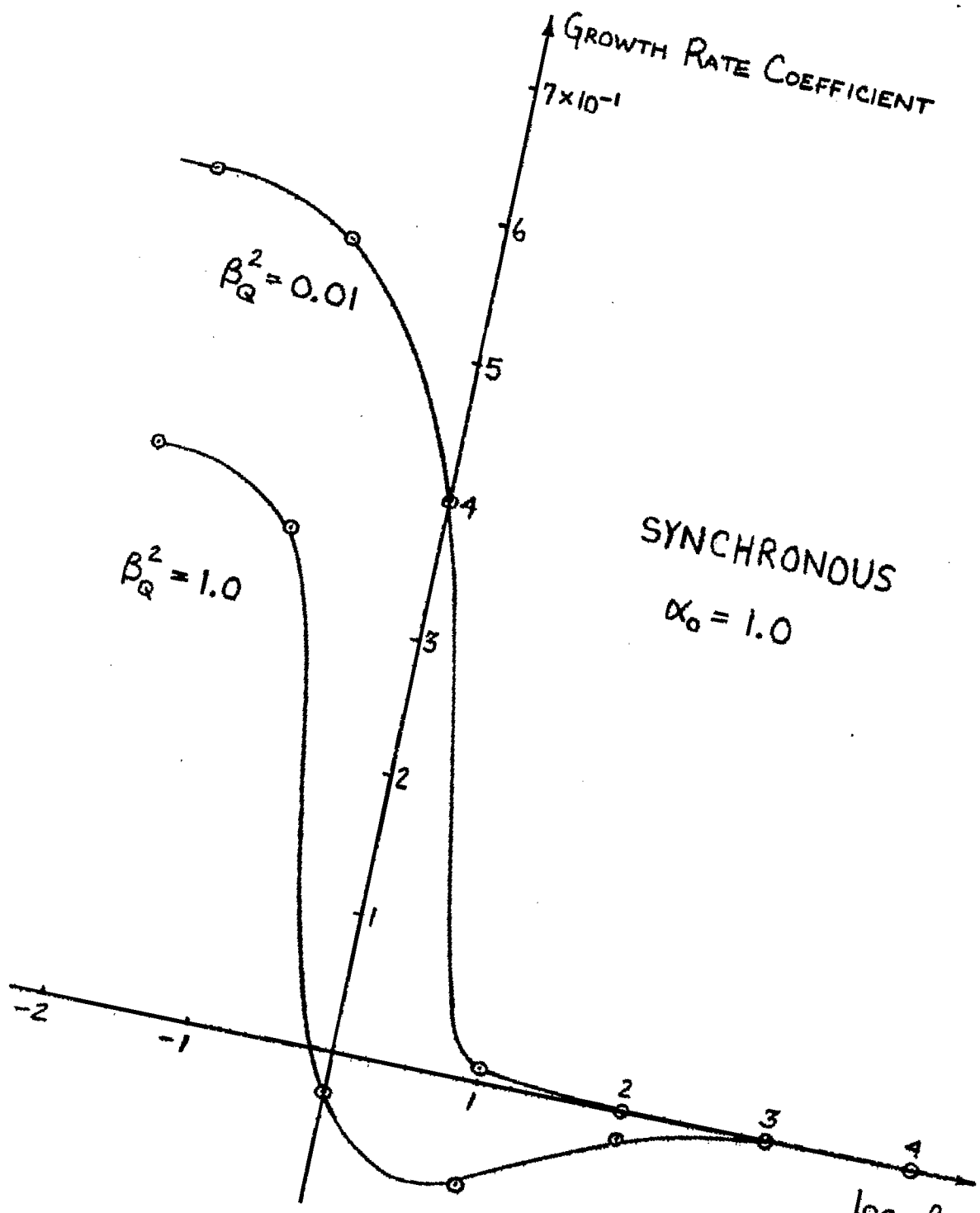
GROWTH RATE COEFFICIENT
7×10-1
6
5
4
3
2
1
$\beta_Q^2 = 0.01$
$\beta_Q^2 = 1.0$
SYNCHRONOUS
$\alpha_0 = 1.0$
-2
-1
1
2
3
4
$\log_{10} \beta_c$

FIGURE 6.2b

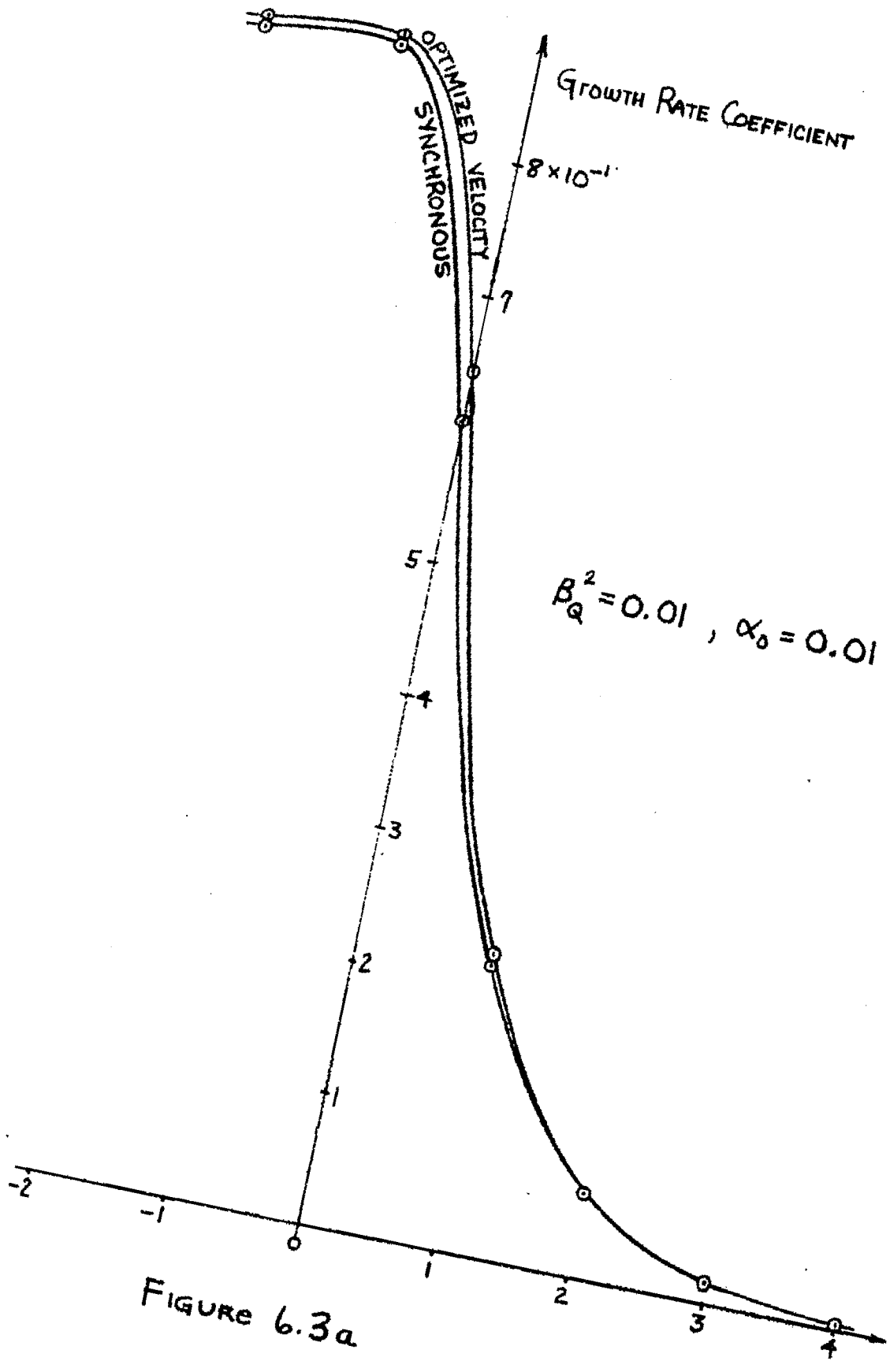
OPTIMIZED SYNCHRONOUS VELOCITY
GROWTH RATE COEFFICIENT
8×10^{-1}
1
5
4
3
2
1
-2
-1
1
2
3
4
$\beta_e^2 = 0.01$, $\alpha_0 = 0.01$

FIGURE 6.3a

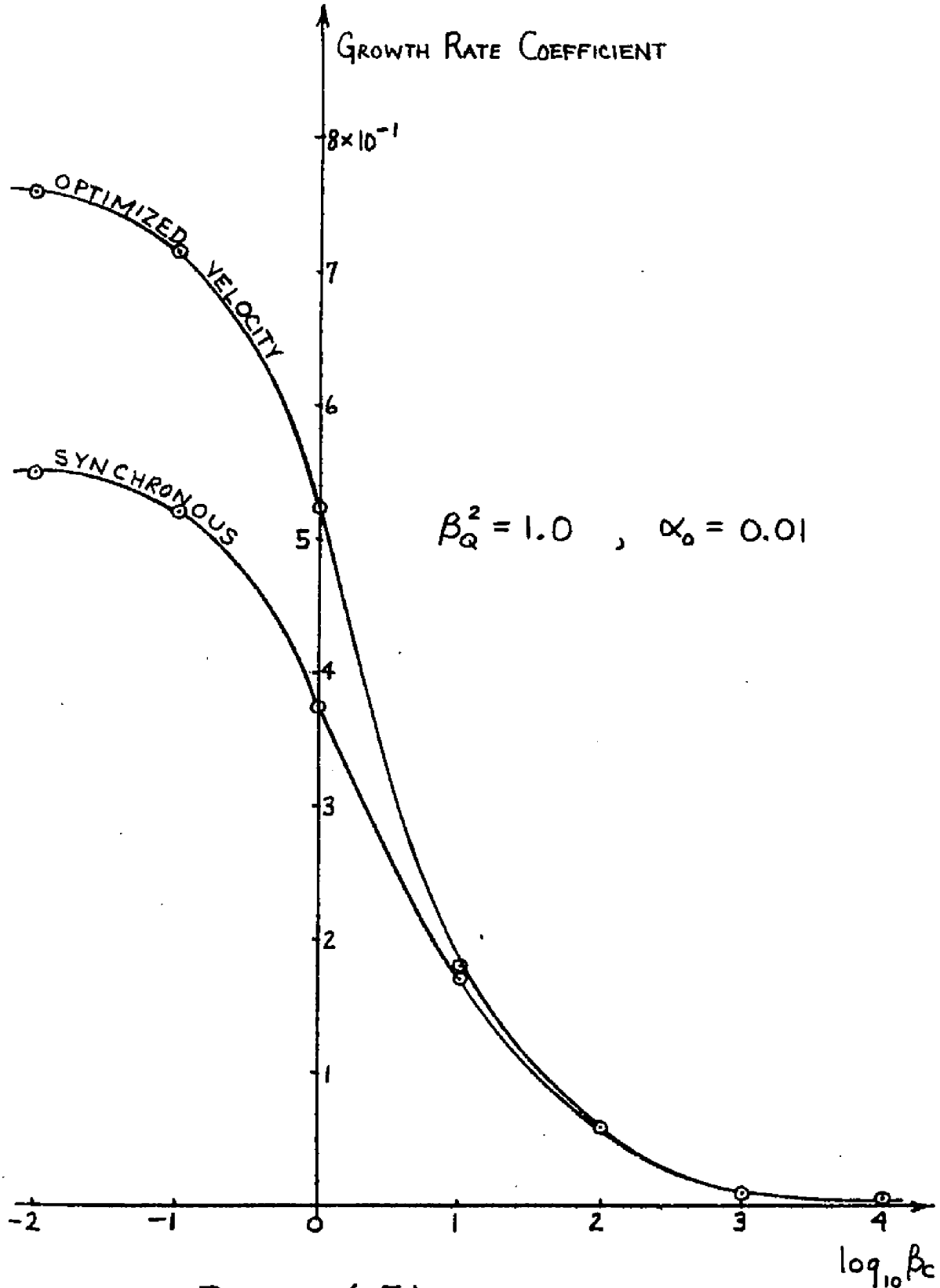
GROWTH RATE COEFFICIENT
8×10⁻¹
7
6
5
4
3
2
1
OPTIMIZED VELOCITY
SYNCHRONOUS
$\beta_Q^2 = 1.0$, $\alpha_0 = 0.01$
-2
-1
0
1
2
3
4
$\log_{10}\beta_c$

FIGURE 6.3b

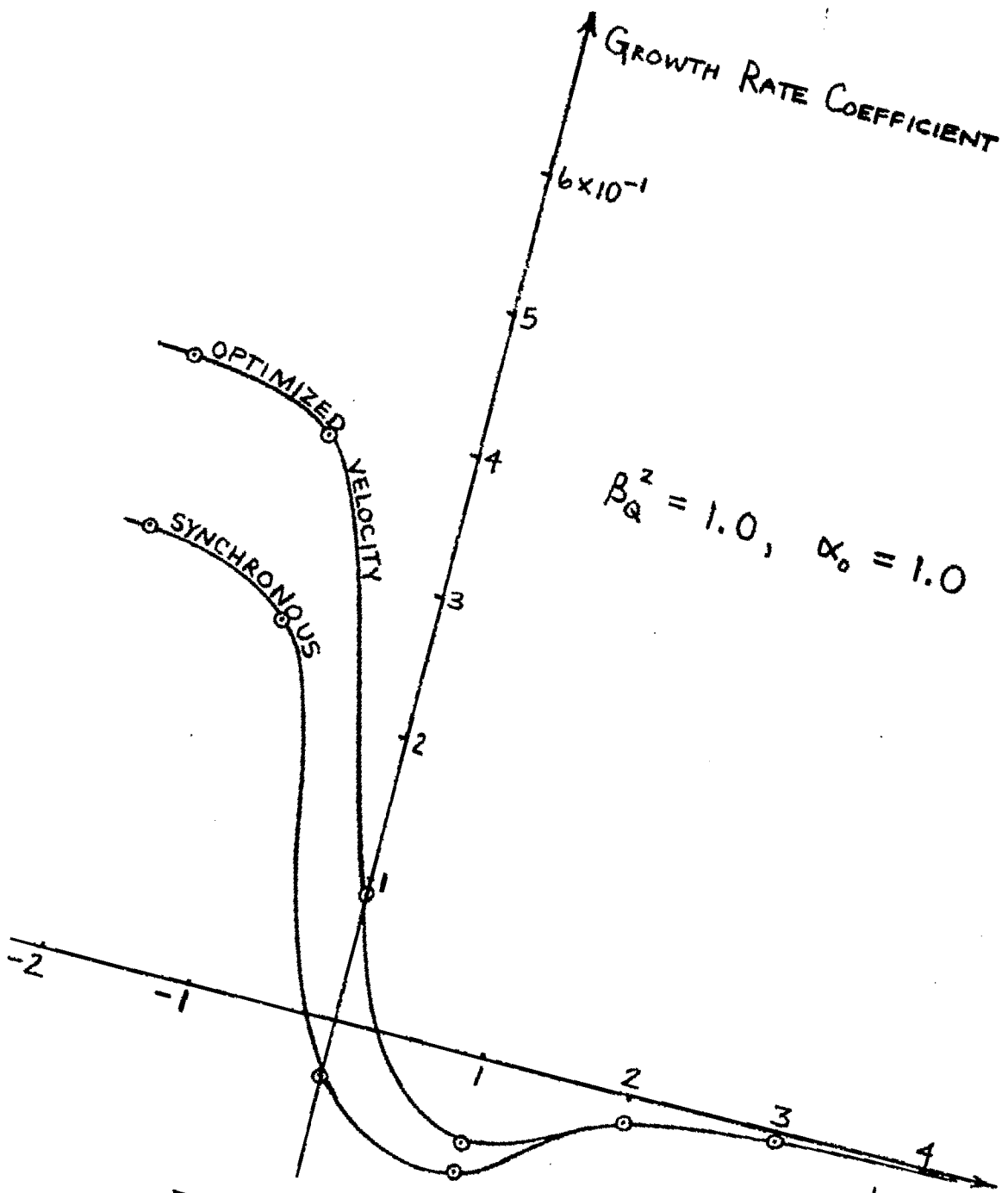
GROWTH RATE COEFFICIENT
6x10⁻¹
5
4
3
2
1
OPTIMIZED VELOCITY
SYNCHRONOUS
$\beta_Q^2 = 1.0, \quad \alpha_0 = 1.0$
-2
-1
1
2
3
4
$\log_{10} \beta_c$

FIGURE 6.3c

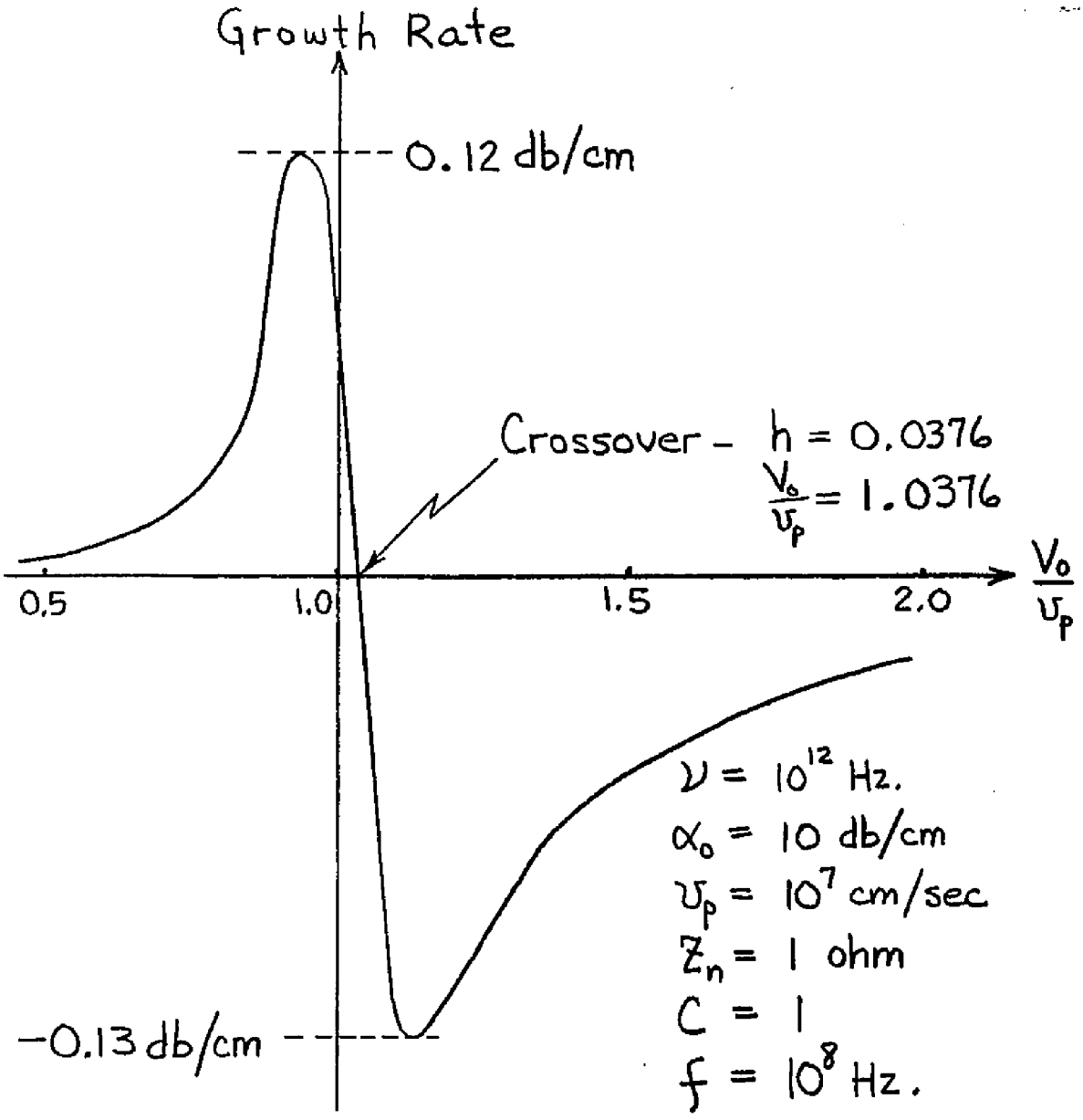

Figure 6.4 Numerical Example

material, calculate its surface admittance, and then equate this to the surface admittance of a developed helix leading to a dispersion equation. A report by Zotter [56] has revealed that Sumi's paper contained several algebraic errors. Zotter subsequently corrected these and numerically evaluated a number of interactions with different materials. His calculations predict gains from 400 to 2000 db/mm for the various materials, a result that has not been experimentally observed.

An extension of the above theory was made by Vural and Steele [57]. Their analysis consists of studying the interaction with a generalized admittance wall rather than the particular one used by Sumi. Unfortunately, for several slow wave circuits of interest, e.g. the stub-loaded meander line, the admittance may not be calculated from the lowest order fields; i.e. when calculated in this manner the admittance is infinite, since for the lowest order fields $H_y=0$.

Sumi [58] has most recently performed an experiment using Indium Antimonide at liquid nitrogen temperature in which he observed a change in transmission through a meander line circuit; i.e., without current in the semiconductor he observed 13 db circuit attenuation at 2 GHz while in the presence of current the circuit attenuation was between 13 and 12 db as shown in Figure 6.5. Using the above mentioned computer programs to calculate the device gain results in a much closer approximation to the experimental results, than any previous method as shown in the figure. It is noted that several of the experimental parameters not supplied by Sumi were estimated and are tabulated in the figure. This model is the only one of the above that takes into account excitation amplitudes and phases of the various modes.

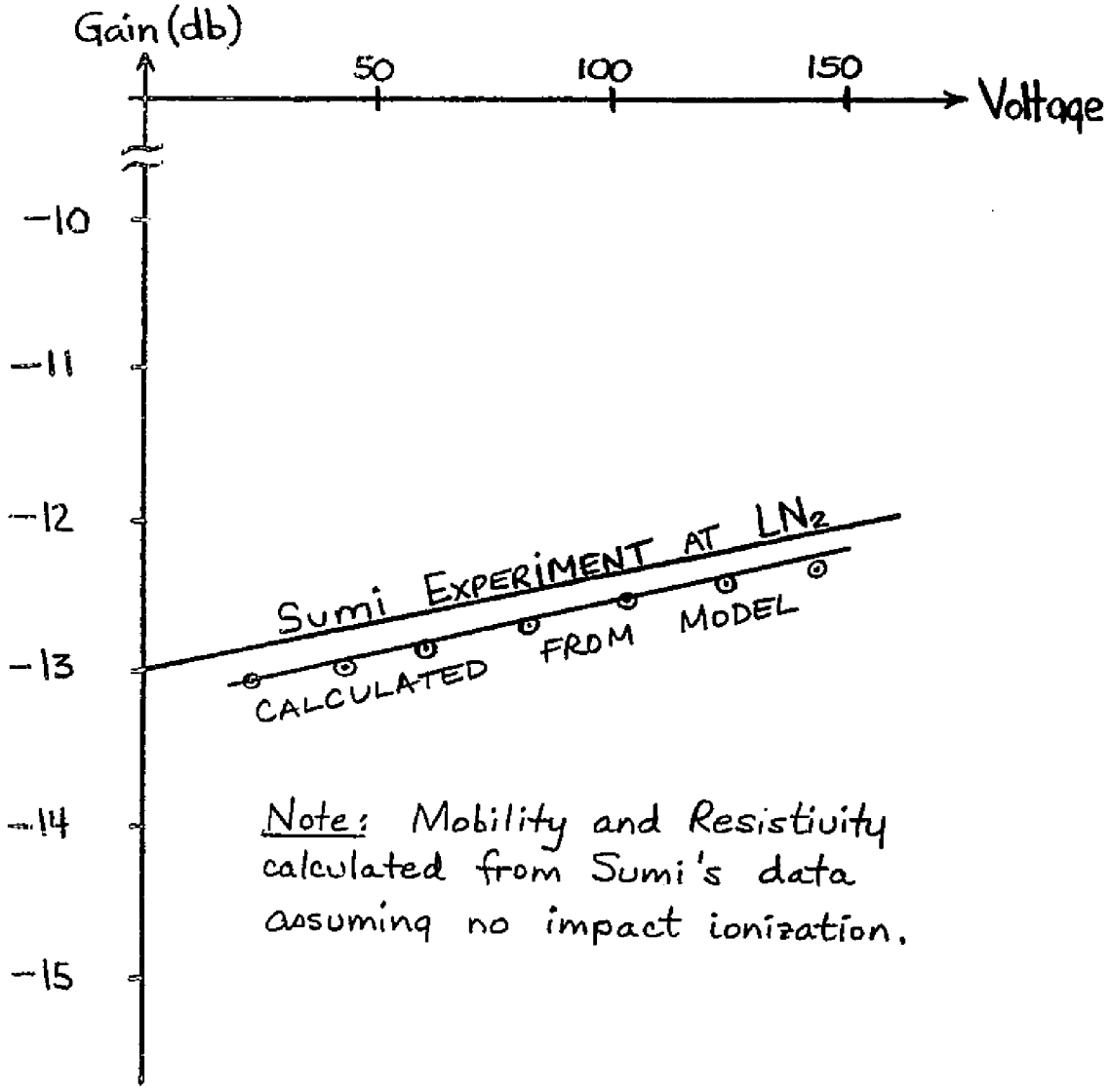

Figure 6-5 Comparison of Numerical Results of One Dimensional Model And Sumi's Experiment.

(circuit width – 640 mils, line thickness – 0.6 mil, dielectric thickness – 50 mils, dielectric permittivity – 16.8, Area – 400 $mils^2$, length – 0.5 cm, α_o – 13 db/cm, $m^* = 0.0132\, m_e$)

6.5 Alternate Numerical Method

Solutions to algebraic equations of degree less than or equal to four are known [59]. These solutions are not in general suitable for machine calculation because excessive roundoff error may propagate through the solution and invalidate its accuracy. Numerical techniques have been developed by Hamming [60] and Richter [61] in which regions of the solution plane are searched along constant phase contours. These techniques, although allowing solution of equations of higher degree, involve the evaluation of the polynomial functions at grid points of decreasing size and are therefore time consuming.

A new method is presented that allows one to generate an equivalent set of equations for the imaginary and real parts of the roots of the original algebraic equation of arbitrary degree such that these equations are separated and linear; i.e., the equation $P^n(S) = 0$ with complex roots $\Gamma_1, \Gamma_2, \cdots \Gamma_n$, will be transformed into a set of equations for $Re(\Gamma_1)$, $Re(\Gamma_2) \ldots Re(\Gamma_n)$, and another set of equations for IM (Γ_1), Im (Γ_2)--- Im (Γ_3).

The required transformation involves generating the coefficients of the test fraction of $P^n(s)$. (See Chapter 5 Section 2) The new set of equations are formed by equating the numerators and denominators of the test fraction to zero, (when possible) and looking for changes in sign of the test fraction coefficients. This method is illustrated by example in Appendix Four.

6.6 Conclusions

The methods used to solve the dominant carrier dispersion equation were outlined and found to require special care to avoid excessive roundoff error. Numerical results were presented for the synchronous and asynchronous cases showing that as the collision wave number, reduced plasma frequency wave number, or cold circuit attenuation increases the

growth rate decreases; in some cases growth does not exist at all.

Examination of Figure 6.2a reveals that for the semiconductor region, $\log_{10} \beta_{CA} \cong 3$, collision damping is the predominant loss mechanism. For semiconductors, $\beta_c \propto T^n$ where n is from 1 to 2.5. Operation at liquid nitrogen temperature decreases $\log_{10} \beta_c$ by the factor $n \log_{10}\left(\frac{293}{77}\right) = 0.58\,n$.

For low resistivity materials the carrier density decreases with temperature therefore decreasing the reduced plasma frequency wave number. The result of operation at liquid nitrogen temperature is a significant increase in the growth rate. While operation at still lower temperature is desirable from the above viewpoints it presents insurmountable difficulties with thermal expansion of the slow wave circuit.

The effect of varying the mean carrier drift velocity was studied showing that the growing mode exists well below synchronism although its growth rate becomes exceedingly small; whereas the growing mode does not exist above synchronism.

Experimental results obtained by Sumi using InSb at liquid nitrogen temperature were compared to values theoretically predicted by this model and found to be in close agreement. The discrepancy between experimental and theoretical values at low voltage is caused by the perturbational assumption $|sC| \ll 1$ not being met.

A new numerical method to be used as an alternative to presently available methods, of use in solving n^{th} degree algebraic equations typically found in wave interaction problems, was derived. This method, illustrated by example in Appendix Four, allows the separate refinement of the real and imaginary parts of a solution.

CHAPTER 7 - SUMMARY AND CONCLUSIONS

The purpose of this chapter is to complete this dissertation by summarizing and drawing conclusions regarding its contents and outlining suggestions for further work

The main subject studied within the dissertation is the interaction of drifting carriers in a semiconductor and slow electromagnetic waves. A one dimensional model for the interaction has been developed including the effects of carrier-lattice collisions, carrier recombination, space charge, diffusion, mean carrier drift velocity and slow wave circuit configuration through its propagation constant and interaction impedance. The model, allowing for two mobile carrier species, results in a sixth degree algebraic equation for growth rates of the various modes. The dominant carrier case which is reduceable to the Pierce model of the vacuum traveling wave tube was studied first by root locus technique and then numerically. The root locus technique surprisingly has not been previously applied to wave interaction problems where it readily reveals the wave dependence on a given parameter.

Another subject studied within the dissertation is the development of a slow wave circuit capable of achieving the required velocity for which a "strong" interaction occurs. A circuit that satisfies the necessary criteria is the stub loaded meander line; a planar evapora-

tion deposited structure constructed on layered media. Theory developed to characterize this device, based on a uniform interline electric field, has been experimentally verified at frequencies up to approximately one-half the cutoff frequency; however, difficulty has been encountered in exciting the forward mode at the higher frequencies. Further work directed toward multiple line excitation is required including the investigation of techniques to lower the VSWR. Extension of the uniform interline electric field approximation to include higher describing functions should improve the predicted dispersion characteristics near cutoff. This may be accomplished by applying a variational technique to refine the interline electric field as outlined below:

1. Express the interline electric field as a traveling wave in the plane of the circuit with a constant and parabolic dependence, i.e.

$$E_z\Big|_{x=0} = \begin{cases} \left(E_0 + E_2 z^2 + \dots\right) e^{-jm\theta_0} e^{-j\varphi}, & \text{between the lines,} \\ 0, & \text{on the lines.} \end{cases}$$

2. Search for the particular set of coefficients, E_0, E_2, ... , that minimizes the stored energy per period while maintaining a constant interline voltage.

3. Having obtained these coefficients as a function of θ_o, calculate $X(\theta_o)$ and the resulting dispersion characteristics.

It is anticipated that the dispersion characteristics so found will more closely model the circuit performance since the interline electric field has been more realistically selected. Unfortunately, the search time rapidly increases with the number of coefficients involved.

The perturbational solution of the dominant carrier dispersion equation was studied by numerically evaluating its solution for various semiconductor materials using the stub loaded meander line as the slow wave circuit. Experiments to verify the one dimensional model have been undertaken using Germanium at room temperature. The technique is to look for a change in RF transmission thru the circuit when the semiconductor carriers are drifted as shown in Figure 7.1. These experiments have not resulted in the observation of the interaction because the small transmission change (less than 0.1 db) is masked by spurious effects; e.g. mixer noise, multiple internal RF reflections, current pulse top ripple, etc.

Numerical analysis indicates that increased gain is obtainable by operation at higher frequency and lower temperature. To operate at higher frequency requires a decrease in the dimensions of the slow wave circuit demanding photolithographic technology for construction that is not yet available. Although this difficulty is

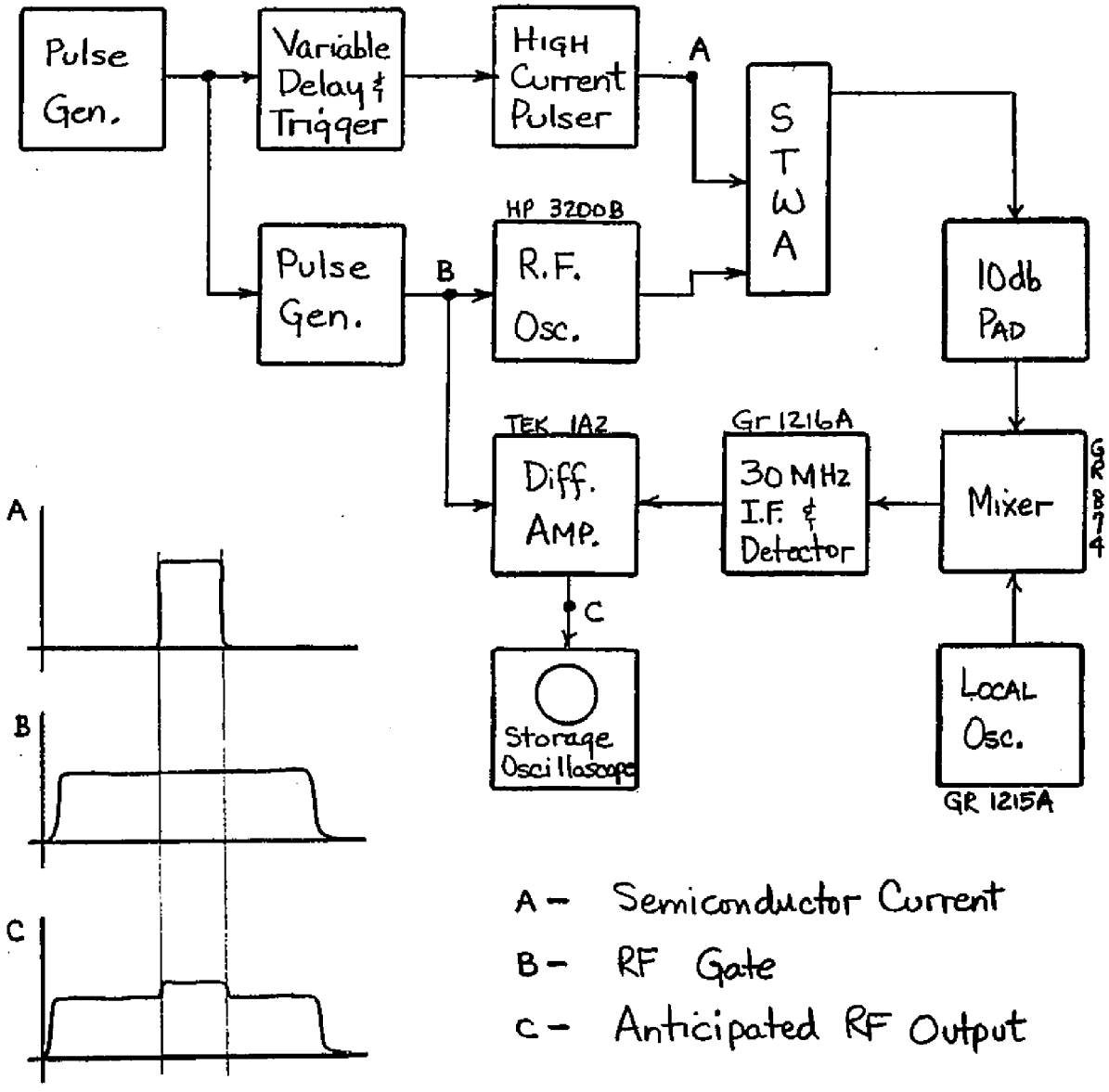

Figure 7.1 EXPERIMENTAL CONFIGURATION

less severe when high dielectric constant materials are utilized operation at X-band is not yet feasible. A possible method for constructing an X-band device has recently been suggested by Ettenberg [62]. This technique consists of constructing the slow wave circuit by diffusing a high conductivity pattern into a high resistivity substrate thus permitting finer line widths to be "etched".

Throughout this dissertation emphasis has been placed on studying the interaction for realizable physical dimensions. The maximum obtainable gain vs. frequency, without regard to the present ability to construct the device, is also of interest. Consider a semiconductor at temperature T, collision frequency ν, with an applied electric field drifting majority carriers at a velocity V_o. The maximum gain-frequency curve is calculated in the following manner. A circuit of width b is excited at a frequency resulting in an interline phase shift as shown in Figure 3.8. The interaction impedance is found from Figure 3.10 and is used to calculate Pierce's coupling coefficient C and the normalized collision wave number β_c'. The maximum gain per wavelength is obtained from Figure 6.3a by selecting the period of the circuit to optimize the phase velocity. The maximum obtainable gain vs. frequency is plotted in Figure 7.2.

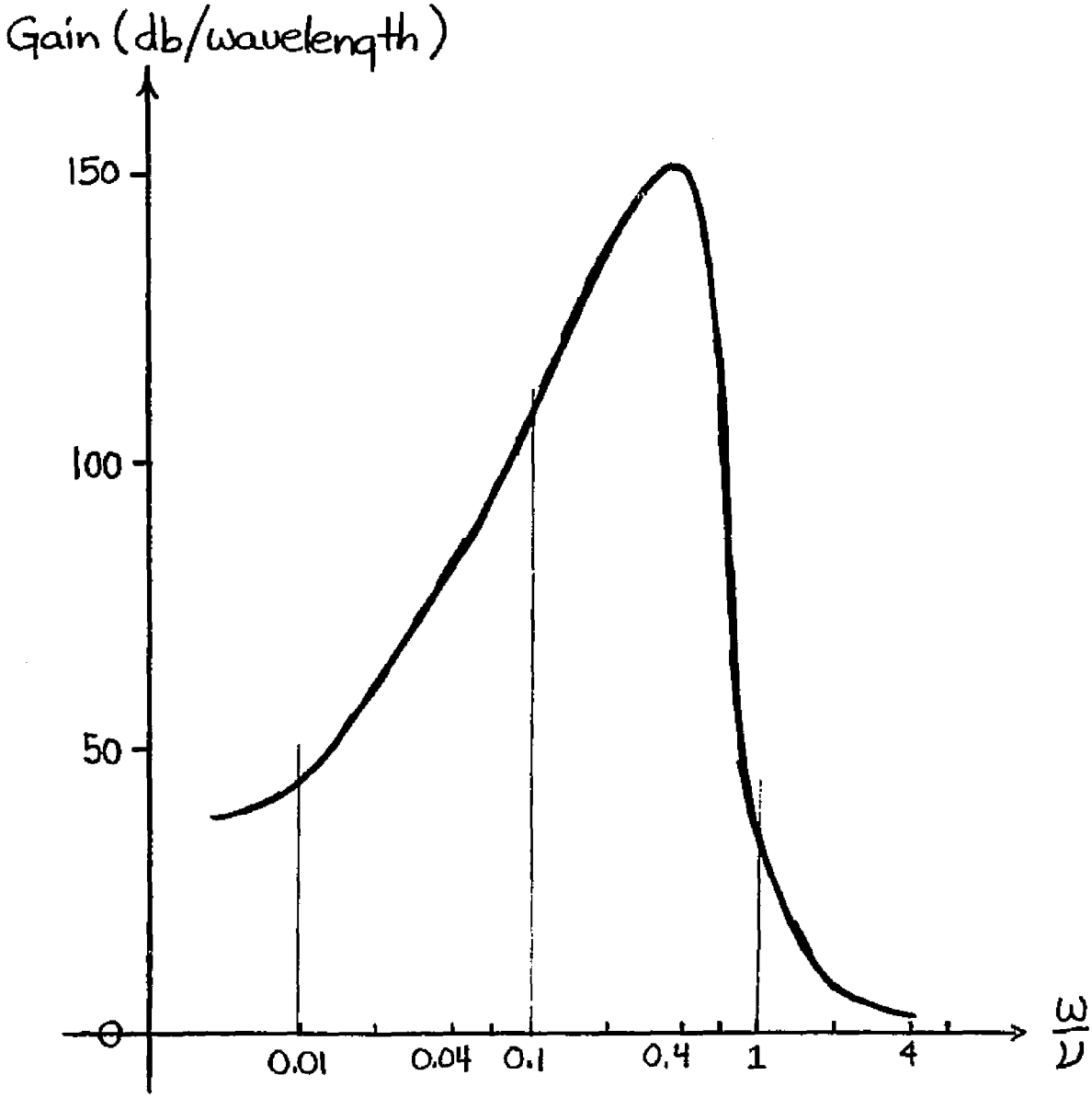

Figure 7.2 Maximum Obtainable Gain vs. Frequency. (high resistivity semiconductor, low loss circuit)

At low frequency the gain increases with frequency since the number of collisions per excitation period decreases rapidly while the interaction impedance remains essentially constant. At high frequency the gain decreases with frequency since the number of collisions per excitation period is negligibly small, i.e. the device is inertia dominated and the interaction impedance decreases rapidly. For this example maximum gain is achieved at $\frac{\omega}{\nu} \approx 0.3$.

For most semiconductors this corresponds to K_a-band excitation of a circuit designed to propagate the collision frequency. Such a circuit when constructed on a dielectric with relative dielectric constant twenty-five would have a line thickness of 125 Å and an overall circuit width of 15 microns; clearly an impractical design. It is additionally noted that Figure 7.2 was calculated for a high resistivity semiconductor, $\beta_Q^2 \approx 0.01$, and a low loss circuit, $\alpha_0 \approx 0.01$.

The problem of calculating the achievable gain while utilizing the narrowest line width that may be constructed at present ($\sim$1 mil) is treated next. Utilizing the approximate formula for cutoff frequency and slowing factor previously developed, one may write $f_c \approx v_p/2p$. Letting the interaction occur at a phase velocity of 3×10^7 cm/sec (limited by the saturated carrier drift velocity of InSb) results in a cutoff frequency of 3×10^9 Hz corresponding to the collision dominant portion of the gain curve. Excitation at maximum ωC product results

in a growth rate S = 0.04 for high resistivity semiconductor and non-lossy circuit; a gain of 2.16 db/wavelength. Experiments performed by Sumi,[63] indicate that a circuit with one mil line width has a cold circuit attenuation of approximately 30 db/cm yielding a 20 db excitation attenuation loss at the input end and decreased growth rate; S = 0.039. Hence at least 18.5 wavelengths ($\sim$ 175 mils) are required to achieve net gain. Taking into account the finite resistivity of the semiconductor (approximately 10 ohm-cm maximum for InSb) decreases the growth rate to 0.43 db/wavelength.

Close agreement has been found between experiments performed at low temperature; e.g. InSb at LN_2 as in Sumi's experiment, and theoretically predicted gain based on the one dimensional model. A new numerical method, based upon the analytic theory of continued fractions, has been developed to facilitate the solution of wave interaction problems resulting in n^{th} degree algebraic equations avoiding excessive roundoff error that is found in presently available methods. This method could be utilized to solve the two carrier dispersion equation for optimum semiconductor resistivity.

Experiments to verify the calculated dispersion characteristics of the stub loaded meander line have resulted in good agreement between theory and experiment. The existence of the slow wave suggests other uses for the circuit.

The stub loaded meander line is being considered for use in

a traveling wave parametric amplifier. Heilmeier [64] and Sills [65] have analyzed a shunt and series traveling wave parametric amplifier using straight transmission line. Sills [66] has constructed a successful series loaded line which however required a separate pump wave for each diode. In 1959 Ettenberg [67] reported on a feasibility study of such a device using an interdigital line. He obtained a strong interaction and reasonable interaction gain, but with the lossy diodes then available, did not achieve a net device gain.

By using a meander line however there are three possible diode configurations, namely; shunt, interline, and series as shown in Figure 7.3 a, b, c. The shunt diodes respond to $E_x(x,np)$ while the interline diodes respond to the field $E_z(0,z)$. Line parameters suitable for propagating a signal at ω_s, a pump at ω_p, and an idler at $\omega_i = \omega_p - \omega_s$ such that $\beta_p \cong \beta_s + \beta_i$, all along the same circuit may be determined in view of the refined meander line analysis. The result of this analysis could make a miniaturized parametric amplifier possible because of the slowing factor involved.

While the main subject investigated in this dissertation is the interaction between drifting carriers in a semiconductor and forward waves on a slow wave circuit, the interaction with backward waves on the circuit could be utilized in the solid state analog of the backward wave oscillator. The interaction with the forward wave may be

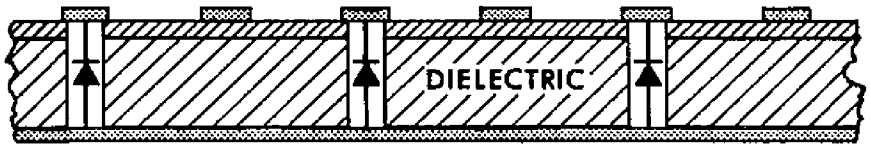

a. Shunt

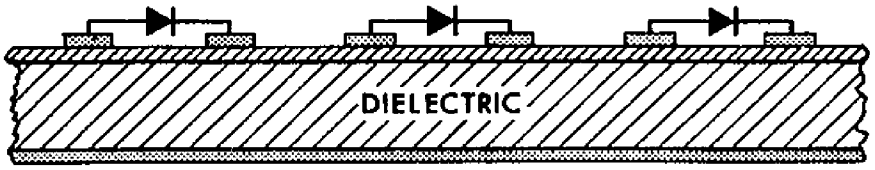

b. Interline

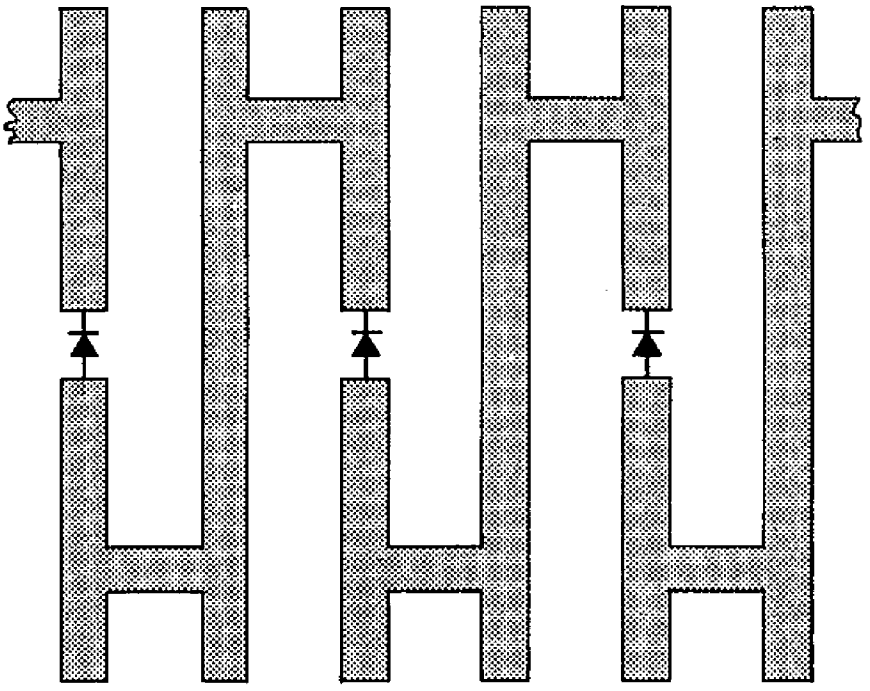

c. Series

Figure 7.3 Diode Configurations
(Lines will be broken for diode biasing when necessary.)

illustrated by a lossless coupled mode diagram as shown in Figure 7.4a. There exists an excitation region for ω_r for which γ pure imaginary does not exist. In this region the solution for γ has a real part and is called a convective instability. As loss increases the growth rate decreases and the bandwidth increases. The anticipated interaction with the backward wave is illustrated in Figure 7.4b. There exists an excitation region for γ_i for which ω pure real does not exist. In this region the solution for ω has an imaginary part and is called an absolute instability. As loss is increased the magnitude of the instability should decrease while it is anticipated that the bandwidth will increase. For semiconductors the starting current may be prohibitively large, whereas for " vacuum " devices the effect of introducing a small amount of loss (e.g. by intentionally introducing inert gas or cold circuit loss) would be to increase the frequency range while increasing the starting current by a tolerable amount.

Extension to a two dimensional model using the transverse interaction impedance concept [68] should be difficult although fruitful in determining the effects of a static transverse magnetic field.

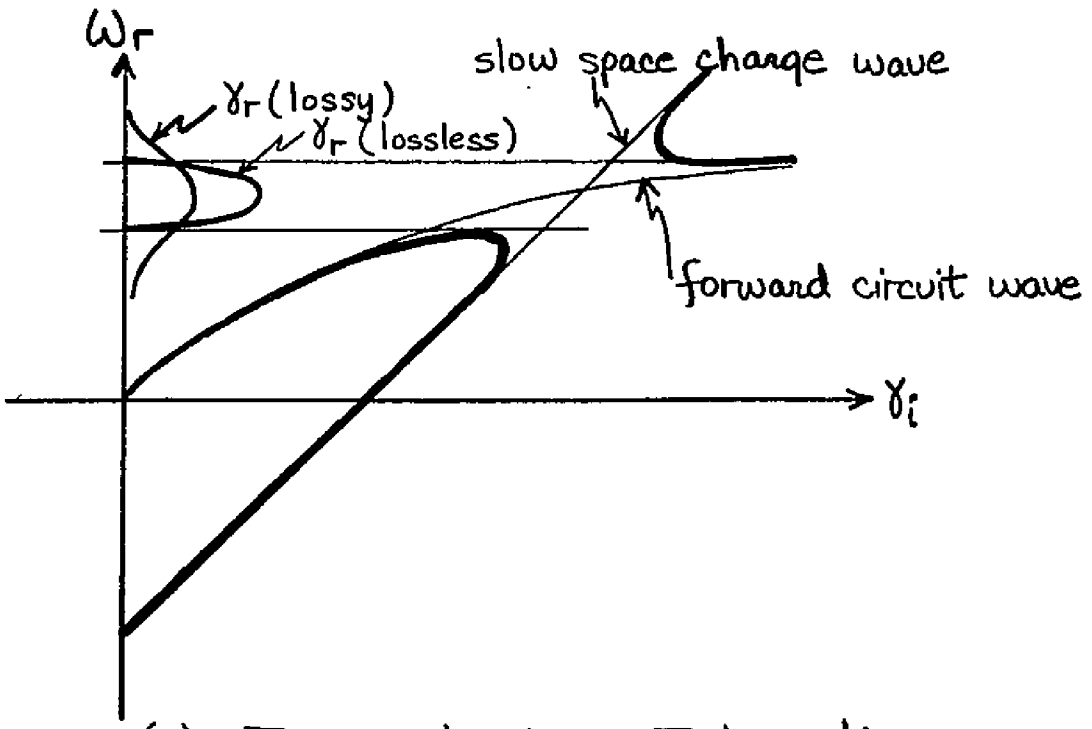

(a) Forward Wave Interaction

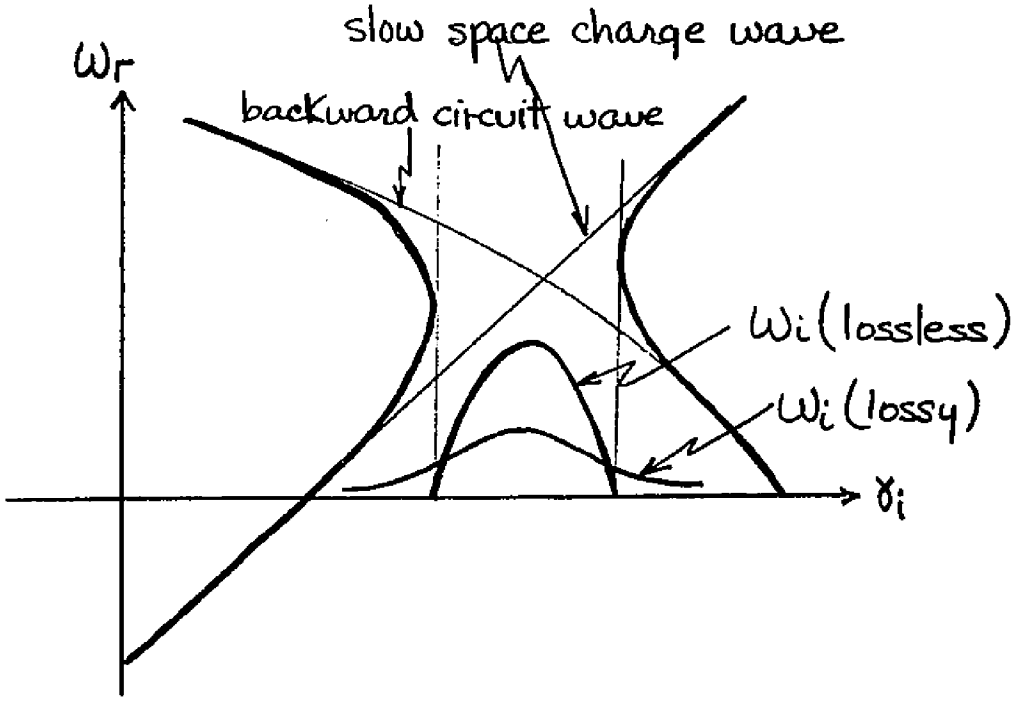

(b) Backward Wave Interaction

FIGURE 7.4 COUPLED MODE DIAGRAMS FOR FORWARD AND BACKWARD INTERACTIONS

APPENDIX ONE

THE EFFECTIVE PERMITTIVITY OF A MULTIPLE COMPOMENT PLASMA

The semiconductor plasma has been represented as a collection of carriers moving in a crystalline medium. It is therefore appropriate to set $\vec{D} = \epsilon_\ell \vec{E}$ thus allowing the effects of the plasma to be represented by convection currents arising from the motion of charged carriers. Alternately the plasma may be characterized as a complex dielectric medium whose effective dielectric constant includes the plasma effects thus not requiring separate knowledge of the density, velocity, etc. This may be developed from the second Maxwell equation, continuity and momentum transfer equations. Using previously defined symbols these are respectively;

$$\nabla \times \vec{H} = J + \epsilon_\ell \frac{\partial E}{\partial t} = \sum_s \rho_s V_s + j\omega \epsilon_\ell E_{T1} \quad , \qquad \text{(I-1)}$$

$$j\omega n_{1s} - \gamma \left(n_{os} V_{1s} + n_{1s} V_{os} \right) = - n_{1s} \tau_{Rs}^{-1} \quad , \qquad \text{(I-2)}$$

$$\left(j\omega - \gamma n_{os} + \nu_s \right) V_{1s} = \eta_s^* E_{T1} + v_{ths}^2 \frac{\gamma n_{1s}}{n_{os}} \quad . \qquad \text{(I-3)}$$

Solving the continuity equation for the density and substituting in the momentum transfer equation results in

$$V_{1S} = \frac{\eta_s^* \omega_{RS} E_{T1}}{\omega_{CS}\omega_{RS} - v_{th_s}^2 \gamma^2} , \tag{I-4}$$

where

$$\omega_{RS} \triangleq (j\omega - \gamma V_{OS} + \tau_{RS}^{-1}) , \tag{I-5}$$

$$\omega_{CS} \triangleq (j\omega - \gamma V_{OS} + \nu_s) , \tag{I-6}$$

and E_{T1} is the total RF electric field in the semiconductor plasma. The convection current is therefore

$$J = \sum_s \rho_s V_s = \epsilon_\ell E_{T1} \sum_s \frac{\omega_{ps}^2 (\omega_{RS} + \gamma V_{OS})}{\omega_{CS}\omega_{RS} - v_{th_s}^2 \gamma^2} \tag{I-7}$$

where the plasma frequency of the s^{th} type carrier is defined as

$$\omega_{ps}^2 \triangleq \frac{q_s n_{os} \eta_s^*}{\epsilon_\ell} . \tag{I-8}$$

Maxwell's second equation becomes, $\nabla \times \vec{H} = j\omega\epsilon_\ell\epsilon_r \vec{E}$

where $\epsilon_l \epsilon_r$ is the effective permittivity of the multiple component semiconductor plasma is the effective permittivity of the multiple component

$$\epsilon_r = 1 - j \sum_s \frac{\omega_{ps}^2 (\omega_{RS} + \gamma V_{os})}{\omega(\omega_{cs}\omega_{RS} - \nu_{th_s}^2 \gamma^2)} \qquad \text{(I-9)}$$

and includes the effects of density, recombination, drift velocity, collision, and diffusion. If s is taken to mean electron and hole carriers this latter equationrealistically represents the semiconductor plasma. It may be expanded to consider heavy and light carriers of each type when the densities of each are known. One dimensional wave propagation may thus be studied by combining the above with Maxwell's first equation resulting in the wave equation

$$\nabla^2 \vec{E} - \mu \epsilon_l \epsilon_r \frac{\partial^2 \vec{E}}{\partial t^2} = \nabla (\nabla \cdot \vec{E}). \qquad \text{(I-10)}$$

For sinuosoidal excitation, the solution to the homogeneous wave equation is of the form

$$\exp\left[j\omega \left(t \pm \sqrt{\mu \epsilon_l \epsilon_r}\, z \right) \right], \qquad \text{(I-11)}$$

thus characterizing the plasma behavior.

APPENDIX TWO

The stub loaded meander line circuit boundary conditions are enumerated in Table 3.1. Substitution of equations (3-6) and (3-9) in the twelve boundary condition equations results in the homogeneous set of equations

$$|M|\,\vec{A} = 0\,, \tag{II-1}$$

where defining

$$t_a \triangleq \tan\left(\frac{2\pi a}{\lambda_{eff}}\right), \tag{II-2}$$

$$t_b \triangleq \tan\left(\frac{2\pi b}{\lambda_{eff}}\right), \tag{II-3}$$

$$T \triangleq j\tan\left(\frac{\theta}{2}\right), \tag{II-4}$$

$$X(\theta_o) \triangleq \frac{Y(\theta_o)}{Y(\theta_o+\pi)}\,, \tag{II-5}$$

and $\vec{A} = \begin{vmatrix} A_1 \\ A_2 \\ \vdots \\ A_{11} \\ A_{12} \end{vmatrix}$,

gives

$$(M) = \begin{vmatrix}
-e^{-jm\pi} & -t_a e^{jm\pi} & t_a & 1 & e^{-jm\pi} & t_a e^{-jm\pi} & -t_a & -1 & 0 & 0 & 0 & 0 \\
e^{-jm\pi} & t_a e^{jm\pi} & t_a & 1 & -e^{-jm\pi} & -t_a e^{-jm\pi} & -t_a & -1 & 0 & 0 & 0 & 0 \\
e^{-jm\pi} & t_a e^{-jm\pi} & -t_a T & -T & 0 & 0 & 0 & 0 & 0 & 0 & 0 & 0 \\
-t_a T e^{-jm\pi} & T e^{-jm\pi} & -X & t_a X & t_a T e^{-jm\pi} & -T e^{-jm\pi} & X & -t_a X & 0 & 0 & 0 & 0 \\
-e^{-jm\pi} & t_a e^{-jm\pi} & -t_a & 1 & 0 & 0 & 0 & 0 & e^{-jm\pi} & -t_a e^{-jm\pi} & t_a & -1 \\
e^{-jm\pi} & -t_a e^{-jm\pi} & -t_a & 1 & 0 & 0 & 0 & 0 & -e^{-jm\pi} & t_a e^{-jm\pi} & t_a & -1 \\
e^{-jm\pi} & -t_a e^{-jm\pi} & -t_a T & T & 0 & 0 & 0 & 0 & 0 & 0 & 0 & 0 \\
t_a T e^{-jm\pi} & T e^{-jm\pi} & X & t_a X & 0 & 0 & 0 & 0 & -t_a T e^{-jm\pi} & -T e^{-jm\pi} & -X & -t_a X \\
0 & 0 & 0 & 0 & -t_b e^{-jm\pi} & e^{-jm\pi} & X & -t_b X & 0 & 0 & 0 & 0 \\
0 & 0 & 0 & 0 & t_b e^{-jm\pi} & -e^{-jm\pi} & X & -t_b X & 0 & 0 & 0 & 0 \\
0 & 0 & 0 & 0 & 0 & 0 & 0 & 0 & t_b e^{-jm\pi} & e^{-jm\pi} & X & t_b X \\
0 & 0 & 0 & 0 & 0 & 0 & 0 & 0 & -t_b e^{-jm\pi} & -e^{-jm\pi} & X & t_b X
\end{vmatrix}$$

Imposing the condition that a non-trivial solution exist; i.e., $\vec{A} \neq 0$, results in the determinantal equation

$$[M] = 0 . \tag{II-8}$$

Diagonalizing the determinant by the Gauss-Jordan algorithm [69] results in

$$t_a t_b X + T^2 = 0 . \tag{II-9}$$

Relational Coefficients

Inspection of the matrix (M) reveals that certain relationships exist between various members of the column vector $\vec{A}$. Letting $A_{i1} = A_1, A_5, A_9$, $A_{i2} = A_2, A_6, A_{10}$, $A_{i3} = A_3, A_7, A_{11}$, and $A_{i4} = A_4, A_8, A_{12}$ for $i = 1, 2, 3$ respectively and defining

$$f_{i3} \triangleq \frac{A_{i3}}{A_{i1}} , \tag{II-10}$$

and

$$f_{i4} \triangleq \frac{A_{i4}}{A_{i2}} , \tag{II-11}$$

it is found that

$$f_{13} = \frac{e^{-jm\pi}}{T t_a} , \tag{II-12}$$

$$f_{23} = f_{33} = \frac{e^{-jm\pi} t_b}{T} , \tag{II-13}$$

$$f_{14} = -\frac{e^{-jm\pi} t_a}{T} , \tag{II-14}$$

and

$$f_{24} = -f_{34} = \frac{e^{-jm\pi}}{T t_b} . \tag{II-15}$$

It is noted that all the relational coefficients are pure imaginary since m is an integer.

Futher inspection of the matrix (M) reveals that

$$A_{i2} = k_i A_{i1} \tag{II-16}$$

where k_i is a real number. Multiplying

$$V_{im} V_{im}^* = \cos^2\varphi \left(A_{i1} A_{i1}^* - f_{i4}^2 A_{i2} A_{i2}^*\right) + \sin^2\varphi \left(A_{i2} A_{i2}^* - f_{i3}^2 A_{i1} A_{i1}^*\right) , \tag{II-17}$$

where use has been made of a relationship derived from equation (II-16),

$$\left(A_{i1}^* A_{i2} - A_{i1} A_{i2}^*\right) = 0 \tag{II-18}$$

Finally equation (II-17) is independent of m, therefore

$$V_i V_i^* = A_{i1} A_{i1}^* \left[\cos^2\varphi \left(1 - f_{i4}^2 k_i^2\right) + \sin^2\varphi \left(k_i^2 - f_{i3}^2\right)\right] . \tag{II-19}$$

APPENDIX THREE

LISTING OF COMPUTER PROGRAMS

1. MAIN PROGRAM
2. SUBROUTINE INIT
3. SUBROUTINE ONE
4. SUBROUTINE TWO
5. SUBROUTINE THREE
6. SUBROUTINE XEDC
7. SUBROUTINE CARDAN
8. SUBROUTINE SELECT

```
C      MAIN PROGRAM
       REAL KB,MU1,MU2,MU3,N1,N2,N3,N3Y,N3YI,NUM,DNM,DNM2,NEFF,VIEFF,KA
       COMMON CTH(20),CEPEFF(20),CNEFF(20),CVIEFF(20),CX(20),CYTH(20),
      1FN3Y(20),SF(20),TH(20),CVPH(20),W(20),WST(20),CVG(20),CZN(20),
      2F(20),AB,R,N1,N2,N3,T,P,D,B,WF1,WF2,EP1,EP2,EP3,VIEFF,NEFF,EPEFF,
      3X,YTH,PI
       PI = 3.1415927
C
C                        DATA REQUIRED
C
C               B - CIRCUIT HALF WIDTH - MILS
C               T - SEMICONDUCTOR THICKNESS - MILS
C               D - PASSIVATION LAYER THICKNESS - MILS
C               P - CIRCUIT INTERLINE SPACING - MILS
C               R - METALLIZATION RATIO
C               AB - ASPECT RATIO
C               MU1 - PERMEABILITY REGION 1
C               MU2 - PERMEABILITY REGION 2
C               MU3 - PERMEABILITY REGION 3
C               EP1 - PERMITTIVITY REGION 1
C               EP2 - PERMITTIVITY REGION 2
C               EP3 - PERMITTIVITY REGION 3
C               MODE
C
    4  WRITE(6,1)
       READ(5,2) AB,T,D,B,P,R,MU1,MU2,MU3,EP1,EP2,EP3,MODE
       N1 = SQRT(MU1/EP1)*377.
       N2 = SQRT(MU2/EP2)*377.
       N3 = SQRT(MU3/EP3)*377.
       WF1 = EP1/EP3
       WF2 = N3/N1
       X1 = 2.*B
       X2 = P*(1.-R)
       X3 = T
       X4 = D
       X5 = FLOAT(MODE)
```

```
      T = T*2.54E-05
      D = D*2.54E-05
      B = B*2.54E-05
      P = P*2.54E-05
      WRITE(6,3) X1,X2,X3,X4,R,AB,EP1,EP2,X5
      CALL INIT
      CALL ONE
      CALL TWO(MODE)
      CALL THREE
      GO TO 4
    1 FORMAT(1H1)
    2 FORMAT(12F5.2,I2)
    3 FORMAT(T43, CIRCUIT WIDTH -  ,1PE10.2,   MILS ,//,
     1       T43, LINE THICKNESS -  ,1PE10.2,   MILS ,//,
     2       T43, DIELECTRIC THICKNESS -  ,1PE10.2,   MILS ,//,
     3       T43, CIRCUIT BOARD THICKNESS -  ,1PE10.2,   MILS ,//,
     4       T43, METALLIZATION RATIO -  ,1PE10.2,//,
     5       T43, ASPECT RATIO -  ,1PE10.2,//,
     6       T43, CIRCUIT BOARD PERMITTIVITY -  ,1PE10.2,//,
     7       T43, DIELECTRIC PERMITTIVTY -  ,1PE10.2,//,
     8       T43, SPACE HARMONIC NUMBER -  ,1PE10.2,////)
      END
```

```
      SUBROUTINE INIT
      REAL KB,MU1,MU2,MU3,N1,N2,N3,N3Y,N3YI,NUM,DNM,DNM2,NEFF,VIEFF,KA
      COMMON CTH(20),CEPEFF(20),CNEFF(20),CVIEFF(20),CX(20),CYTH(20),
     1FN3Y(20),SF(20),TH(20),CVPH(20),W(20),WST(20),CVG(20),CZN(20),
     2F(20),AB,R,N1,N2,N3,T,P,D,B,WF1,WF2,EP1,EP2,EP3,VIEFF,NEFF,EPEFF,
     3X,YTH,PI
C
C                          THIS SECTION INITIALIZES
C                               THE ARRAYS
C
      DO 13 I = 1,20
      CTH(I) = 0.
      CEPEFF(I) = 0.
      CNEFF(I) = 0.
      CVIEFF(I) = 0.
      CX(I) = 0.
      CYTH(I) = 0.
      FN3Y(I) = 0.
      SF(I) = 0.
      CVPH(I) = 0.
      W(I) = 0.
      WST(I) = 0.
      CVG(I) = 0.
   13 CZN(I) = 0.
      RETURN
      END
```

```
      SUBROUTINE ONE
      REAL KB,MU1,MU2,MU3,N1,N2,N3,N3Y,N3YI,NUM,DNM,DNM2,NEFF,VIEFF,KA
      COMMON CTH(20),CEPEFF(20),CNEFF(20),CVIEFF(20),CX(20),CYTH(20),
     1FN3Y(20),SF(20),TH(20),CVPH(20),W(20),WST(20),CVG(20),CZN(20),
     2F(20),AB,R,N1,N2,N3,T,P,D,B,WF1,WF2,EP1,EP2,EP3,VIEFF,NEFF,EPEFF,
     3X,YTH,PI
      WRITE(6,101)
C
C                     THIS SECTION SETS THE FREQUENCY
C
      THPR = 0.0
    2 DO 1 I = 1,20
      KB = FLOAT(I)*0.16
      TESTA = ABS(COS(AB*KB))
      TESTB = ABS(COS(KB))
      IF(TESTA-0.001) 71,73,73
   73 IF(TESTB-0.001) 71,74,74
   74 FA = SIN(AB*KB)/COS(AB*KB)
      FB = SIN(KB)/COS(KB)
      IF(FA*FB) 70,71,72
   71 WRITE(6,114) I,KB
      GO TO 25
   70 WRITE(6,115) I,KB
      GO TO 25
C
C
C                     THIS SECTION SOLVES THE EQUATION
C
C
   72 THL = 0.0000001
      THH = 3.1415920
      DO 3 J = 3,12
      TH(J) = (THH+THL)/2.
      THETA = TH(J)
      CALL XEDC(THETA,R,N1,N2,N3,T,P,D,WF1,WF2,EP3,VIEFF,NEFF,EPEFF,X,
     1YTH)
```

```
      IF(J-12) 4,3,3
    4 TN = SIN(TH(J)/2.)/COS(TH(J)/2.)
      FT = FA*FB*X-TN*TN
      IF(FT) 300,301,302
  300 THH = TH(J)
      GO TO 3
  302 THL = TH(J)
    3 CONTINUE
  301 THETA = THETA - PI
      IF(THETA-THPR) 25,26,26
   26 THPR = THETA
      CTH(I) = THETA
      CEPEFF(I) = EPEFF
      CNEFF(I) = NEFF
      CVIEFF(I) = VIEFF
      CYTH(I) = YTH
      CX(I) = X
      WRITE(6,102)I,KB,CTH(I),CEPEFF(I),CNEFF(I),CVIEFF(I),CYTH(I),CX(I)
    1 CONTINUE
   25 CONTINUE
      RETURN
  101 FORMAT(20X,3H  I,3X,12H         KB   ,12H      CTH I   ,12H   CEPEFF I
     1 ,12H    CNEFF I ,12H   CVIEFF I ,12H    CYTH I   ,12H     CX I    ,
     2/)
  102 FORMAT(20X,I3,3X,1P7E12.2)
  114 FORMAT(20X,I3,3X,1PE12.2,15X,24HDEGENERATE PI ROOT FOUND)
  115 FORMAT(20X,I3,3X,1PE12.2,15X,19HSTRUCTURE IS CUTOFF)
      END
```

```
      SUBROUTINE TWO(MODE)
      DIMENSION WVLNTH(20), WVLMTH(20)
      REAL KB,MU1,MU2,MU3,N1,N2,N3,N3Y,N3YI,NUM,DNM,DNM2,NEFF,VIEFF,KA
      COMMON CTH(20),CEPEFF(20),CNEFF(20),CVIEFF(20),CX(20),CYTH(20),
     1FN3Y(20),SF(20),TH(20),CVPH(20),W(20),WST(20),CVG(20),CZN(20),
     2F(20),AB,R,N1,N2,N3,T,P,D,B,WF1,WF2,EP1,EP2,EP3,VIEFF,NEFF,EPEFF,
     3X,YTH,PI
      THPR = 0.
      DO 80 I = 1,20
      IF(CTH(I)) 81,80,81
   81 SF(I) = CTH(I)*B/(P*0.16*FLOAT(I))
      CVPH(I) = CVIEFF(I)/SF(I)
      W(I) = CVPH(I)*CTH(I)/P
      CVPH(I) = CVPH(I)*CTH(I)/(CTH(I)+PI*FLOAT(MODE))
      CVG(I) = (P*CVIEFF(I)/B)*(0.16/(CTH(I)-THPR))
      THPR = CTH(I)
   80 CONTINUE
C
C                    THIS SECTION SOLVES FOR THE
C                       INTERACTION IMPEDANCE
C
      WRITE(6,103)
      DO 12 I = 1,20
      IF(W(I)) 11,12,11
   11 IF(CVG(I)) 12,13,13
   13 X = CX(I)
      THETA = CTH(I)
      TT = SIN(THETA/2.)/COS(THETA/2.)
      TT = TT*TT
      KB = FLOAT(I)*0.16
      KA = AB*KB
      FA = SIN(KA)/COS(KA)
      FB = SIN(KB)/COS(KB)
      TA = FA*FA
      TB = FB*FB
      F13SQ = 1./(TT*TA)
```

```
      F14SQ = TA/TT
      F23SQ = TB/TT
      F24SQ = 1./(TT*TB)
      F33SQ = TB/TT
      F34SQ = 1./(TT*TB)
      C1 = (X*THETA-FA*FB*TT)/(X*THETA*TA*FB-FA*TT)
      C2 = FB
      C3 = -FB
      D5 = (1.+C1*FA)/(1.+FA*FB)
      D9 = (1.-C1*FA)/(1.+FA*FB)
      C11 = (1.+C1*C1*F14SQ)
      C12 = C1*C1+F13SQ
      C21 = (1.+C2*C2*F24SQ)*D5*D5
      C22 = (C2*C2+F23SQ)*D5*D5
      C31 = (1.+C3*C3*F34SQ)*D9*D9
      C32 = (C3*C3+F33SQ)*D9*D9
      WS1 = 4.*KA*(C11+C12)+2.*SIN(2.*KA)*(C11-C12)
      WS2 = 2.*(KB-KA)*(C21+C22)+(C21-C22)*(SIN(2.*KB)-SIN(2.*KA))
      WS3 = 2.*(KB-KA)*(C31+C32)+(C31-C32)*(SIN(2.*KB)-SIN(2.*KA))
      WST(I) = CYTH(I)*(WS1+WS2+WS3)/(2.*W(I)*P)
      THN = THETA+2.*PI*FLOAT(MODE)
      G1 = SIN(THETA/2.)*SIN(THN*R/2.)/(THN*R/2.)
      G1SQ = G1*G1
      G4 = COS(THETA/2.)*COS(THN*R/2.)/(R*(THN+PI)/2.)
      G4SQ = G4*G4
      FNMAG2 = 4.*(G1SQ+F14SQ*C1*C1*G4SQ)/(P*P)
      CZN(I) = P*P*FNMAG2/(2.*THN*THN*WST(I)*CVG(I))
      F(I) = W(I)/(2.*PI)
      WVLNTH(I) = 100.*CVPH(I)/F(I)
      THETA=-THETA+PI
      CALL XEDC(THETA,R,N1,N2,N3,T,P,D,WF1,WF2,EP3,VIEFF,NEFF,EPEFF,X,
     1YTH)
      WVLMTH(I)=16.*VIEFF*P*FLOAT(I)/(THETA*B*F(I))
      WRITE(6,104)I,F(I),WVLNTH(I),WVLMTH(I),CVPH(I),CVG(I),WST(I),CZN(I
     1)
   12 CONTINUE
```

```
      RETURN
  103 FORMAT(1H0,19X,3H  I,3X,12H      F(I)  ,12H      FWL(I) ,12H      BW
     1L(I) ,12H    CVPH(I) ,12H     CVG(I) ,12H     WST(I) ,12H     CZN(
     2I) ,/)
  104 FORMAT(20X,I3,3X,1P7E12.2)
      END



      SUBROUTINE THREE
      REAL*4KA,KB,MU1,MU2,MU3,N1,N2,N3,N3Y,N3YI,NUM,DNM,DNM2,NEFF,VIEFF,
     1H,I1,I2,I3,NU,JO,LD,PRAL,PRH,PRBC,MR,ME,MU,NO,K,EIMAG,ID(20),LEN0,
     2LEN1,MR1,ER1,TE1,AREA1,ALPHA1,RES1,MU0
      COMMON CTH(20),CEPEFF(20),CNEFF(20),CVIEFF(20),CX(20),CYTH(20),
     1FN3Y(20),SF(20),TH(20),CVPH(20),W(20),WST(20),CVG(20),CZN(20),
     2F(20),AB,R,N1,N2,N3,T,P,D,B,WF1,WF2,EP1,EP2,EP3,VIEFF,NEFF,EPEFF,
     3X,YTH,PI
      COMPLEX*8 E1EI,E2EI,E3EI,EOUT1,EOUT2,EOUT3,Y0,Y1,Y2,Y3,ROOT,
     1CS1,CS2,CS3
      COMPLEX*16 A21,A22,A23,A31,A32,A33,M1,M2,M3,DET
      COMMON/A1A/ CS1,CS2,CS3
      DIMENSION CV0(20),CGAIN(10,20),CVPHCM(20),IN(10),CVOLT(20),
     1CCS1(10,20)
      WRITE(6,111)
      K  = (1.38E-23)
      ME = (9.1E-31)
      EC = (1.6E-19)
      ETA = (1.76E+11)
      E0 = (8.86E-12)
      READ 5,6  N
      DO 1 J1=1,N
C
C          REQUIRES LENGTH IN CM, ALPHA IN DB/CM,
C          RESISTIVITY IN OHM-CM, AND AREA IN MILS-SQUARE
```

```
C
      READ(5,20) RESCM,MR,ER,MU,TE,AREA,ALPHA,LEN0,LEN1,RQP,MU0
      READ(5,40) (IN(II),II=1,10)
      RES1 = RESCM
      MR1 = MR
      ER1 = ER
      MU1 = MU
      TE1 = TE
      AREA1 = AREA
      ALPHA1 = ALPHA
      RES = RESCM/100.0
      MU = MU/1.0E+04
      MU0 = MU0/1.0E+04
      ALPHA = ALPHA*100./8.68
      AREA = AREA*2.54E-05*2.54E-05
      LEN0 = LEN0*0.01
      LEN1 = LEN1*0.01
      N0 = 1./(EC*MU0*RES)
      RH0 = N0*EC
      TAU = MR*MU/ETA
      VTH = SQRT(K*TE/(ME*MR))
      DC = VTH*VTH*TAU
      WP2 = ETA/(E0*MR*ER*RES*MU)
      DO 2 J2 = 1,9
      CVOLT(J2) = 20.*FLOAT(J2)
      V0 = CVOLT(J2)*MU0/LEN0
      CV0(J2) = V0*100.
      J0 = RH0*V0
      I0(J2) = J0*AREA
      BP2 = WP2/V0/V0
      LD = DC/(WP2*TAU)
      WRITE(6,3) RES,MR,ER,MU,TE,AREA,ALPHA,WP2,V0
      WRITE(6,108)
      DO 14 I = 1,20
      CVPHCM(I) = CVPH(I)*100.
      IF(W(I)) 14,14,16
```

```
16 IF(CZN(I)) 14,14,17
17 BE = W(I)/VO
   C3 = CZN(I)*JO*ETA*AREA/(2.*VO*VO*MR)
   C = EXP((ALOG(C3))/3.)
   BEC = BE*C
   BC = 1./(VO*TAU)
   PRBC = BC/BEC
   PRAL = ALPHA/BEC
   IF(LD) 15,15,18
18 SWL = CVIEFF(I)/(SF(I)*F(I))
   IF((SWL/LD)-10.) 23,23,19
23 WRITE(6,106) SWL,LD
19 IF((SWL/LD)-10.) 15,15,21
21 IF((SWL/LD)-100.) 22,22,15
22 WRITE(6,107) SWL,LD
15 CONTINUE
   X = VO/CVPH(I)
   PRBP2 = BP2/BEC/BEC
   PBQ2 = RQP*RQP*PRBP2*(1.+LD*LD*BE*BE)
   PRH = W(I)*(1./CVPH(I)-1./VO)/BEC
   R1 = PRBC+PRAL
   I1 = PRH
   R2 = PRBC*PRAL+PBQ2
   I2 = PRBC*PRH
   R3 = PRAL*PBQ2
   I3 = PRH*PBQ2 +(2.*X/(1.+X))
   YO = CMPLX(1.0,0.0)
   Y1 = CMPLX(R1,I1)
   Y2 = CMPLX(R2,I2)
   Y3 = CMPLX(R3,I3)
   CALL CARDAN(YO,Y1,Y2,Y3)
   CALL SELECT
   CCS1(J2,I) = REAL(CS1)
   A21 = 1./ (CS1*(CS1+PRBC)+PBQ2)
   A22 = 1./ (CS2*(CS2+PRBC)+PBQ2)
   A23 = 1./ (CS3*(CS3+PRBC)+PBQ2)
```

```
      A31 = A21*CS1
      A32 = A22*CS2
      A33 = A23*CS3
      M1 = A22*A33 - A23*A32
      M2 = A21*A33 - A31*A23
      M3 = A21*A32 - A31*A22
      DET = M1-M2+M3
      E1EI = M1/DET
      E2EI = -M2/DET
      E3EI = M3/DET
      PI2 = 2.*PI
      PH1 = AIMAG(CS1)*LEN1*BEC
      PH2 = AIMAG(CS2)*LEN1*BEC
      PH3 = AIMAG(CS3)*LEN1*BEC
      PH1 = AMOD(PH1,PI2)
      PH2 = AMOD(PH2,PI2)
      PH3 = AMOD(PH3,PI2)
      AM1 = REAL(CS1)*LEN1*BEC
      AM2 = REAL(CS2)*LEN1*BEC
      AM3 = REAL(CS3)*LEN1*BEC
      IF(AM1-170.) 42,42,41
   41 CGAIN(J2,I) = 0.0
      GO TO 45
   42 EOUT1 = EXP(AM1)*CMPLX(COS(PH1),SIN(PH1))*E1EI
      EOUT2 = EXP(AM2)*CMPLX(COS(PH2),SIN(PH2))*E2EI
      EOUT3 = EXP(AM3)*CMPLX(COS(PH3),SIN(PH3))*E3EI
      EOUT = CABS(EOUT1+EOUT2+EOUT3)
      CGAIN(J2,I) = 20.*ALOG10(ABS(EOUT))
      E1MAG = CABS(E1EI)
   45 WRITE(6,109) I, E1MAG ,CS1,CS2,CS3,BE,C,CGAIN(J2,I)
   14 CONTINUE
      WRITE(6,110)
      IF((FLOAT(J2)/3.)-FLOAT(J2/3)) 30,30,2
   30 WRITE(6,111)
    2 CONTINUE
      WRITE(6,4) (IN(II),II=1,10),MR1,ER1,MU1,TE1,AREA1,VTH,LEN0,LEN1,
```

```
     1ALPHA1,RES1,(IO(L),L=1,9),(CVOLT(L),L=1,9),(CVO(L),L=1,9)
      WRITE(6,5) (F(L),CZN(L),CVPHCM(L),(CGAIN(M,L),M=1,9),L=1,10)
      WRITE 6,111
      WRITE(6,4) (IN(II),II=1,10),MR1,ER1,MU1,TE1,AREA1,VTH,LEN0,LEN1,
     1ALPHA1,RES1,(IO(L),L=1,9),(CVOLT(L),L=1,9),(CVO(L),L=1,9)
      WRITE(6,5) (F(L),CZN(L),CVPHCM(L),(CCS1 (M,L),M=1,9),L=1,10)
      WRITE(6,111)
    1 CONTINUE
      RETURN
    3 FORMAT(T26,       RES        MR         ER         MU        TEMP
     1 AREA      ALPHA       WP2         VO    ,/,26X,1P9E10.2)
    4 FORMAT(T38, MATERIAL -  ,10A4,//,
     1       T38, RELATIVE MASS -  ,1PE10.2,//,
     2       T38, RELATIVE PERMITTIVITY -  1PE10.2,//,
     3       T38, MOBILITY -  ,1PE10.2,T60, CM*2/VOLT-SEC ,//,
     4       T38, TEMPERATURE -  ,1PE10.2,T65, DEG. KELVIN ,//,
     5       T38, AREA -  ,1PE10.2,T58, MILS*2 ,//,
     6       T38, THERMAL VELOCITY -  ,1PE10.2,T70, CM/SEC ,//,
     7       T38, SEMICONDUCTOR LENGTH -  ,1PE10.2,T75, METERS ,//,
     8       T38, SLOW WAVE CIRCUIT LENGTH -  ,1PE10.2,T78, METERS ,//,
     9       T38, COLD CIRCUIT ATTENUATION -  ,1PE10.2,T78, DB/CM ,//,
     1       T38, RESISTIVITY -  ,1PE10.2,T65, OHM-CM ,////,
     2       T30, CURRENT ,T41,1P9E10.2,/,
     3       T30, VOLTAGE ,T41,1P9E10.2,//,
     4       T30, VO CM/SEC  ,T41,1P9E10.2,//,
     5       T10, FREQUENCY ,T20, INT. IMP ,T31, CVPHCM ,/)
    5 FORMAT(7X,1P3E10.2,3X,1P9E10.2,/)
    6 FORMAT(I2)
   20 FORMAT(5E10.2)
   40  FORMAT(10A4)
  106 FORMAT(1H0,10X,24HFLUID MODEL IS NOT VALID,10X,6HSWL = ,1PE10.2,5X
     1,5HLD = ,1PE10.2)
  107 FORMAT(1H0,10X,27HFLUID MODEL IS QUESTIONABLE,7X,6HSWL = ,1PE10.2,
     15X,5HLD = ,1PE10.2)
  108 FORMAT(1H0,6X,3H I ,11H    E1MAG  , 12H      RCS1  ,12H       ICS1
     1 ,12H      RCS2  ,12H      ICS2  ,12H      RCS3  ,12H      ICS3  ,
```

```
   212H        BE    ,12H        C     ,12H       GAIN   ,/)
109 FORMAT(6X,I3,1P10E12.3)
110 FORMAT(1H0,/)
111 FORMAT(1H1)
    END



    SUBROUTINE XEDC(THETA,R,N1,N2,N3,T,P,D,WF1,WF2,EP3,VIEFF,NEFF,
   1EPEFF,X,YTH)
    DIMENSION F1(50),F3(50),F4(50),F5(50),FN3Y(10)
    REAL N1,N2,N3,NUM,NEFF
    PI = 3.1415927
    NUM = 0.0
    DNM = 0.0
    DNM2 = 0.0
    DO 4 K=1,2
    FN3Y(K) = 0.0
    IF(K-2) 6,7,7
  7 THETA = THETA + PI
  6 TEST = -1.
    F2 = 2.*(1.-R)*SIN(THETA/2.)
    DO 5 M=1,49
    TEST = -TEST
    THM = THETA+6.2831854*FLOAT(M-25)
    F1(M) = (SIN((1.-R)*(THM/2.))*SIN(R*(THM/2.)))/((1.-R)*R*(THM/2.)*
   1(THM/2.))*TEST
    SGNM = -1.
    IF(FLOAT(M-25)+0.5) 9,8,8
  8 SGNM = -SGNM
  9 F3(M) = N2*TANH(THM*T/P)/N1
    F4(M) = TANH(THM*D/P)
    F5(M) = (1.+F4(M)*F3(M))/(F4(M)+F3(M))
    IF(K-2) 10,5,5
```

```
   10 NUM = NUM+F1(M)*(SGNM+WF1*F5(M))
      DNM = DNM+F1(M)*(SGNM+F5(M))
      DNM2 = DNM2+F1(M)*(SGNM+WF2*F5(M))
    5 FN3Y(K) = FN3Y(K) + F1(M)*F2*(SGNM+WF2*F5(M))/N3
      IF(K-2) 11,4,4
   11 EPEFF = EP3*NUM/DNM
      NEFF = N3*DNM/(DNM2*377.)
      VIEFF = 3.E+08/(NEFF*EPEFF)
    4 CONTINUE
      X = FN3Y(1)/FN3Y(2)
      YTH = FN3Y(1)
      RETURN
      END



      SUBROUTINE CARDAN(A0,A1,A2,A3)
C
C                        THIS SECTION FINDS THE
C                      ROOTS OF THE GAIN EQUATION
C                        USING CARDANS SOLUTION
C                           DUE TO TARTAGLIA
C
      REAL*8 THR3,SQR3
      COMPLEX*8 A0,A1,A2,A3,CS1,CS2,CS3
      COMPLEX*16 CW,CP,CG,CPCUBE,CQ,XH,XG,Z1,Z2,SUM
      COMMON/A1A/ CS1,CS2,CS3
      Z1 = A1/3.
      Z2 = A2/3.
      XH = A0*Z2-Z1*Z1
      XG = A0*A0*A3-3.*A0*Z1*Z2+2.*Z1*Z1*Z1
      SUM=A3*A3-6.*A3*Z1*Z2+4.*A3*Z1*Z1*Z1-3.*Z1*Z1*Z2*Z2
     1+4.*Z2*Z2*Z2
      SUM = SUM*A0*A0
```

```
      CPCUBE = -XG/2.-0.5*CDSQRT(SUM)
      IF(CDABS(CPCUBE)) 11,10,11
   11 CP = CDEXP((CDLOG(CPCUBE))/3.)
      IF(CDABS(CP)) 12,10,12
   12 CQ = -XH/CP
      THR3 = 3.
      SQR3 = DSQRT(THR3)/2.
      CW = (-0.5,0.)+SQR3*(0.,1.)
      CS1 = (CP+CQ-Z1)/A0
      CS2 = (CP*CW*CW+CQ*CW-Z1)/A0
      CS3 = (CP*CW+CQ*CW*CW-Z1)/A0
      GO TO 20
   10 CS1 = (0.,0.)
      CS2 = (0.,0.)
      CS3 = (0.,0.)
   20 CONTINUE
      RETURN
      END


      SUBROUTINE SELECT
C
C                              THIS SECTION ORDERS THE ROOTS
C
      COMPLEX CS1,CS2,CS3
      COMMON/A1A/ CS1,CS2,CS3
      DIMENSION CR(20),CI(20)
      CR(1) = REAL(CS1)
      CR(2) = REAL(CS2)
      CR(3) = REAL(CS3)
      CI(1) = AIMAG(CS1)
      CI(2) = AIMAG(CS2)
      CI(3) = AIMAG(CS3)
```

```
      DO 21 K=1,2
      DO 21 J=1,2
      IF(CR(J)-CR(J+1)) 22,21,21
   22 TEMP1 = CR(J)
      TEMP2 = CI(J)
      CR(J) = CR(J+1)
      CI(J) = CI(J+1)
      CR(J+1) = TEMP1
      CI(J+1) = TEMP2
   21 CONTINUE
      CS1 = CMPLX(CR(1),CI(1))
      CS2 = CMPLX(CR(2),CI(2))
      CS3 = CMPLX(CR(3),CI(3))
      RETURN
      END
```

APPENDIX FOUR

EXAMPLE OF NEW NUMERICAL METHOD

Consider the trivial algebraic equation

$$S^3 + j = 0 , \tag{IV-1}$$

whose roots are known,

$$\begin{aligned} r_1 &= +j , \\ r_2 &= 0.5(\sqrt{3} - j) , \\ r_3 &= 0.5(-\sqrt{3} - j) . \end{aligned} \tag{IV-2}$$

The real parts of the solution using the above method are determined first. Letting $X = S - S_o$, where S_o is pure real, results in reducing equation(IV-1) to

$$X^3 + 3S_oX^2 + 3S_o^2X + S_o^3 + j = 0 . \tag{IV-3}$$

Generating the test fraction coefficients yields

$$C_1 = (3S_o)^{-1} , \tag{IV-4a}$$

$$C_2 = \left(\frac{8}{9}S_o\right)^{-1} , \tag{IV-4b}$$

and

$$C_3 = \frac{512S_o^5}{3(64S_o^6 - 27)} . \tag{IV-4c}$$

Investigation of the test fraction coefficients reveals that sign changes of occur at $S_o = \frac{\pm\sqrt{3}}{2}$, and $S_o = 0$ as shown in Figure IV-1. Counting

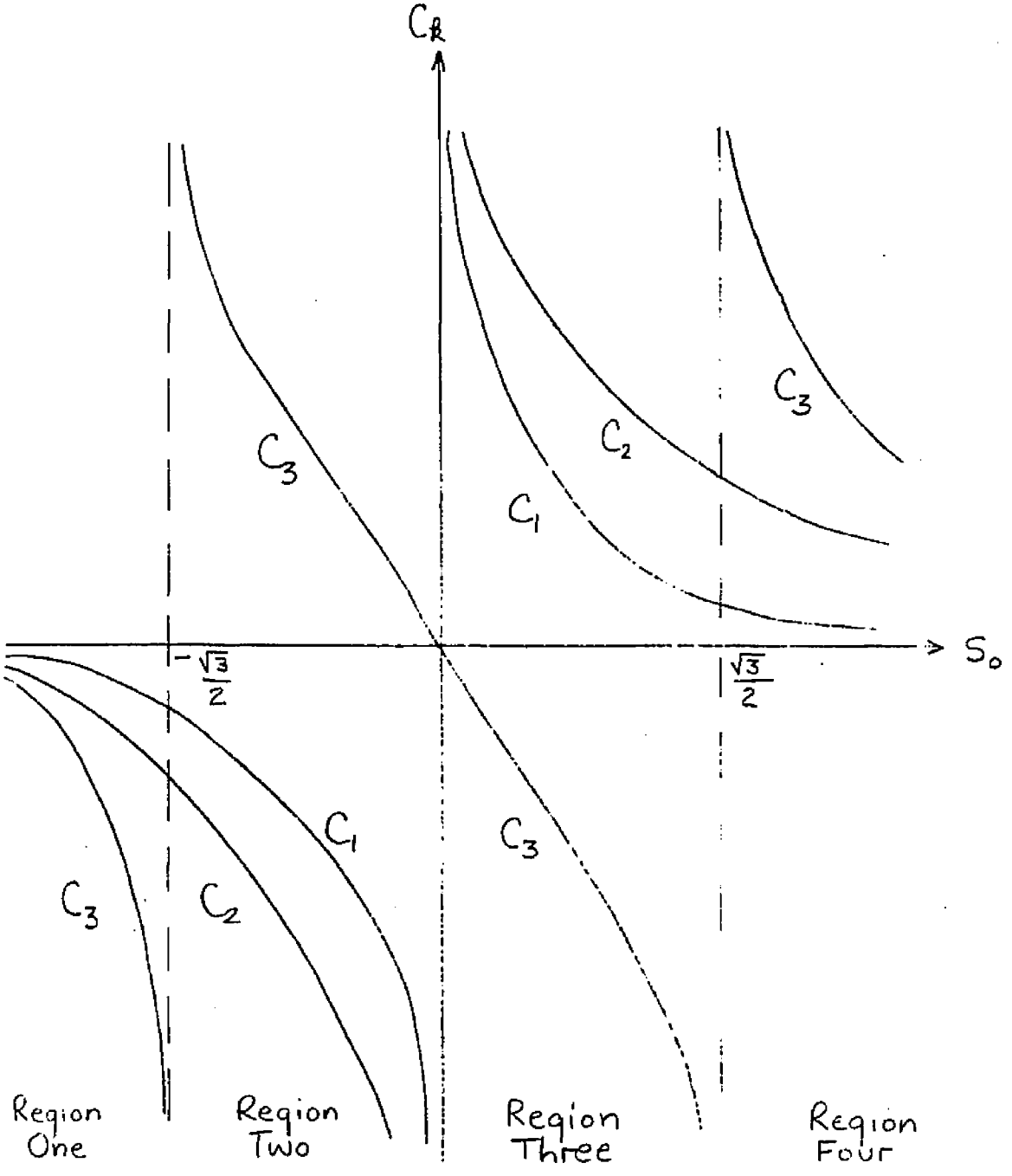

Figure IV - 1 Test Fraction Coefficients for the Real Part of the Roots of $s^3 + j = 0$.

the number of test fraction coefficients that are negative for any value of S_o reveals the number of roots with real part greater than or equal to S_o. Thus the singularities of the test fraction coefficient represent all the possible solutions for the real part of the roots of $P^n(s) = 0$. For example in region three of Figure IV-1 there is only one negative test coefficient, hence there is only one root with real part greater than any value of S_o in this region.

The imaginary parts of the solution are found next. Letting $X = -jS - S_o$, where S_o is pure real, results in reducing equation (IV-1) to

$$X^3 + 3S_oX^2 + 3S_o^2X + S_o^3 - 1 = 0. \qquad \text{(IV-5)}$$

Generating the test fraction coefficients yields

$$C_1 = (3S_o)^{-1}, \qquad \text{(IV-6a)}$$

$$C_2 = \frac{9S_o^2}{8S_o^3 + 1}, \qquad \text{(IV-6b)}$$

and

$$C_3 = \frac{3S_o(8S_o^3 + 1)}{S_o^3 - 1}. \qquad \text{(IV-6c)}$$

Investigation of the test fraction coefficients reveals that sign changes occur at $S_o = -\frac{1}{2}$, $S_o = 0$, and $S_o = +1$ as shown in Figure IV-2. Although sign change does occur at $S_o = 0$ the number of negative test coefficients does not change; therefore, there is no root with zero real part.

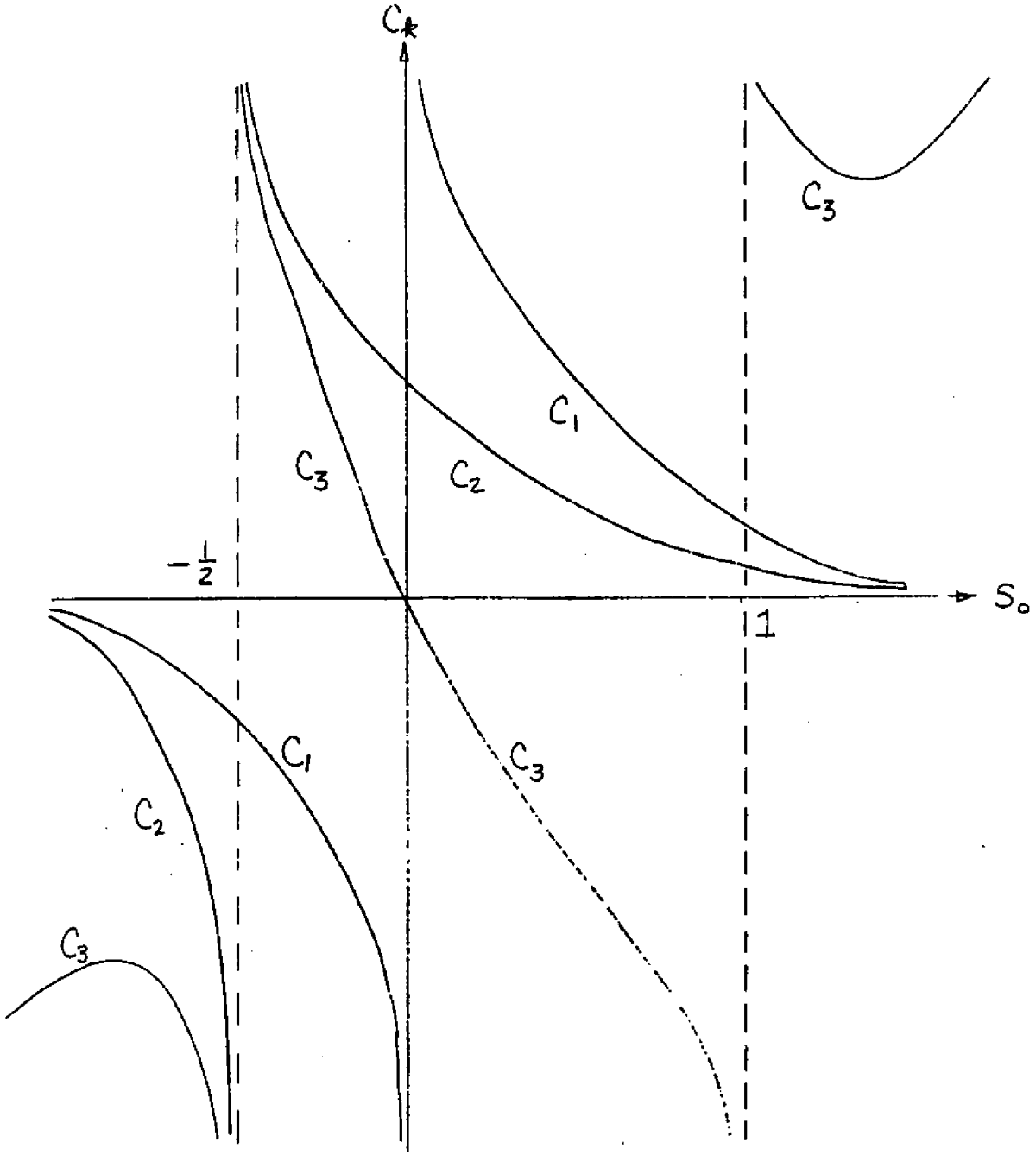

Figure IV-2 Test Fraction Coefficients for the Imaginary Part of the Roots of $S^3 + j = 0$.

Combining the above results in six possible solutions to the equation $P^n(s) = s^3 + j = 0$ as shown in Figure IV-3. The remainders of the function are evaluated at each possible solution. The correct solutions are chosen by comparing the remainders; i.e. choosing the three with smallest remainder.

The effects of roundoff error in the test coefficients are not serious for the following reasons. Consider the two cases shown in Figure IV-4 where an error in numerical evaluation occurs in C_3 at $S_o = O$. Both cases indicate that an error has occured and must be corrected; the indication being that the number of roots with real part greater than S_o must be a monotonic function of S_o as is not the case herein.

This numerical method is extremely useful in refining only the real part of a root; this being of major concern when determining the growth rate of various waves in interaction type problems.

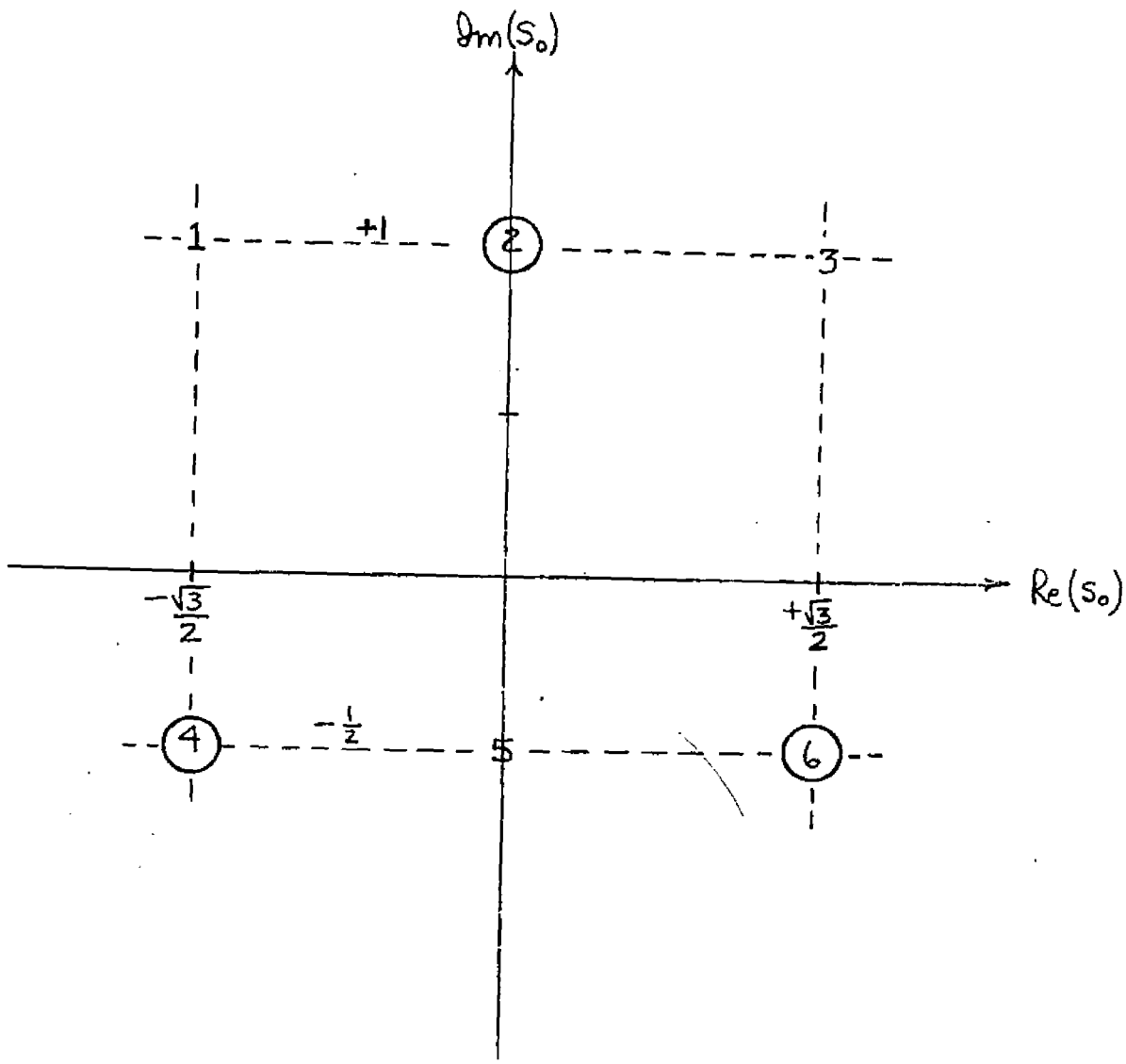

Figure IV-3 Solutions of $S^3+j=0$ Generated by Numerical Method. Correct solutions (encircled) are found by testing the remainders.

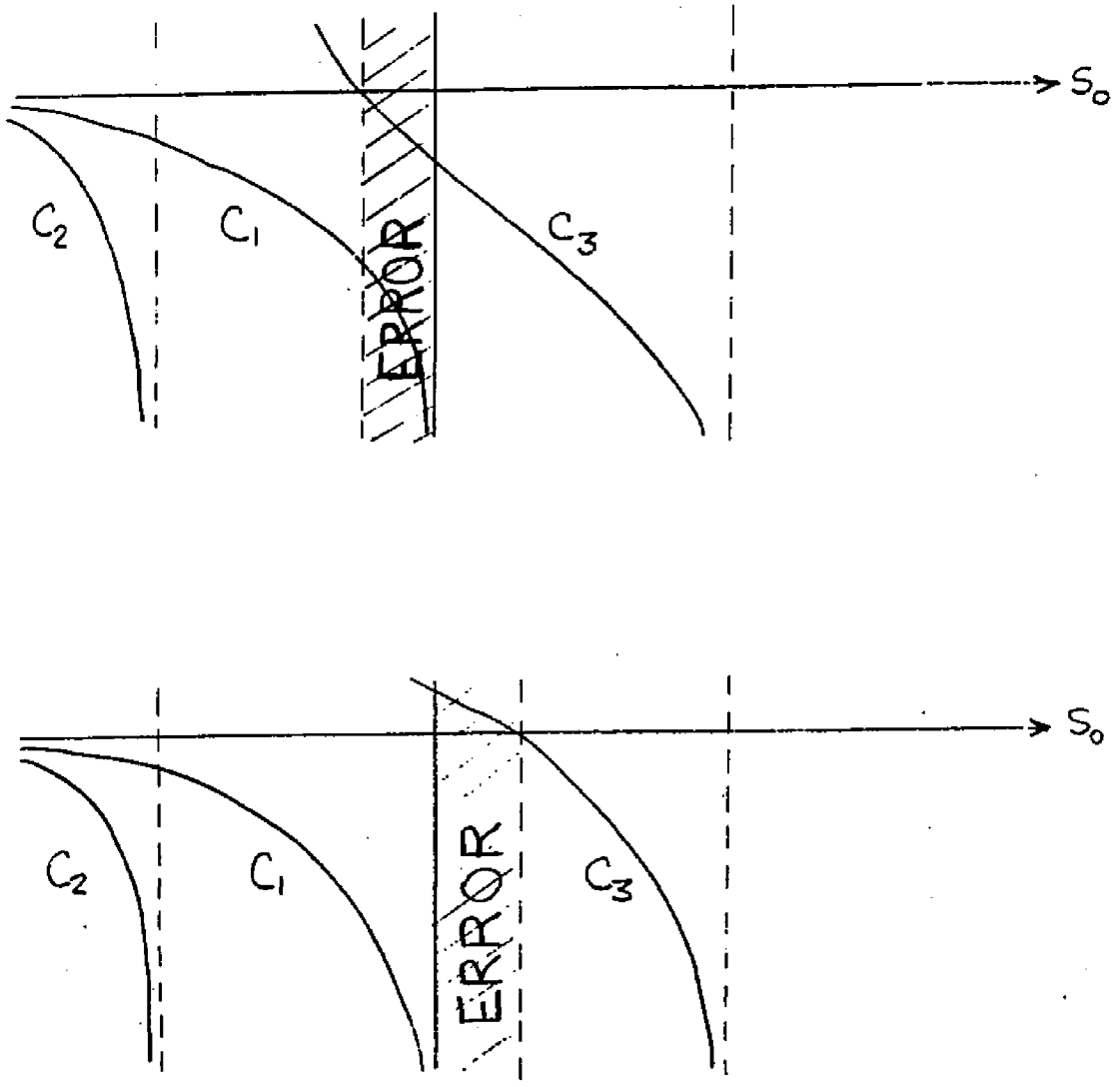

Figure IV-4 Error Indication Caused by Roundoff in the C_3 Test Coefficient

REFERENCES

1. PIERCE, J. R.
   U. S. Patent No. 2,743,322

2. SANDBANK, HEEKS, KING, WASSE, SOLYMAR and ASH
   "Velocity Modulation of Charge Carriers in Semiconductors"
   Report RP7-25, Standard Telecommunications Lab., LTD, London 1965

3. BUTCHER, P. N.
   "The Coupling Impedance of Tape Structures", J.I.E.E. Vol. 104B, pp.177-187, March 1957

4. SUMI, M.
   "Traveling-Wave Amplification by Drifting Carriers in Semiconductors", APL, Vol. 9, No. 6, pp.251-253, 15 Sept. 1966 (Expanded version - J.J.A.P., Vol. 6, No. 6, pp. 688-698, June 1967)

5. ROBINSON, B. B., and SWARTZ, G. A.
   "Two-Stream Instabilities in Semiconductor Plasmas", J.A.P., Vol 38, No. 6, pp. 2461-2465, May 1967

6. BEAGLEHOLE, D.
   "Optically Excited Surface Plasmons", C.C.N.Y. Conference on Wave Interactions in Solids", Feb. 7, 1969

7. ZOTTER, B.
   "Traveling-Wave Amplification by Drifting Carriers in Semiconductors", U.S. Army ECOM-2958, April 1968

8. VURAL, B., and STEELE, M.
   "Solid-State Plasma and Wave Interactions in Semiconductors", Chapter 11, McGraw-Hill (to be available May 1969)

9. HAMMER, J. M.
   "Coupling Between Slow Waves and Convective Instabilities in Solids", RCA Report PTR-2227, Feb. 1967

10. HAMMER, J. M.
    "Coupling Between Slow Waves and Convective Instabilities in Solids", APL, Vol. 10, No. 12, pp. 358, June 15, 1967

11. WANG, S.
    "Solid State Electronics", McGraw-Hill, 1968, Ch. 4.1

12. TANNENBAUM, B.
    "Plasma Physics", McGraw-Hill, 1967, Ch. 4.1

13. DELCROIX, J.
    "Plasma Physics", Wiley, 1965, Ch. 7.1, 2

14. SMITH, R. A.
"Wave Mechanics of Crystalline Solids", Chapman & Hall, 1963, Ch. 8.8

15. JONSCHER, A. K.
"Transport of Hot Injected Plasmas in Semiconductors", Proc. Phys. Soc., Vol. 84, 1964, pp. 767-779

16. CHAPMAN & COWLING
"Mathematical Theory of Non-Uniform Gases", Cambridge Press, London, 1953, Ch. 3.1

17. HANSON, D. C.
"Microwave Circuit Considerations for Bulk GaAs Oscillators", Report RADC-TR-67-97, Feb. 1967

18. Ibid

19. ZIMAN, J.
"Principles of the Theory of Solids", Cambridge Press, London, 1965, Ch.7.1.

20. ERLBACH & GUNN
"Noise of Hot Electrons in Germanium", Proc. Int. Conf. on Semiconductors, London 1962, pp. 128-132

21. ECKSTEIN, S.
"Resonant Amplification of Sound by Conduction Electrons", Phys. Rev., Vol. 131, 1963, pp. 1087

22. CHODOROW & SUSKIND
"Fundamentals of Microwave Engineering", McGraw-Hill, 1964, Ch. 4.3b

23. BRANCH & MIHRAN
"Plasma Frequency Reduction Factors in Electron Beams", I.E.E. Trans. Elec. Devices, April 1955, pp. 3-11

24. PIERCE, J. R.
"Effect of Passive Modes in Traveling-Wave Tubes", Proc. I.R.E. Aug. 1948, pp. 993-997

25. BRANCH & MIHRAN
op. cit.

26. SOLYMAR, L. and ASH, E.
"Velocity Modulation of Charge Carriers in Semiconductors", Report RP7-25, Std. Telecommunications Lab. LTD, London 1964, Appendix 2

27. PIERCE, J. R.
"Theory of Beam-Type Traveling Wave Tubes" Proc. IRE, Feb. 1947, pp. 111-123.

28. SOLYMAR and ASH
op. cit.

29. ABRAMOWITZ and STEGUN
"Handbook of Mathematical Functions", National Bureau of Standards Publ. AMS 55, 1966, p. 17

30. FLETCHER, R. C.
"A Broad-Band Interdigital Circuit for Use in Traveling-Wave Type Amplifiers", Proc. IRE, Vol. 40, Aug. 1952, pp. 951-958

31. WALLING, J. C.
"Interdigital and Other Slow Wave Structures", J. Electronics and Control, Vol. 3, Series 1, July 1957, pp. 239-258

32. CHEN, F. S.
"The Comb-Type Slow Wave Structure for TWM Applications", BSTJ, Vol. 43, May 1964, pp. 1035-1065

33. HADDAD, G. I.
"Characteristics of Dielectrically Loaded Ladder Lines for Traveling-Wave Masers and Other Applications", IEEE Trans. M.T.T., Vol. 14, No. 3, March 1966, pp. 120-129

34. WATKINS, D. A.
"Topics in Electromagnetic Theory", Wiley, 1958, pp. 12-14

35. BRILLOUIN, L.
"Wave Guides for Slow Waves", JAP, Vol. 19, Nov. 1948, pp. 1023-1041

36. BUTCHER, P. N.
"Coupling Impedance of Tape Structures", J.I.E.E., Vol. 104B, March 1957, pp. 177-187

37. ASH, E. and STUDD, A.
"A Ladder Structure for Millimeter Waves", IRE Trans. Elec. Devices, Vol. 8, July 1961, pp. 294-302

38. HADDAD, G. I.
op. cit.

39. HADDAD, G. I.
"Characteristics of Dielectrically Loaded Ladder Lines for Traveling Wave Masers and Other Applications", Report No. 65, University of Michigan Electron Physics Lab., Dec. 1963

40. HAMMING, R.
"Numerical Methods for Scientists and Engineers", McGraw-Hill, 1962 Ch. 28.2

41. EPSTEIN and MOURIER
"Definition, Mesure et Caracteres Des Vitesses De Phase Dans Les Systemes, A Structure Periodique", Annales De Radio Electricite, No. 39, Jan. 1955, p. 70

42. NICOLSON, A
"Broad band Microwave Transmission Characteristics From a Single Measurement of the Transient Response", IEEE Trans. Inst. & Meas., Vol. 17, Dec. 1968, pp. 395-402

43. EPSTEIN and MOURIER
op. cit., pp. 67-69

44. Ibid., p. 69

45. JOHNSON, C. C.
"Field and Wave Electrodynamics", McGraw-Hill, 1965, p. 270

46. Ibid, p. 230

47. ASH, E. and STUDD, A.
op. cit.

48. WALL, H. S.
"Analytic Theory of Continued Fractions", D. Van Nostrand, 1948, Sec. 40

49. Ibid, Theorem 48.1

50. SUMI, M.
op. cit.

51. ZOTTER, B.
op. cit.

52. VURAL, B. and STEELE, M.
op. cit.

53. SUMI, M. and SUSUKI, T.
"Evidence for Directional Coupling Between Semiconductor Carriers and Slow Circuit Waves", App. Phys. Letters, Vol. 13, No. 9, 1 Nov. 1968, pp. 326-327

54. ABRAMOWITZ and STEGUN
op. cit.

55. SUMI, M.
op. cit.

56. ZOTTER, B.
op. cit.

57. VURAL, B. and STEELE, M.
op. cit.

58. SUMI, M. and SUSUKI, T.
op. cit.

59. ABRAMOWITZ and STEGUN
op. cit., p. 18

60. HAMMING, R.
Chapter 3 of new book in preparation and personal conference.

61. RICHTER, S.
Private communication

62. ETTENBERG, M.
Personal conference

63. SUMI and SUSUKI
op. cit.

64. HEILMEIER, G. H.
"An Analysis of Parametric Amplification in Periodically Loaded Transmission Lines" RCA Review, Vol. 20, No. 3, 1959

65. SILLS, A. D.
"A Strip-Form Iterated Traveling Wave Parametric Amplifier Using Series Connected Diodes", DDC Report No. AD 642 766, Nov. 1966

66. Ibid

67. ETTENBERG, M.
"Microwave Traveling Wave Parametric Amplifier", 1959 Solid State Device Research Conf., Cornell University

68. CHODOROW and SUSKIND
op. cit.

69. HAMMING, R.
"Numerical Methods for Scientists and Engineers", McGraw-Hill, 1962, Ch. 29.3

VITA

Joseph Stanley Nadan, born in Brooklyn on April 16, 1942, is married and has one child.

Mr. Nadan attended elementary school in Brooklyn and graduated from George W. Wingate High School in June 1958. At City College, Mr. Nadan majored in electrical engineering and was president of the I.R.E. and editor-in-chief of TECH NEWS. Upon graduation in June 1963 he entered graduate school at the City College of New York and received his Master's degree in electrical engineering in June 1964.

In September 1964, Mr. Nadan became a Lecturer in the Department of Electrical Engineering, where he became interested in microwave semiconductors. In 1967, he became a full time student at the City University of New York working towards his PhD. In February 1968, Mr. Nadan was awarded a National Science Foundation Science Faculty Fellowship during the tenure of which the majority of the work on this dissertation was completed.

Mr. Nadan is presently a member of Eta Kappa Nu, I.E.E.E., and the American Society of Engineering Education.